1-1-2015

Experimental Investigation On Combustion And Ionization During Cold Starting And Idling Of A Diesel Engine

Sahil Deodatta Sane
Wayne State University,

EXPERIMENTAL INVESTIGATION ON COMBUSTION AND IONIZATION DURING COLD STARTING AND IDLING OF A DIESEL ENGINE

by

SAHIL DEODATTA SANE

THESIS

Submitted to the Graduate School

of Wayne State University,

Detroit, Michigan

in partial fulfillment of the requirements

for the degree of

MASTER OF SCIENCE

2015

MAJOR: Mechanical Engineering

Approved by:

_____

Advisor Date

DEDICATION

This thesis is dedicated to my parents and my sister, who are always being a source of inspiration to work hard towards my goal and provided me an endless support to achieve my dream.

Also, I dedicate this wok to all my friends, who helped me in all the possible ways from the day I arrive in USA till the date.

ACKNOWLEDGEMENTS

I would like to express my deepest and sincere gratitude to my adviser Prof. Dr. Naeim A. Henein, who gave me the opportunity to work in Center for Automotive Research and to contribute in the research work. I would also like to thank him for his continuous guidance, support and motivation without which this work would be difficult. His abundant knowledge and an extra-ordinary will power contributed as a greater source of motivation which helped me to achieve continuous improvement in my work.

I would also like to thank Dr. Walter Bryzik, Dr. Nabil Chalhoub, Dr. Marcis Jansons, Dr. Dinu Taraza and Dr. Trilochan Singh for being my thesis committee members and providing me with a continuous support and valuable feedback for my research work. I also acknowledge the help from Eugene and Marvin for the machine shop support.

I would also like to thank Shenouda Mekhael for his support during the instrumentation of MSFI sensor. I would like to thank my lab mates Dr. Amit Shrestha, Rojan George and Saikumar for sharing their thoughts and ideas and providing help with experimentation and analysis. I would like to thank all my colleagues from Center for Automotive Research particularly Sanket Gujarathi, Dr. Ziliang Zheng, Dr. Umashankar Joshi for their valuable feedback and support. Finally, I would especially want to thank Dr. Tamer Badawy for guiding and helping me in every possible way.

TABLE OF CONTENTS

LIST OF FIGURES

LIST OF TABLES

CHAPTER 1

INTRODUCTION

Diesel engines are gaining more popularity based on their high thermal efficiency and flexibility to operate on the variety of alternative fuels. With the use of advanced electronic control over injection systems, diesel engines can undergo multiple injections with high injection pressure, reducing the specific fuel consumption. These systems are equipped with high speed piezo injectors, through which 5 to 8 injections are achieved minimizing the undesirable NOx and soot emissions. Since the combustion process in the compression ignition (CI) engines is characterized by auto-ignition, which in turn has an overall lean air-fuel mixture resulting in lower specific fuel consumption at a given power rating. Turbocharging further helps the combustion process at high loads, which in turn improves the fuel economy and power output. Since the emission regulations are getting more and more stringent, the auto industry faces a big challenge seeking the balance between fuel economy and emissions without compromising engine performance. Although most of these situations are successfully handled with the help of modern techniques, cold starting in diesel engines is still recognized as a major issue which produces high amount of unburnt hydrocarbon emissions in the form of white smoke. Cold starting in diesel engines is distinguished by rough engine operation while cranking affecting the engine startability. During this operation, the engine experience incomplete/late combustion or complete misfiring causing a high cycle-to-cycle variation. This in turn gives rise to combustion instability which deteriorates the engine performance. It mainly depends on the ambient temperature, gas temperature and pressure near TDC and fuel properties. Therefore, in order to understand the in-cylinder combustion process, a reliable and robust feedback system is required.

Over the years, the ion current sensing technology has been successfully implemented in SI engines to detect engine knock and misfire. It is also used for closed loop control to obtain a close correlation with the combustion parameters for a various operating conditions. Hence, a detailed investigation of cold starting process using traditional as well as alternative fuels needs to be carried out with the help of ionization signal.

This thesis presents a detailed cycle by cycle analysis of auto-ignition, combustion and ionization characteristics of ULSD and JP8 fuels and their impact on combustion instability during cold starting. Experiments were conducted on a high speed direct injection diesel engine at normal room temperature (25˚C). In addition, a comparison is made between the ion current signals measured by two sensors during cold starting and low idling operation.

CHAPTER 2

LITERATURE REVIEW

2.1 Introduction

With the Federal and EURO regulations for emissions getting more stringent, engine manufacturers are facing the challenge of reducing both NOx and PM emissions, without any impact on fuel economy. Many emission standards have been met by applying electronic injection controls and using stacked piezo injectors, after-treatment devices, VTG etc. and seeking a balance between performance, fuel economy reduced emissions, and cost. In spite of all these advances, cold starting of diesel engines is still a problem, causing combustion instability and unburned hydrocarbon emissions in the form of white smoke [11]. To solve this problem and meeting more stringent NOx and particulate emissions in the future, there is a need for an in-cylinder combustion sensor that would produce a feedback signal to the ECU (Engine Control Unit).

Most of the previous research and development on in-cylinder combustion sensors focused on the pressure transducer which has been widely used in research. The research on ion current sensors has been limited, mainly, because of the lack of reproducibility of the ion current signal from cycle to cycle. However, recent research at Wayne State University showed that the lack of reproducibility of the ion current signal is an indication of the characteristics of combustion and its variation from cycle to cycle.

Due to its availability in many diesel engines and low production cost, the glow plug has been modified to act as an ion current sensor, in addition to its main function of heating the charge during the cold starting process. Unlike SI engines where the charge is homogeneous, the charge in the diesel engine is heterogeneous and the ion current is sensitive to the local equivalence ratio.

In diesel engines without a glow plug, the fuel injector has been used as an ion current sensor and referred to as MSFI (Multi-Sensing Fuel Injector) because it can sense the injection command timing and duration [29].

Currently, there is a great interest in developing alternate petroleum based fuels as well as renewable duels for different types of combustion engines. Also, the single fuel policy requires military engines to operate on JP8 aviation fuel. This chapter gives a review of previous research on the effect of different fuels on cold starting and the ion current signal.

2.2 Cold Starting in diesel engines

Problems in the cold starting of diesel engines are related to the high sensitivity of the autoignition processes to changes in the air temperature near the end of the compression stroke. Low compression temperatures during cold starting reduce the rate of the autoignition processes cause combustion to start late in the expansion stroke and drop in IMEP which eventually result in complete failure of the engine to start. Cold starting of diesel engines is characterized by long cranking periods and combustion instability leading to an increase in fuel consumption and emission of undesirable unburned hydrocarbon which appear as white smoke.

The problem of cold starting is influenced by many operating parameters such as ambient temperature, altitude, injection strategy, spray properties such as cone angle, spray penetration and wall impingement, and fuel properties such as cetane number and volatility. These problems would certainly be reduced by improved injection strategy which can further control the combustion phasing in the initial stages. Thus, a detailed cycle to cycle analysis is required in order to understand the effect of these parameters on combustion during cold starting.

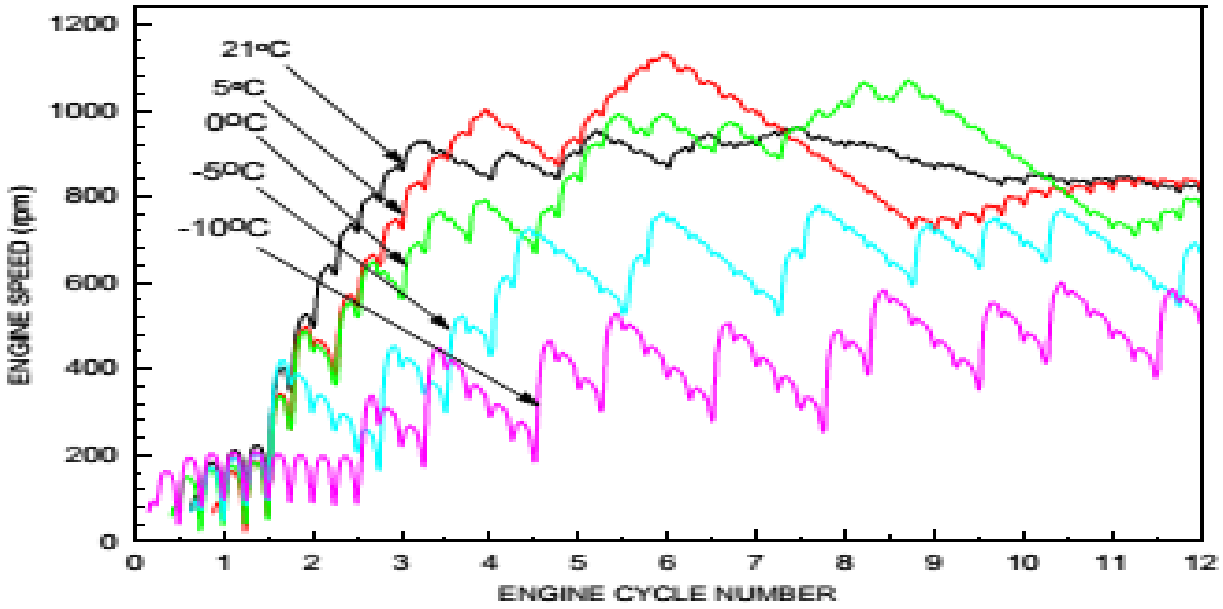

Figure 2-1 Engine speed variation with ambient temperature [11]

Figure 2-1 shows the transient engine speed at five different ambient air temperatures. Zhiping et al [11] showed that, the number of the cranking cycles almost doubled when the ambient temperature dropped from -5˚C to-10˚C. They also observed that the number of misfiring cycles increased with the drop in ambient temperature, which decreased as the engine got warmed up. This type of combustion instability was discussed in details in references [6-11]. They also developed a model for ignition delay in order to build speed-injection timing maps to identify misfiring zones at different temperatures, speeds and cetane number of fuel. This is further explained in figure 2-2 and figure 2-3.

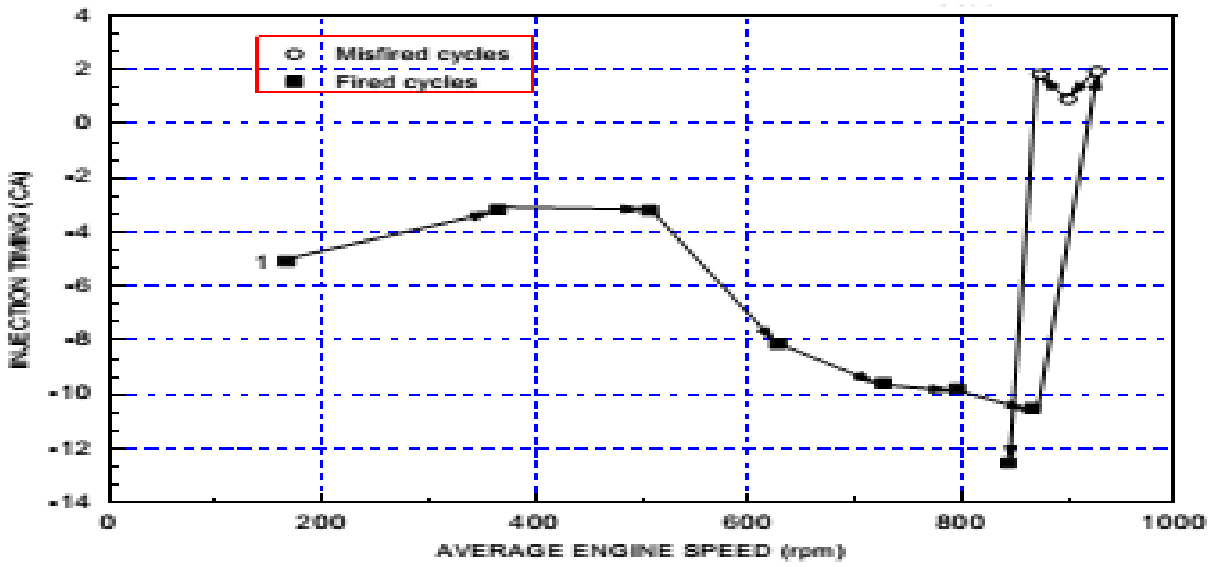

Figure 2-2 Transient engine speed-injection timing map [11]

Figure 2-2 displays the effect of injection timing for transient engine operation at 21˚C indicating firing and misfiring cycles. It shows that, as the engine accelerates to 800 rpm, the injection timing retards from 10.5˚bTDC to 2˚aTDC and the engine undergoes misfiring for cycles 8, 9 and 10 until it advances back to 12.7˚bTDC. It was found that, a mismatch between the injection timing and the engine speed caused most of the instability and misfiring.

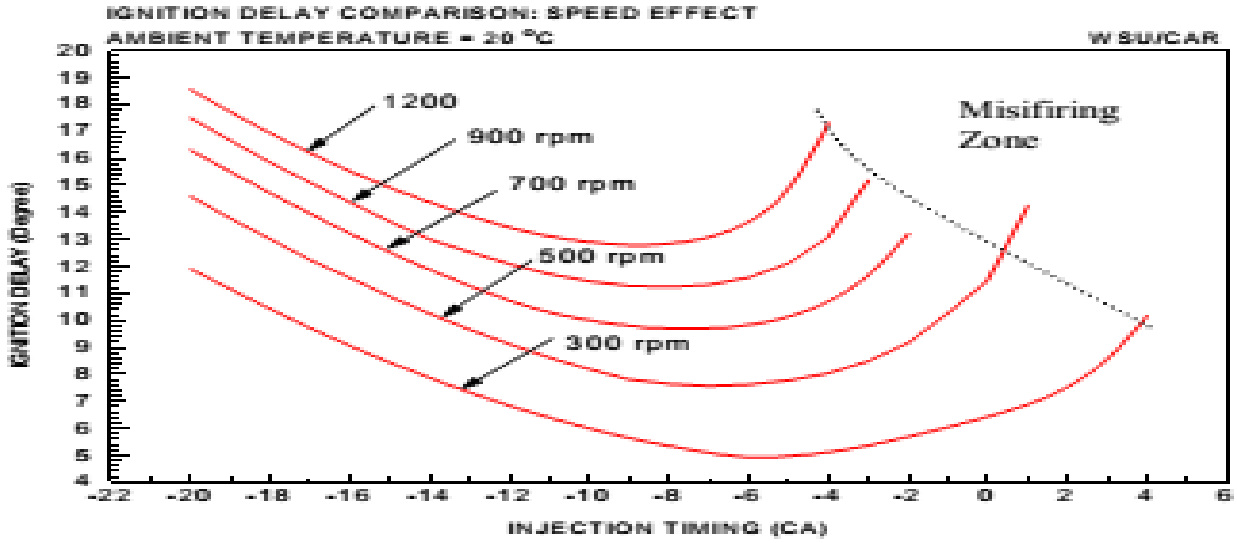

Figure 2-3 Effect of injection timing on ignition delay [11]

Figure 2-3 demonstrates the effects of engine speed on ignition delay and misfiring zones at 21˚C. It shows that at for higher engine speeds the minimum ID delay and the misfiring zone shift slightly towards the advanced injection timing. It is due to the fact that, as engine speed rises, the time available for the fuel-air mixture to react near TDC becomes less. They have also concluded that, the firing zones get narrower and combustion instability increases as the ambient temperature and CN drops.

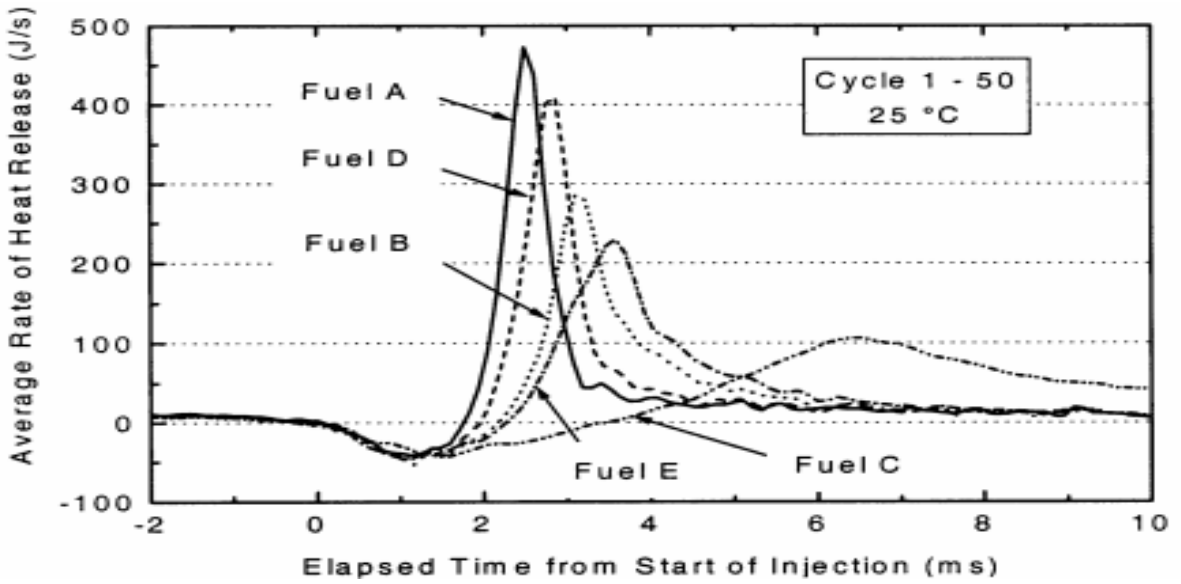

Figure 2-4 Effect of fuel properties on RHR at 25˚C [10]

Figure 2-4 shows the effect of fuels with different cetane numbers on average rate of heat release for cycles 1-50. Hiroaki et al. [10] showed that, cetane number of the fuel does not affect the rate of endothermic reactions at room temperature, which can be seen through figure 2-4. Consequently, cetane number of the fuel controls the rate of exothermic reactions and thus combustion phasing to a greater extent. It can be seen that, the average heat release is the lowest for fuel C, which also has the lowest cetane number (30.8). They also showed that, the number of cycles the engine takes to reach steady speed, is better as the cetane number of the fuel increased.

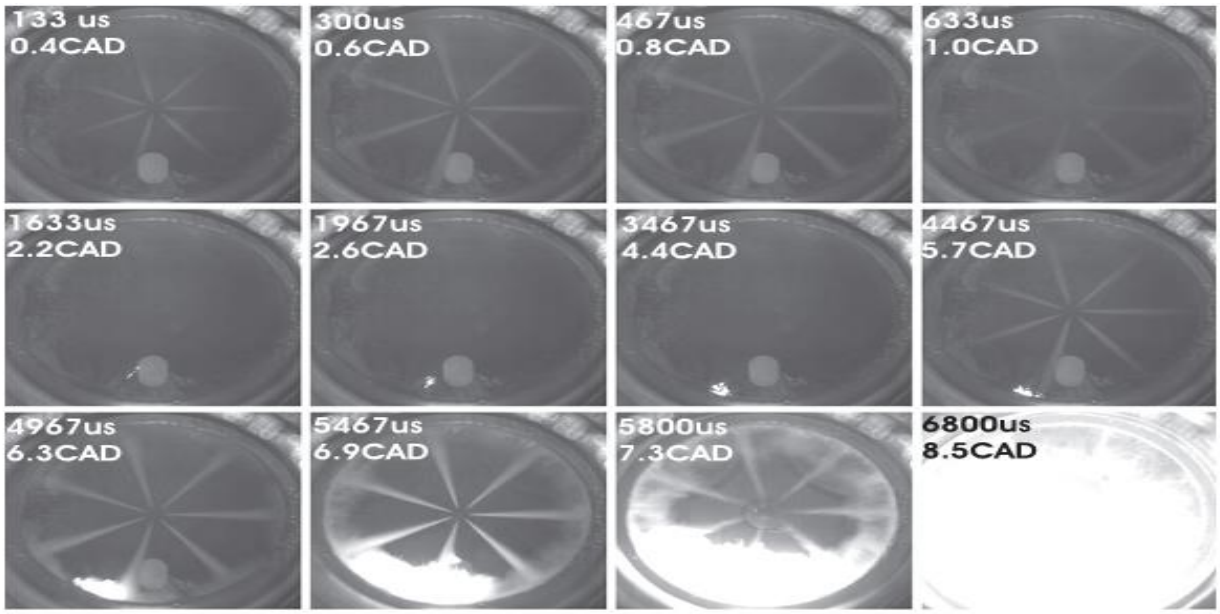

Figure 2-5 Combustion development during cold starting with pilot-main strategy [15]

Pastor J. et al. [15] showed the combustion development in a glow plug assisted HSDI engine under simulated low temperature cold start conditions using high speed visualization in an optical engine and explains the influence of spray glow plug configuration on cold starting. Figure 2-5 shows high speed images obtained under cold starting conditions with pilot-main injection strategy. The pilot injection (6 mg) starts at TDC while main injection (24 mg) starts at 5˚ aTDC with rail pressure being 370 bar. It can be seen that, sprays rapidly reaches the wall in a short time at 300μs, but no reaction has been observed till 1˚aTDC. At 2.2˚aTDC (1633μs), some small radiation spots were detected near the vicinity of glow plug and the fuel continues to burn. The combustion from main injection starts as soon as the closest spray to the glow plug touches the pilot flame. The flame further starts propagating in down and up-swirl directions at 5467μs. At the end they concluded that, injection strategies with low pressure and short duration are favorable to create a strong pilot flame for cold starting, as a better transport of fuel towards the glow plug after the end of pilot injection can be achieved.

2.3 Ionization in internal combustion engines

Ionization in hydrocarbon flames is mainly carried out by two peculiar events, Chemi-ionization and thermal-ionization [24, 25]. Its amplitude depends on the local fuel-air ratio of the charge mixture and the in-cylinder combustion temperature [25, 26]. Since the spark-ignition engines operate close to the stoichiometric fuel-air ratio with a homogeneous charge throughout the chamber, the formation of ions through chemi and thermal ionization is very high and appear as two distinct peaks. On the contrary, combustion in diesel engines is initiated by auto-ignition reaction of fuel-air mixture, which is lean and heterogeneous in nature. In addition, the characteristics of ion current formed in diesel engines are not repetitive as compared to SI engines and mainly depend on local equivalence ratio and in-cylinder temperatures. Thus, depending on engine load, it can have up to 3-4 peaks based on number of injections.

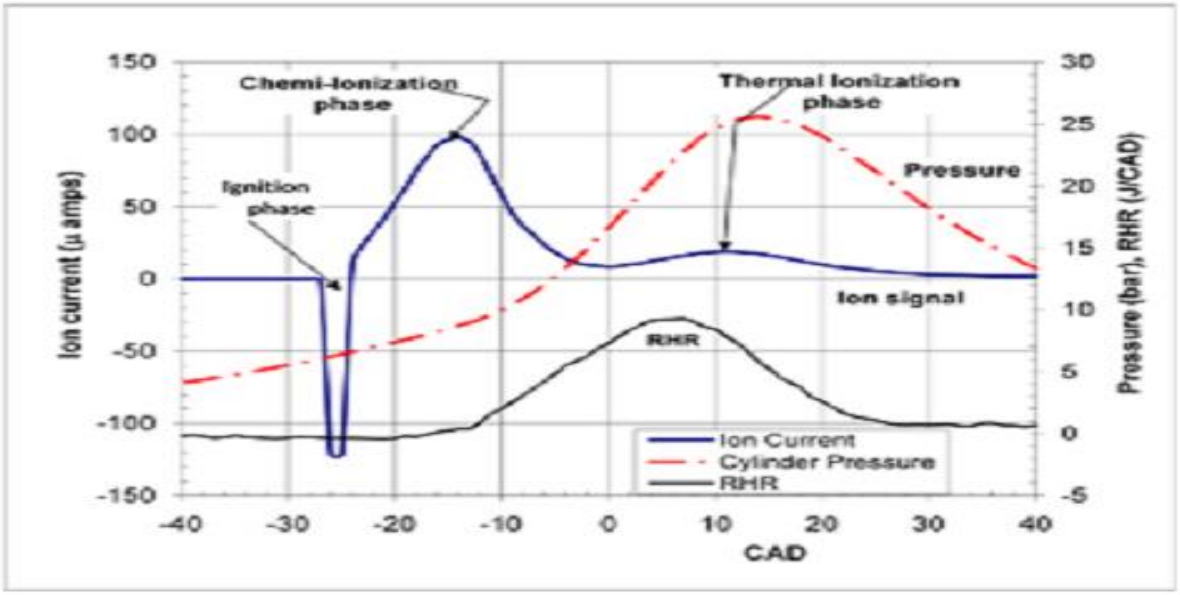

Figure 2-6 Ion current Signal in SI engine (speed = 1300 rpm and Torque = 20Nm) [25]

Figure 2-6 shows traces for in-cylinder pressure, RHR and ion current signal in a SI engine at 1300 rpm. Here, the spark plug is used as an ion current sensor which shows two distinct peaks

for the ion current signal. It can be seen that, the first peak is mainly caused by chemi-ionization in the flame front zone around the spark plug gap, while the second peak is the result of thermal-ionization of the gases due to an increase in temperature [25-27]. Many studies over the past decade indicated that the ionization characteristics in SI engines mainly depend on the equivalence ratio, in-cylinder combustion temperatures, EGR rate and the location of the sensor in the combustion chamber [25, 26].

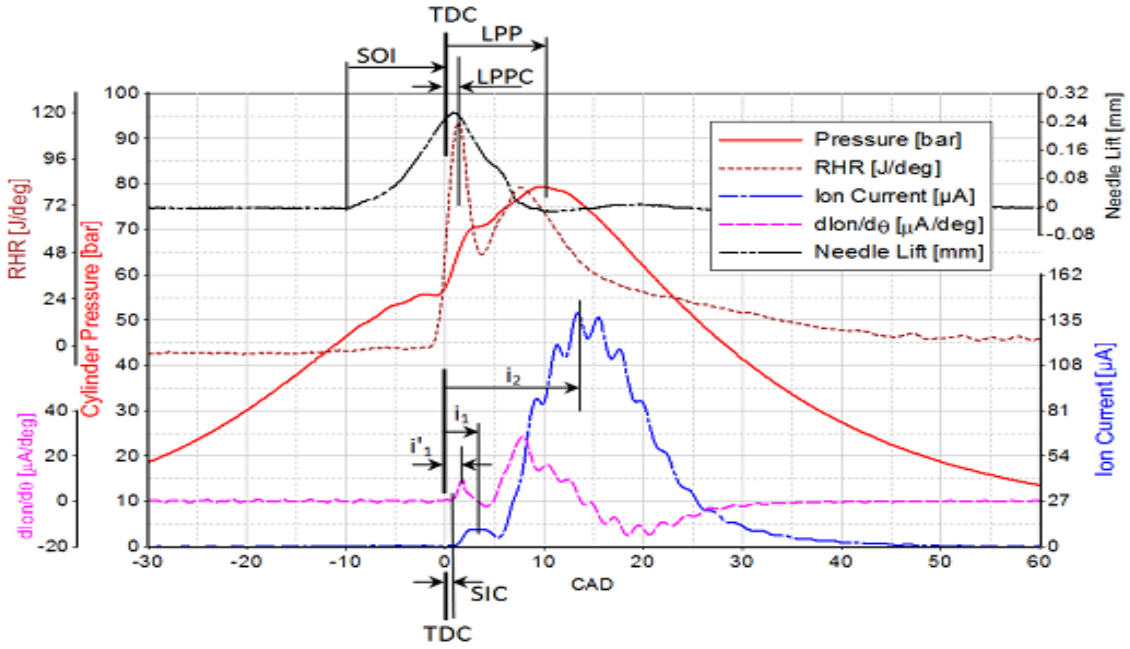

Figure 2-7 Ion current Signal in CI engine (Speed/IMEP=1800rpm/8 bar) [28]

Figure 2-7 shows ionization characteristics in a diesel engine along with cylinder pressure, RHR and needle lift traces at 1800 rpm and 8 bar. Badawy et. al [28] used ion current signal to develop a closed loop feedback control in diesel engines. For this purpose, a modified glow plug sensor is used to obtain ionization characteristics in a diesel engine. They also developed a linear relationship between SIC and LPPC where start of ion current showing reproducible property. They showed that ion current feedback is a good source in controlling the combustion phasing

under steady as well as transient state. In addition to this, the ionization characteristics in a diesel engine are explained in detail in reference [27], where Rai et. al showed that the number of ion current peaks in a diesel engine depend on engine load, injection pressure and probe length. Further George et. al [5] showed the effect of fuel properties on ionization characteristics in a high speed diesel engine under steady state, which can be seen from figure 2-8.

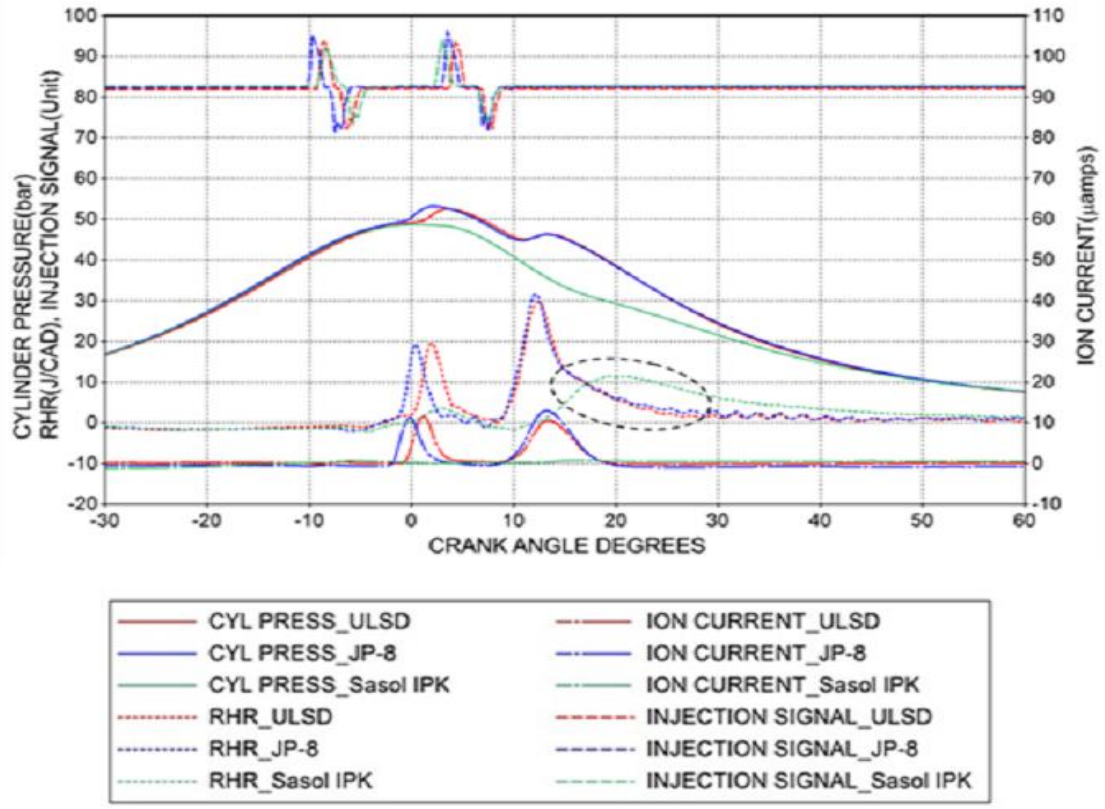

Figure 2-8 Ion current signal at no load operation, 1800 rpm with different fuels [5]

Figure 2-8 shows typical ion current traces at no load and 1800 rpm on a high speed direct injection turbocharged engines. It also shows the in-cylinder pressure, RHR and injection timing using three different fuels ULSD, JP8 and Sasol-IPK. Two distinct combustion events occur for pilot and main injection, when ULSD and JP8 fuel were used. These can be clearly seen with the help of pressure, RHR and ion current traces. On the other hand, despite of having higher volatility,

no distinct combustion event was observed for Sasol-IPK, while RHR trace showing low heat release and retarded LPPC for pilot as well as main injection. In this event, ion current signal was also not detected.

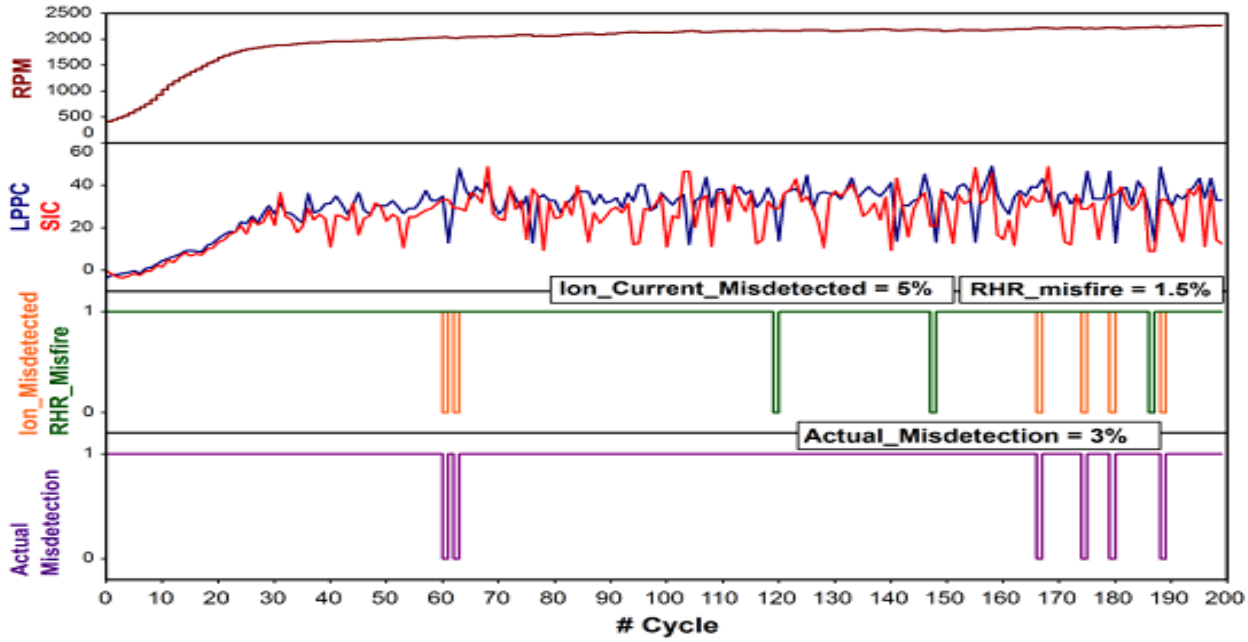

Figure 2-9 Correlation of SIC- LPPC and ion current misdetection for cold starting at 2000 rpm using large probe diameter and length [4]

Figure 2-9 shows the correlation for SIC and LPPC during cold starting at 2000 rpm. Gujarathi et al. [4] showed that ion current measured by glow plug could be misdetected even if the engine undergoes normal combustion. A detailed cycle to cycle analysis was performed using different sizes of glow plug and applied voltage. They showed that detection of ion current mainly depends on the area of the sensor exposed in the combustion chamber which also improves the ion current detection at cold starting and no load operations to a greater extent.

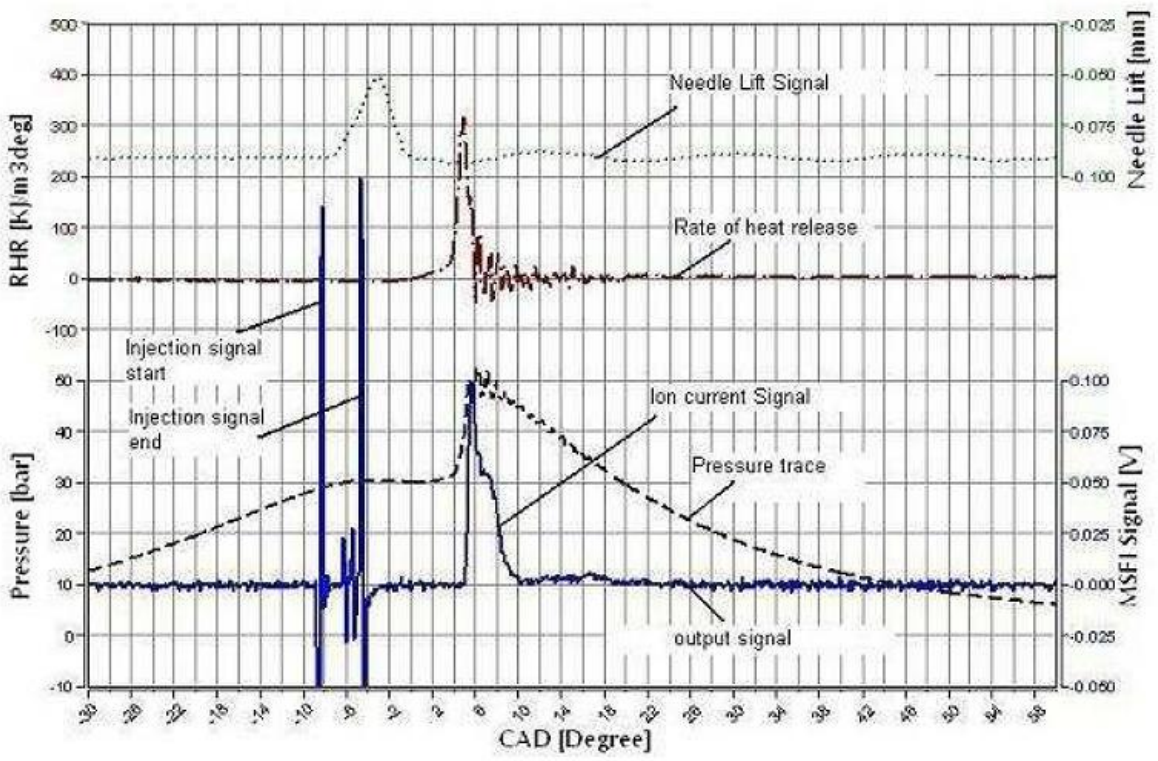

Figure 2-10 MSFI signal using solenoid injector for a successful combustion [29]

Estefanous et al. [29] developed a new technique to use the fuel injector as a multi-sensor (MSFI), ion current as well as injection command and duration. They showed that this new technique has an advantage over ion probes to detect fuel leakage or dribbling. A control algorithm was developed for the use of the MSFI output signal in the feedback loop to the ECU for injection timing and injection and combustion diagnostics. Figure 2-10 shows traces of ion current using MSFI for a successful combustion event along with pressure and RHR trace.

2.4 Ionization Mechanism

The ionization mechanism consists of chemi and thermal ionization phases [5]:

Chemi-Ionization

$CH + O \longrightarrow CHO^+ + e^-$ …… (1)

$CH + C_2H_2 \longrightarrow C_3H_3^+ + e^-$ …… (2)

Charge Transfer

$CHO + CH_2 \longrightarrow CH_3^+ + CO$ …… (3)

$CHO^+ + H_2O \longrightarrow H_3O^+ + CO$ …… (4)

Recombination

$H3O^+ + e^- \longrightarrow H_2O + H$ …… (5)

Thermal Ionization

$M + E_{ion} \longrightarrow M^+ + e^-$ …… (6)

Reactions (1) and (2) show the chemi-ionization phase, where the CH radical initiates the ion formation reaction. Charge transfer takes place with CO as a byproduct as shown by reaction (3) and (4). H_3O^+ gains an electron and forms stable products in the form of H_2O and H which is known as recombination reaction. Reaction (6) shows the thermal ionization mechanism, where ions were formed at high gas temperatures which can be correlated to the formation of NO.

2.5 Conclusions

This literature review explains the cold starting phenomena in diesel engines, being a major challenge faced in today's world. It also shows the influences of various parameters on misfiring and combustion instability which affects the engine startability. It gives a brief insight on effect of ambient temperature, injection timing and cetane number on combustion instability. An improved injection strategy with an appropriate spray-glow plug configuration could act as a good remedy.

Ion current technology has been successfully used as a feedback sensor in SI engines to detect misfire and knocking. Being an inexpensive and reliable technology, it is also implemented in diesel engines over a past decade to understand the heterogeneous combustion process. The review of ionization characteristics for both SI and diesel engines hold an importance for ion current signal as it gives a detailed information about the combustion process. Recently, it was also used to get a feedback using alternative fuels at various operating conditions. Also, a new technique to measure ionization characteristics by using fuel injector (MSFI) is shown which has a good correlation with combustion parameters.

As the industry faces more challenges improving combustion instability, a detailed research is required in order to get a deeper insight of the cold starting problem by using different fuels.

CHAPTER 3

ENGINE SET UP AND INSTRUMENTATION

3.1 Engine Set Up

The cold starting experiments were conducted on a 4-cylinder, 4-stroke, 2.0 Litre turbocharged direct injection, Volkswagen Industrial Engine, which has exhaust gas recirculation and a charge air intercooler. It has four valves per cylinder, driven by overhead belt-driven camshafts. It is equipped with a high pressure common rail injection system which is instrumented with piezo operated injectors. The exhaust gas recirculation system was isolated in this investigation in order to reduce the cylinder to cylinder variations. It originally has a diesel particular filter (DPF) that meets the EURO 5 emissions standards. But DPF was removed in this investigation in order measure the emissions without any after treatment hardware. The engine was mounted on a docking cart and coupled to a water brake dynamometer. A radiator was also mounted on the cart which provided the cooling for the turbocharged intake air. The in-cylinder pressure measurements were taken using a gas pressure transducer installed in the glow plug opening of cylinder #1. Ion current signal is measured using a modified glow plug ion current sensor in cylinder #4. Injector #1 was electrically insulated from the engine body to measure the ionization signal as well as injection pulse signal from cylinder #1. The engine was operated using an industrial/OEM ECU and hence all the engine operating parameters such as injection timing, pulse width and no. of events, fuel injection pressure were controlled by the OEM ECU. A detailed description of engine instrumentation along with DAQ system, emission analyzers and other sensors used in this thesis are explained in detail in the following sections. Figure 3-1 shows the experimental engine set up and instrumentation.

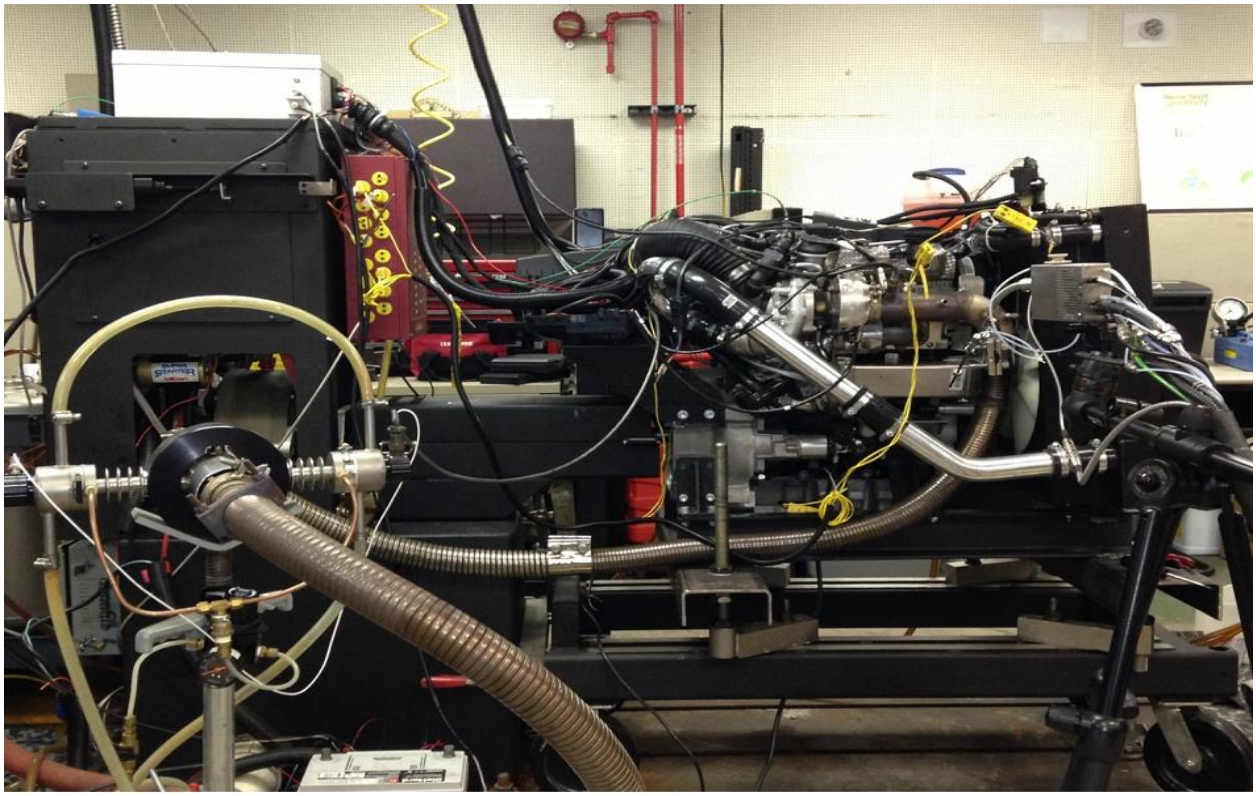

Figure 3-1 Experimental Set Up (Exhaust Side)

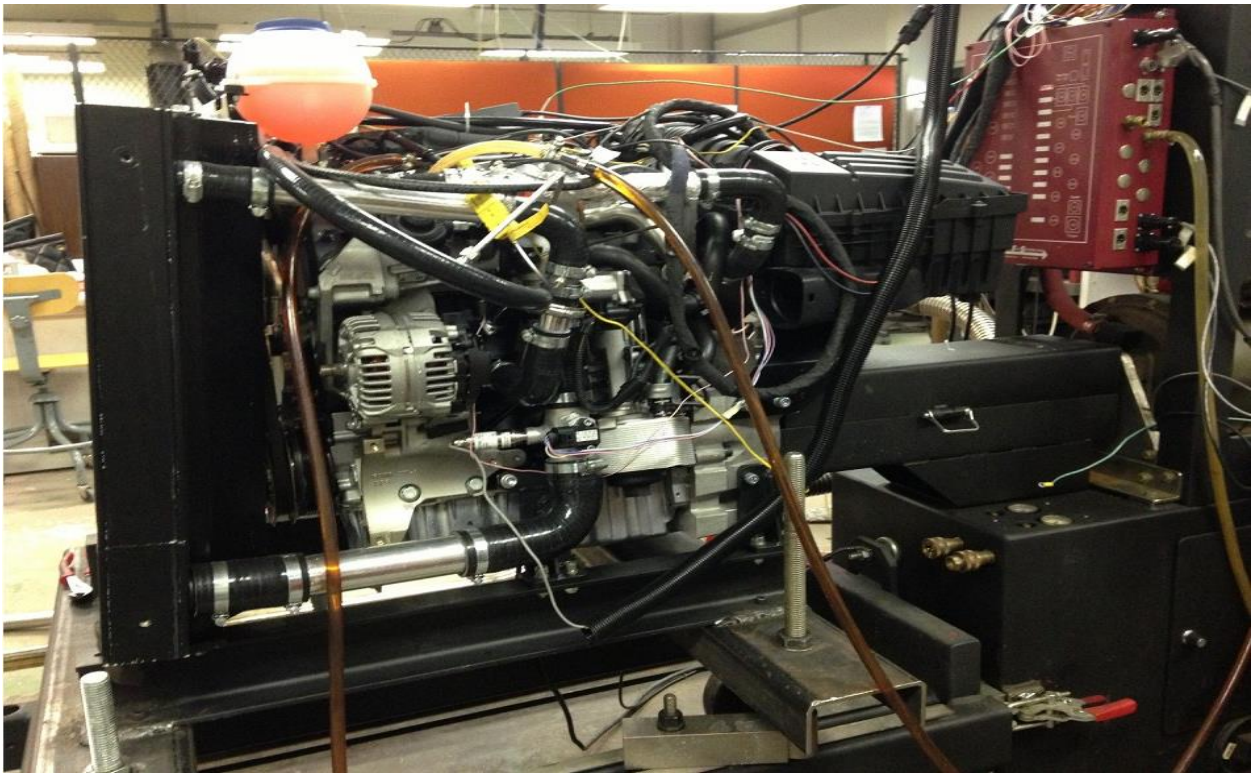

Figure 3-2 Experimental Set Up (Intake Side)

3.2 Engine Specifications

The specifications and technical details of the engine are provided in Table 3-1 and Figure 3-3 shows the permissible operating angles.

Table 3-1 Specification and technical data of 2.0L VW TDI [2, 3]

Engine Type	Diesel, 4 – Stroke
No. of Cylinders	4
Bore/Stroke	81/95.5 (mm)
Connecting Rod Length	144 (mm)
No. of Valves Per Cylinder	4 (DOHC)
Injection System	Common Rail (1800 bar) with Piezo Injectors
Compression ratio	16.5:1
Displaced Volume	1968 CC
Maximum Output	103 kW (140 hp) at 4000 rpm
Maximum Torque	320Nm (236 lb-ft) 1750 rpm up to 2500 rpm
Lower idling Speed	830 rpm +50/-25
Engine Management	Bosch EDC 17 (Common Rail Control Unit)
Lubrication Oil Capacity	4.5 liters
Maximum Tilting	12˚

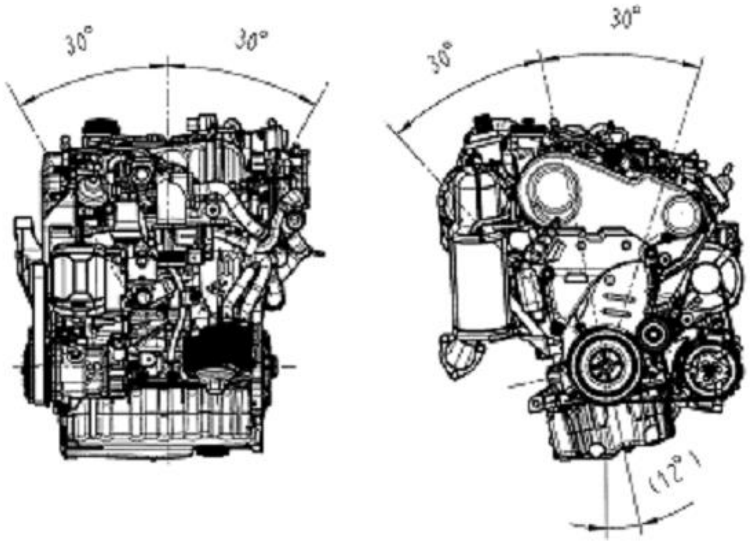

Figure 3-3 The permissible operating angles of the engine [3]

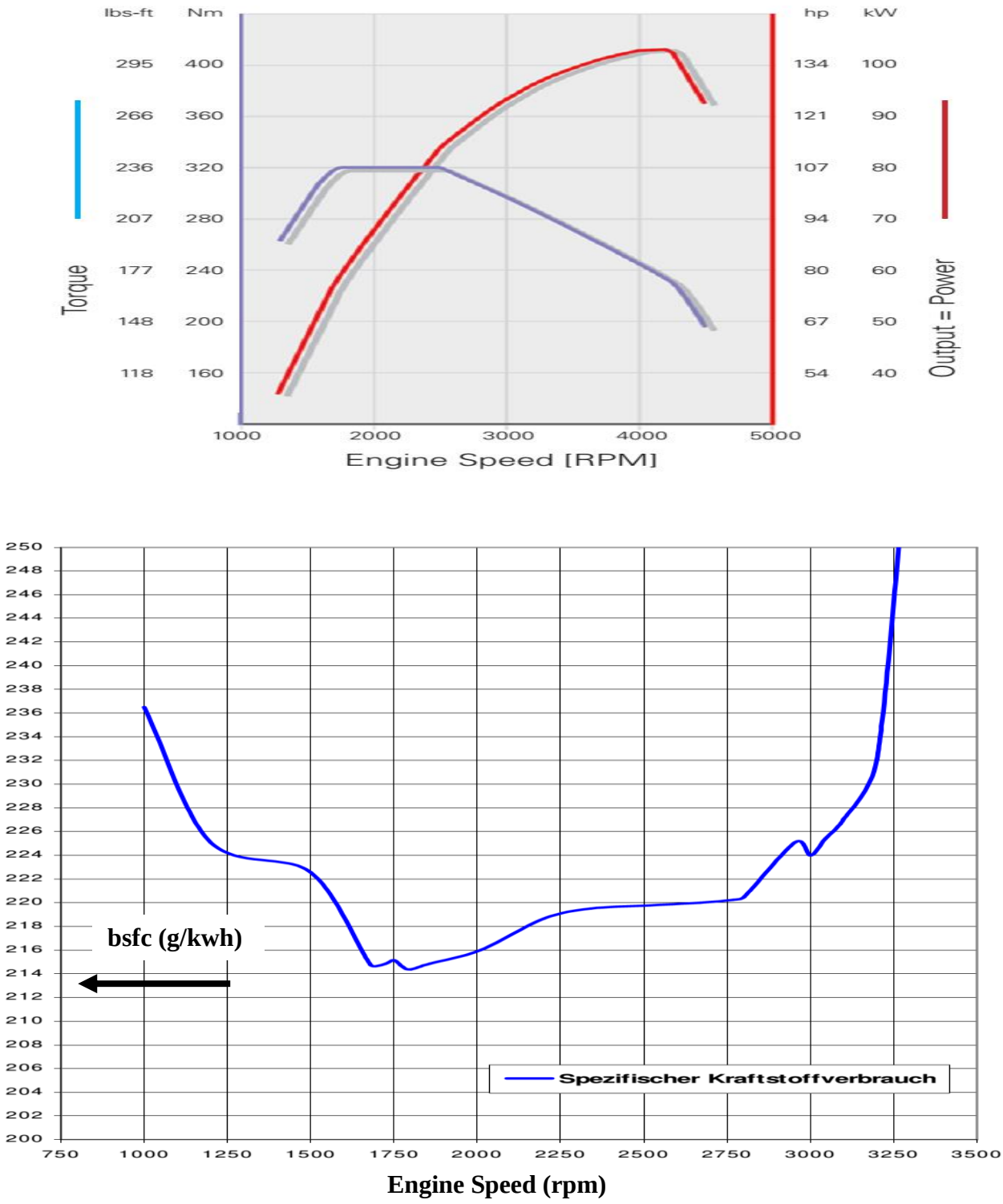

Figure 3-4 Engine output curve and fuel consumption curve [2, 3]

The peak torque of the engine is 320 Nm at 1750 rpm up to 2500 rpm and maximum power output of 103 kW occurs at 4000rpm. It can be also seen that the minimum bsfc for the engine is

214 g/kwh which is obtained at 1750 rpm. The engine torque curve and brake specific fuel consumption curves are shown in Figure 3-4.

3.3 Cylinder head and piston geometry

The cylinder head of the engine is a cross flow aluminum head with two intake and two exhaust valves per cylinder which are arranged vertically overhead. The pistons of this engine come with no valve pockets contrary to the old designs. This reduces the clearance volume of the cylinder and enhances the formation of swirl inside the cylinder. The piezo operated injectors are centrally located over the more flat, wider and shallow piston bowl chamber.

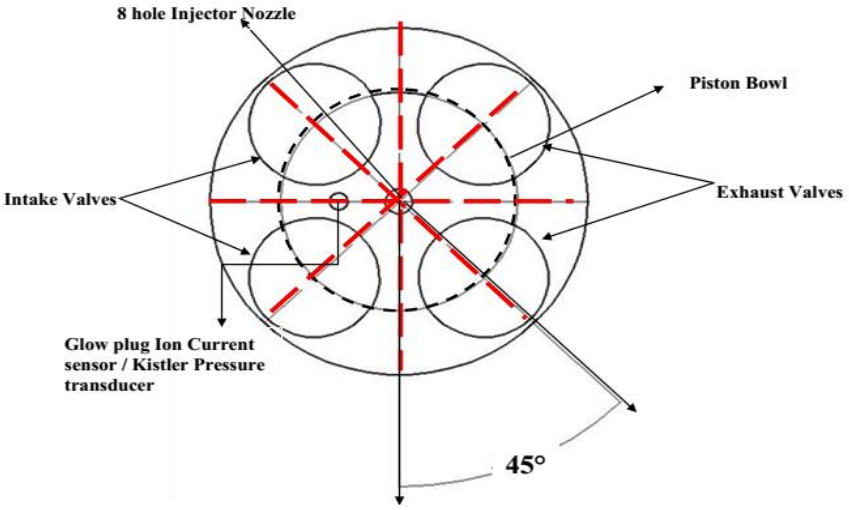

Figure 3-5 Top view of the combustion chamber showing locations of the sprays, Ion sensor, piston bowl and the valves [5]

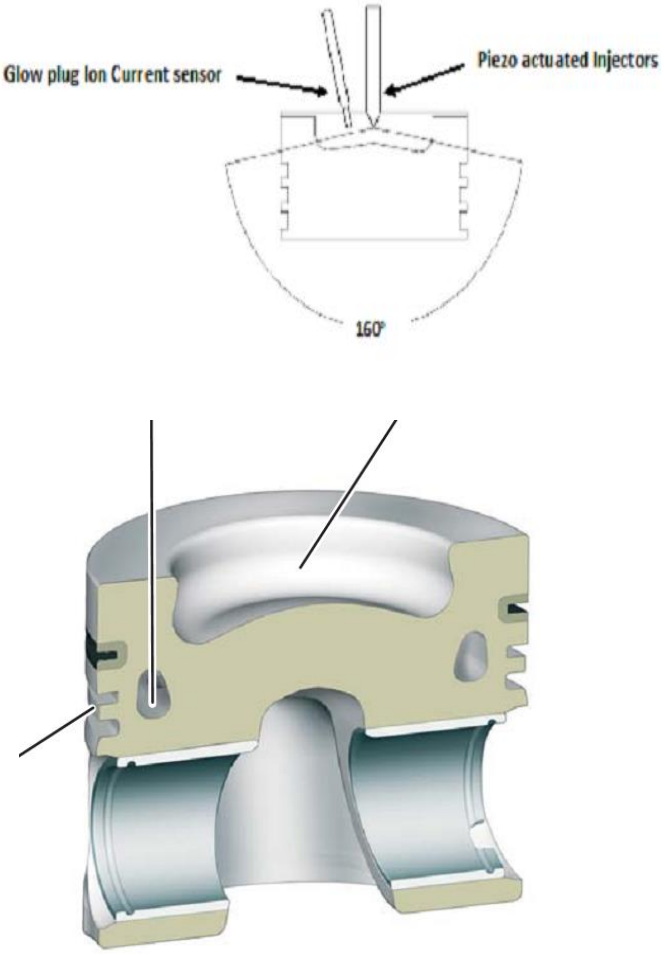

Figure 3-6 Front view of the combustion chamber [2, 5]

3.4 Common rail system equipped with Piezo-Injectors

VW 2.0 L engine is equipped with an electronically controlled high pressure common rail fuel injection system which consists of a separate high pressure pump which generates the pressurized fuel upto 1800 bar. The pressurized fuel is accumulated in the high common rail and supplied to the injectors. The rail pressure varies from 230 bar to 1800 bar depending on the engine operating conditions. The common rail system is instrumented with piezo injectors which are controlled using a piezo actuator stacks. Piezo injectors have certain advantages over regular solenoid injectors. It approximately has 4 times faster switching speeds and 75% less moving mass

at the injector needle. It can deliver up to 5 injection events per working cycles with comparatively less injection delay. Due to the very short switching times of the piezo injectors, injection quantities and phases can be precisely controlled [21]. Figure 3-7 shows a sectional view of piezo injector while figure 3-8 displays the common rail system. A detailed working of the piezo operated injectors and driver signal details are provided in references [20, 22].

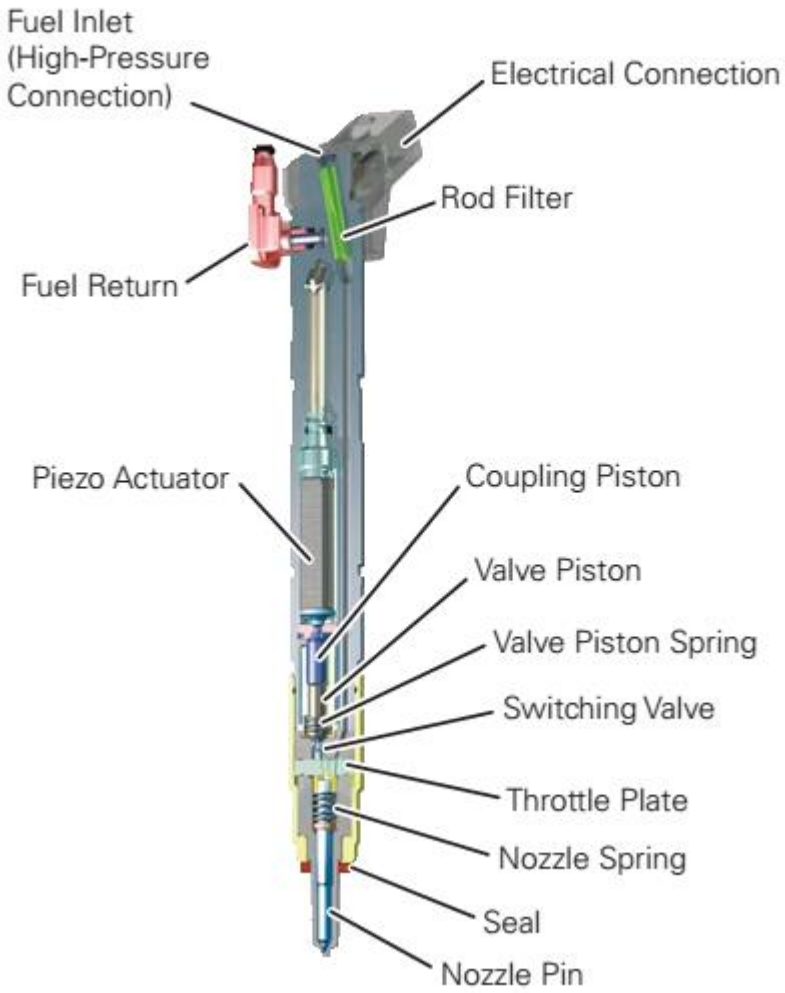

Figure 3-7 Sectional view of Piezo Injector [2]

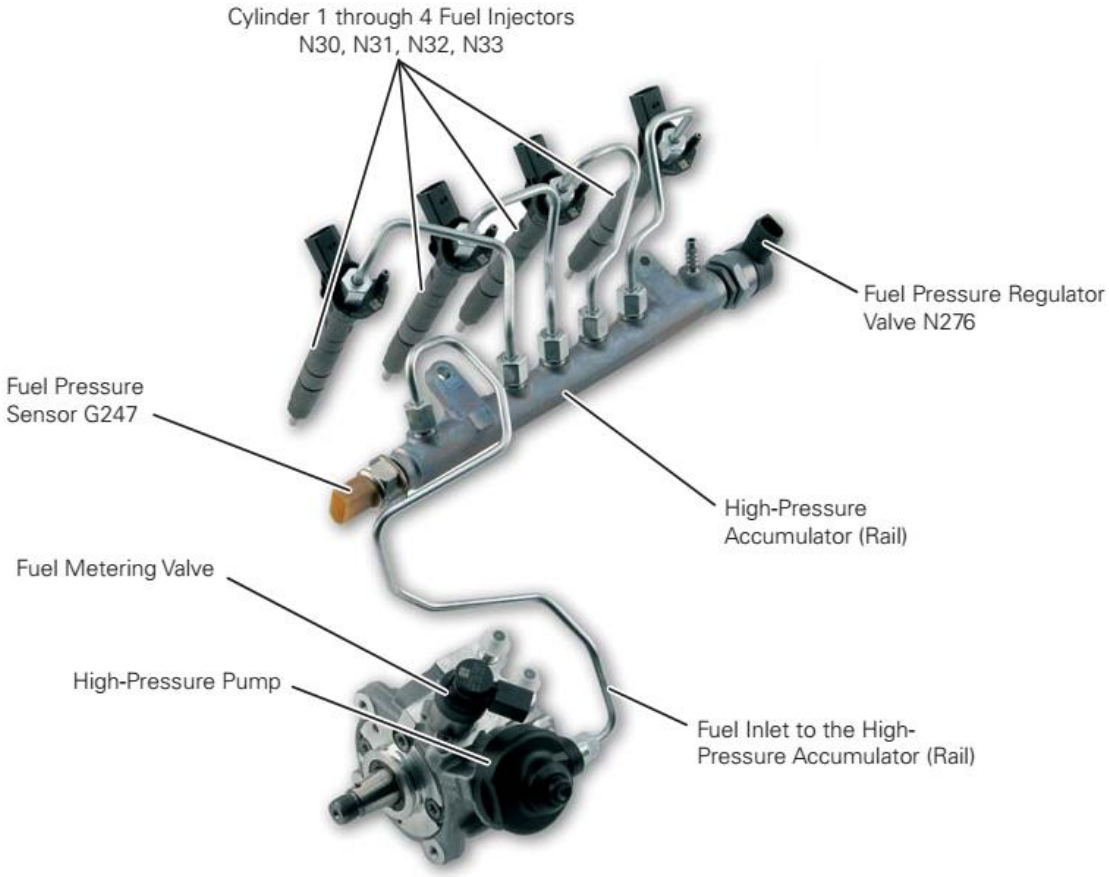

Figure 3-8 Common Rail System with Piezo Injector [2]

3.5 Engine instrumentation

The engine is instrumented with numerous sensors, measurement and control devices in order to operate as well as to monitor the combustion, performance, emissions and ionization characteristics. Various instrumentation on the engine is described in the following subsections.

3.5.1 Dynamometer control set-up

The engine is coupled to a water brake hydraulic dynamometer by means a splined shaft and a constant velocity (CV) coupling in order to allow a smooth engine operation even in the case of slight misalignment. The dyno system consists of a built in control system as well as a time

based slow speed data acquisition system. It is equipped with a speed sensor, a load cell, a slow response thermocouples and pressure sensors. The control software of the dynamometer calculates the speed, engine torque, and brake power, various thermocouple readings such as cooling water temperature, intake and exhaust temperatures, oil pan temperature and room temperature. The water pressure for the dynamometer operation is controlled using a pressure regulator valve where the water pressure is maintained at 5 bar pressure. Figure 3-9 and figure 3-10 show the dynamometer control interface, display and the block diagram of the dynamometer set up along with its various parts respectively.

Figure 3-9 Dynamometer control unit display

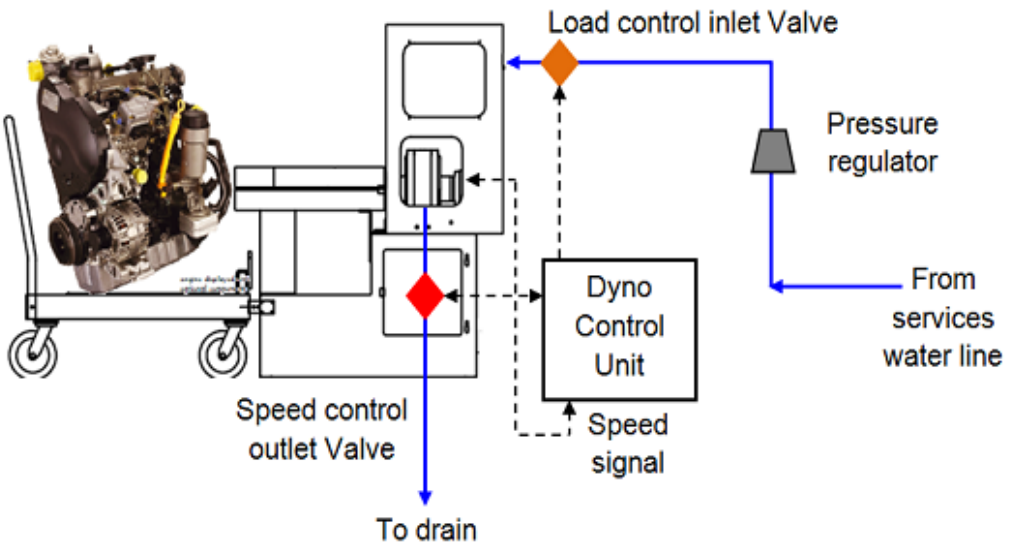

Figure 3-10 Dynamometer setup

3.5.2 Optical encoder

An optical encoder is installed on the camshaft to measure the instantaneous crank angle degree. It was supported by using a bracket to balance in case of any vibration or misalignment that could come between the encoder shaft and camshaft. This optical shaft encoder has the resolution of 0.25 pulses/degree. A resolution of 0.25 CAD was selected since any higher resolution would induce more noise and lesser resolution would result in the loss of combustion data. It sends the TDC pulses as well as the crank angle pulses to the high speed data acquisition system. The TDC of the engine was matched with the TDC of the encoder in order to eliminate any offset. This feature gives 2880 data points per cycle.

3.5.3 Pressure transducer

A Kistler Pressure Transducer-Type 6052A is installed in the glow plug opening in Cylinder #1. It is connected to a charge amplifier of Type 5010 which converts the electrical charge

produced by the piezoelectric sensors into a voltage signal. This voltage signal is then recorded by the DAQ and displays as the in cylinder pressure signal. Figure 3-11 shows the Kistler pressure transducer, Type 6052-A, assembly set up. The pressure in the common rail fuel system is measured using a Kistler high pressure piezo resistive sensor of Type 4067A2000. The pressure sensor is installed on the high pressure fuel line of cylinder #1 using a special mounting clamp. The location of the sensor was selected such that is it should be as close as possible to the fuel injector such it can capture the drop in fuel line pressure which in turn indicate start of the fuel injection. A charge amplifier, Type 4618A, is used to convert the electrical charge produced by the rail pressure sensor into a voltage signal. The high speed DAQ converts and records this voltage signal as the fuel rail pressure in bars. The set-up for the rail pressure sensor assembly is shown in figure 3-12.

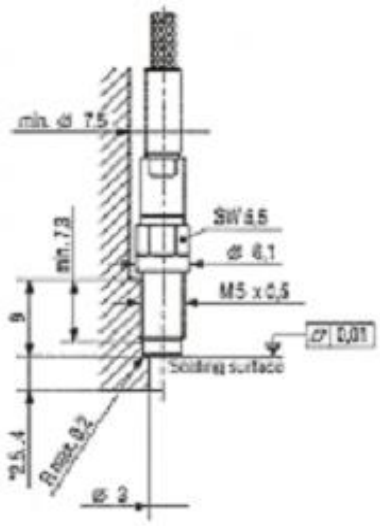

Figure 3-11 Pressure transducer assembly [36]

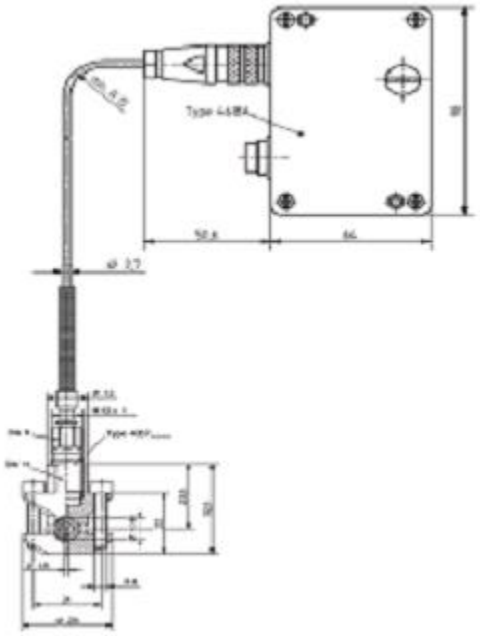

Figure 3-12 Rail pressure sensor assembly [37]

3.5.4 Intake temperature and pressure

An Omega pressure transducer (PX209 30-V85G5V) is used in order to supervise the intake pressure. The intake manifold was machined to accommodate the pressure sensor. It is monitored to provide a support to the in cylinder pressure trace, as the intake pressure variable due to the boosting provided by the turbocharger. The intake air temperature is measured using a K-type thermocouple installed on the intake manifold. It can vary due to the presence of the turbo charging and the exhaust gas recirculation (EGR).

3.5.5 Fuel supply and measuring circuit

The fuel is delivered, using a low pressure pump, from the fuel tank to the engine. It passes through a fuel filter and a flow meter, from Max Machinery Inc (Model 710), before reaching the intake of the engine driven high pressure common rail pump. The fuel from the return line of the high pressure pump returns to the fuel circuit through a heat exchanger, which is water cooled.

The cooled fuel is then circulated back to the fuel tank and again flows towards the common rail. The flow meter measures the fuel consumption rate in centimeters cubes per minute (cc/min). A circuit diagram showing the flow supply and fuel flow metering circuit is shown in Figure 3-13, whereas figure 3-14 shows a pictorial view of the same.

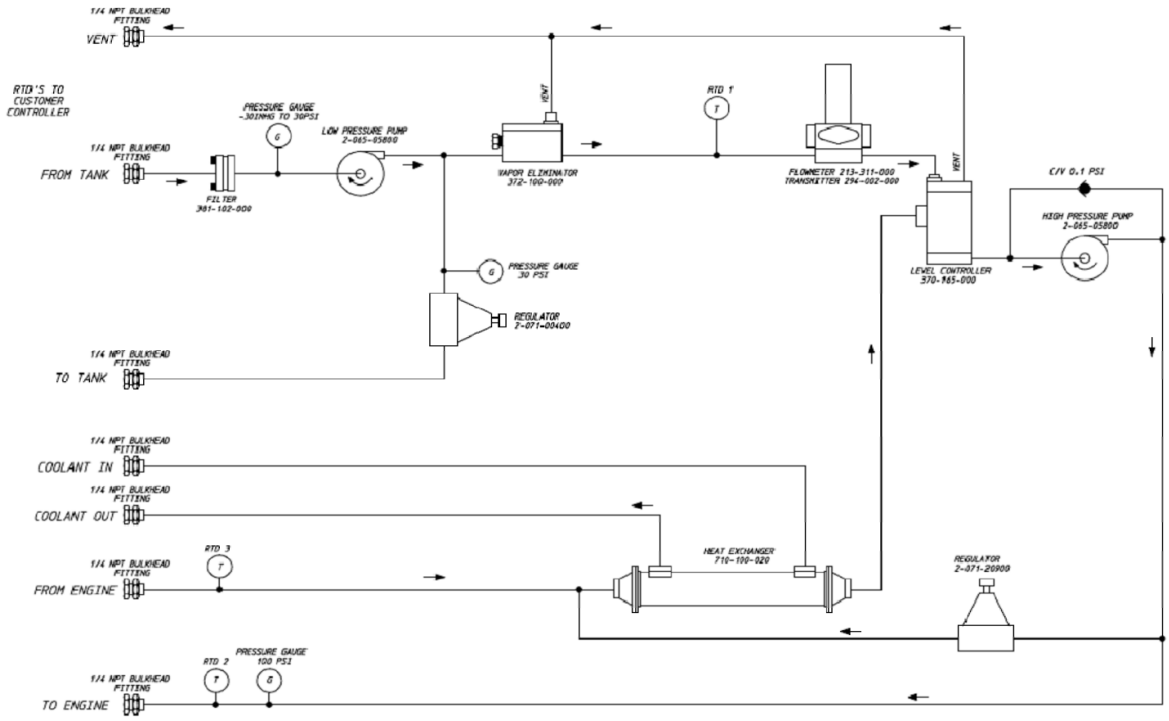

Figure 3-13 Fuel flow and measuring circuit [38]

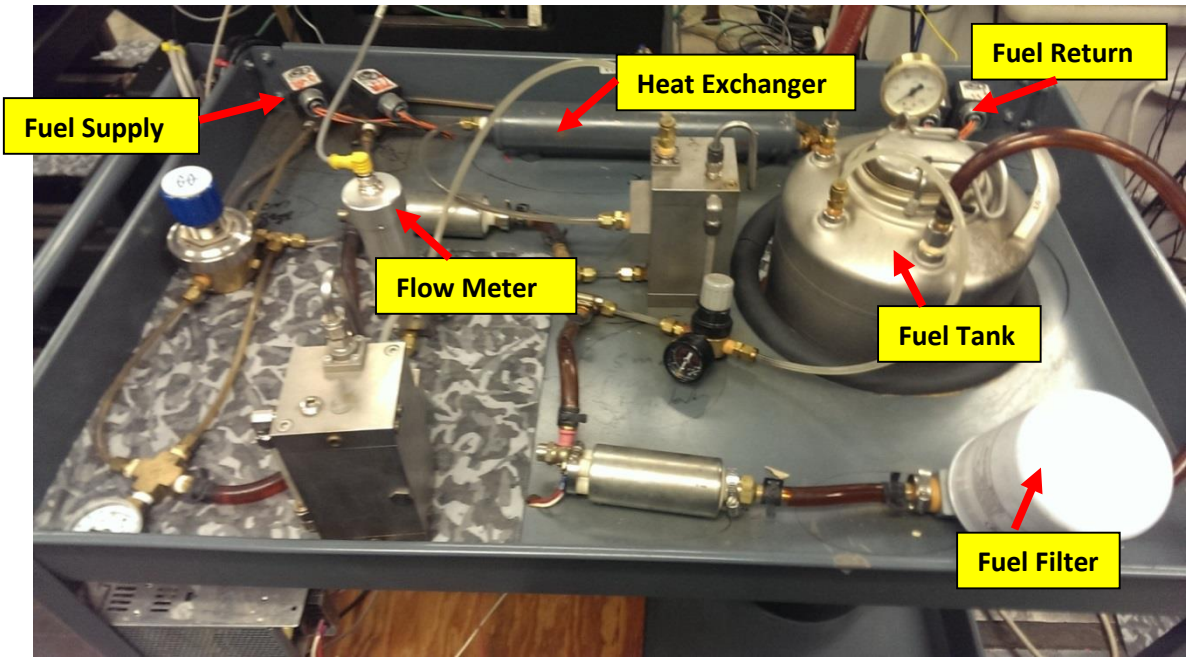

Figure 3-14 Fuel flow and measuring circuit (Pictorial view)

3.5.6 Current probe sensor

A current probe sensor is attached to the electrical connection of the piezo injector of Cylinder #1 in order to capture the start of the injection pulse, injection pulse width and number of injection events occurring per cycle. The current probe captures the current signal waveform passing to the injector. The sample piezo injector signal is explained in the figure 3-15.

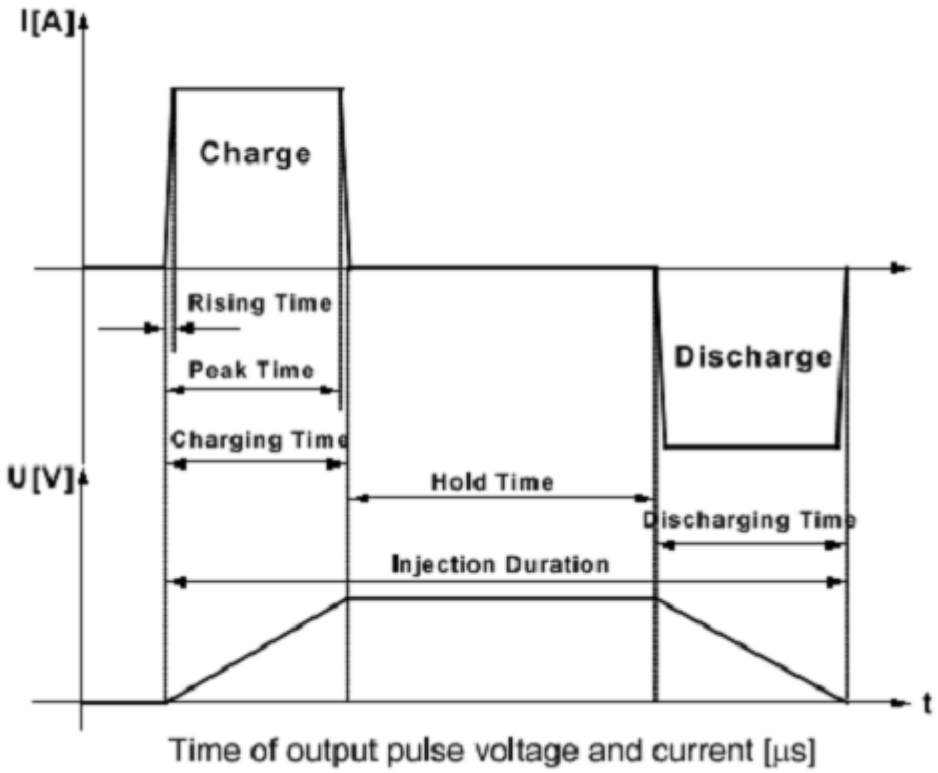

Figure 3-15 Current and voltage waveform which drives the piezo injector [22]

3.5.7 Lambda Sensor

The engine was instrumented with a lambda sensor in the exhaust manifold after turbocharger. The lambda (λ) in the exhaust stream can be obtained in a real time manner and is connected to the data acquisition system. Lambda sensors also referred to as oxygen probes which are used to the measure the oxygen contained in the exhaust emissions. The working principle of lambda sensor is based on the oxygen ion conductance of zirconium oxide at high temperature. It measures the difference between the amount of oxygen in the exhaust gas and amount of oxygen in air. The fuel–air equivalence ratio can be obtained by taking the reciprocal of the value provided by the lambda sensor.

3.5.8 Temperature measurements

The temperature at various engine locations has been monitored and recorded in order to make sure the steady state engine operation and supervise the ambient conditions. Slow response K-Type thermocouples are used to monitor the temperatures from the following locations.

1. Cooling water (in/out) temperature

2. Oil temperature in the sump

3. Compressed air temperature in the intake manifold

4. Exhaust manifold temperature

5. Room temperature

The thermocouples connections from various engine parts are plugged into the dyno control system which contains the built in time based data acquisition system.

3.6 Data acquisition system and engine combustion analyzer

A high speed data acquisition system was used to capture the engine data either time based or crank angle based depending on the type of the signal. The crank angle based high speed DAQ is used to record vital signals like in-cylinder combustion pressure, intake manifold pressure, fuel line pressure, ionization signal, and current probe injection signal and exhaust emissions such as NO and Opacity%. It is provided through Electro Mechanical Associates (EMA). As described in the previous sections, the time based data acquisition is used for recording various slow speed temperature measurements along with the dyno water pressure. The signal from the optical shaft encoder is used as an input to the high speed DAQ to record data on a crank angle basis. The

software of the DAQ allows the user to define the constants for the sensor such as the offset, slope and the coefficients in order to calibrate. The data acquired by the DAQ can be displayed in real time or as an average of many cycles. Smoothening is applied to signals wherever applicable, in order to reduce the noise during capturing the signals. The system includes engine combustion analyzer software which calculates many engine parameters and displays them. Those are IMEP, peak cylinder pressure and location, indicated torque, mean engine speed, mass burnt fraction and coefficient of variation of different parameters.

3.7 Emission measurements

Diesel engine exhaust emissions mainly consists of NO and Soot, which are harmful and have adverse effects on the health and environment. Following subsections explain the principle and the instruments used to measure NO (ppm) and Opacity (%).

3.7.1 NO measurement

A CLD (Chemiluminescence Detector) 500 Fast NOx analyzer from "Cambustion" was used to measure the concentration of NO (ppm) in the engine exhaust emissions. It works on the principle of chemiluminescence, where the reaction between NO and ozone results in the production of light. The produced light (photons) is detected by a photo multiplier tube (PMT). The voltage from the CLD 500 is proportional to the concentration of NO in ppm. The reaction of light production is very fast and hence it reduces the response time of the analyzer. The response time is approximately 2.5 milliseconds. A sampling probe was used in an opening provided on tail pipe to measure NO emissions.

3.7.2 Opacity measurement

A Model 107 in-line smoke meter provided by Telonic Berkeley was installed on the exhaust tail pipe of the engine. It works on the basic principle of attenuation of intensity of light by smoke aerosol absorption and scattering from exhaust gases. To achieve this, light was passed from an emitter through the exhaust stream from the engine and the collector end detects the loss in the amount of light received. The loss of light energy is then converted into opacity percentage and smoke density. The values are digitally displayed on the unit as well as obtained on the DAQ. Air supply at 1.5 bar and high pressure water cooling is provided for maintaining the optical sensors from high temperature exhaust gases. Figure 3-16 displays the opacity measurement principle and figure 3-17 shows the opacity meter used for this research.

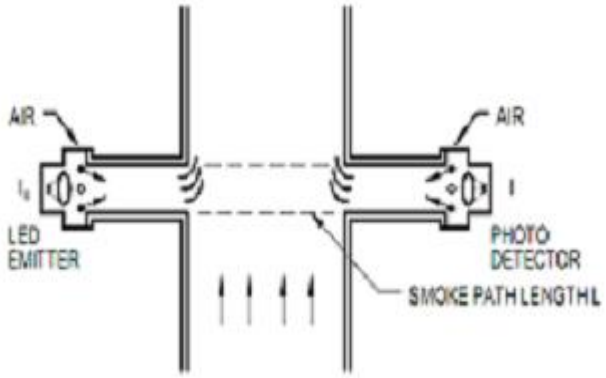

Figure 3-16 Opacity Measurement Principle

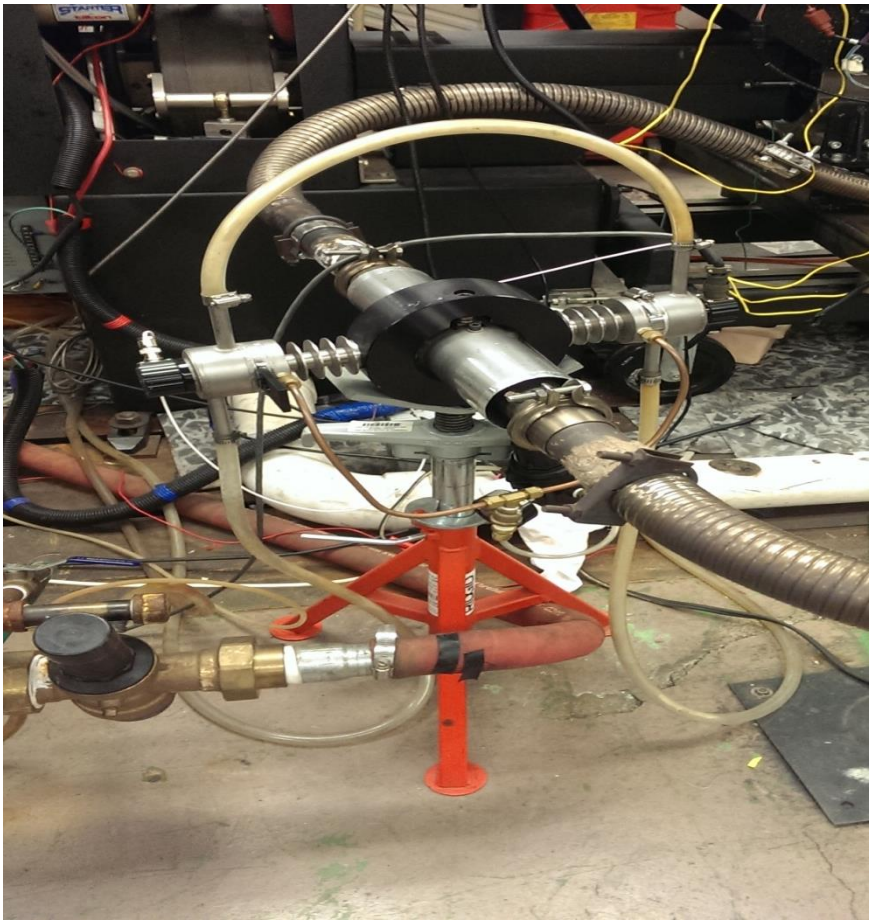

Figure 3-17 Opacity Meter

3.8 Ion current circuit

A glow plug was machined and modified to measure ionization signal which could perform both the functions of a glow plug as well as an ion current sensor. A modified ion current sensor along with the original glow plug is shown in figure 3-20. The heating plug was insulated from the engine body which serves as one electrode for ion current sensor, whereas the cylinder head or the engine ground acts as the other electrode. The heater plug was isolated from the cylinder head by applying high temperature ceramic coating. It uses a supply voltage 100 V DC where the heater surface acts as the anode whereas the cylinder head acts as the cathode. This circuit uses a 100 Ω resistor and a new signal conditioning module - 8B40 to amplify the signal which is displayed as

output in terms of CAD by means of DAQ. A detailed fabrication procedure for the manufacture of the glow plug ion current sensor is described in reference [39].

The ion current amplifier signal box and power supply set up box can be seen in figure 3-18. The ion current probe used for this research purpose is shown in figure 3-19. The amplifier/control box, being designed for a four cylinder engine, can support four ion current sensors. Applied voltage as well as polarity can be changed with the use of ion current box. Moreover, the MSFI sensor was also connected to the ion current box using the similar principle which is explained in section 3.9.

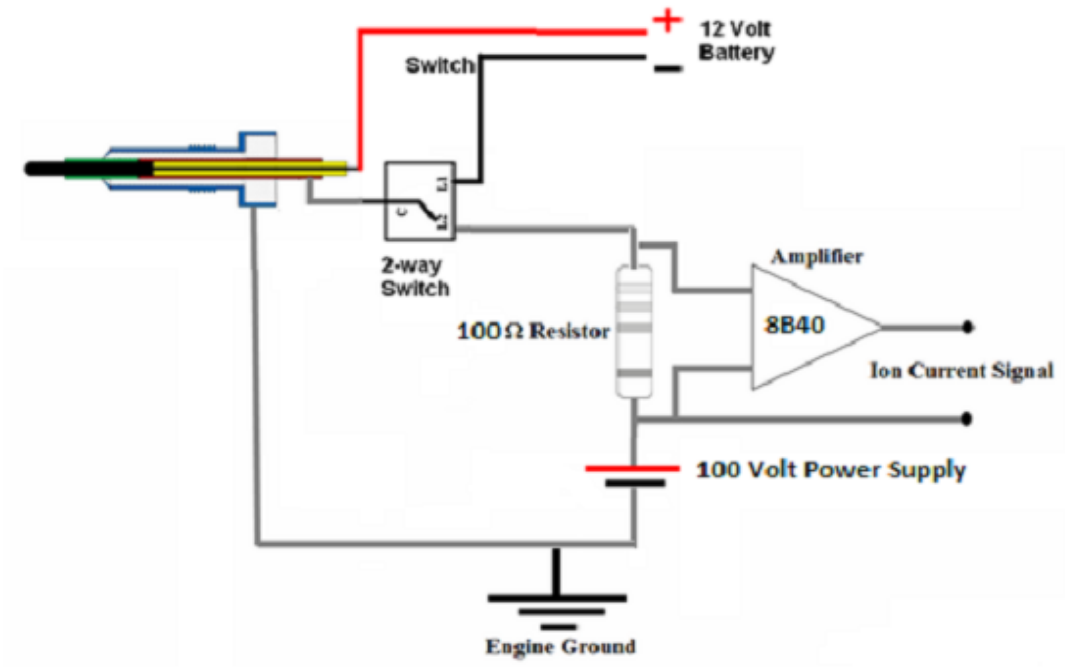

Figure 3-18 Ion current measuring circuit

Figure 3-19 Ion current signal amplifier and power supply box

Figure 3-20 Original glow plug and integrated glow plug/ion sensor

3.9 MSFI (Piezo Injector)

Figure 3-21 shows the schematic diagram of MSFI system. The system consists of electrically isolated electrodes, where the piezo injector acts as one electrode (+ve) and engine block acts as another electrode (-ve). As explained earlier, it is connected to the ionization detection circuit includes 100 V DC power supply using the same ion current box. It not only captures ion current signal at the center of the combustion chamber but also detects the injection events and injection pulse width.

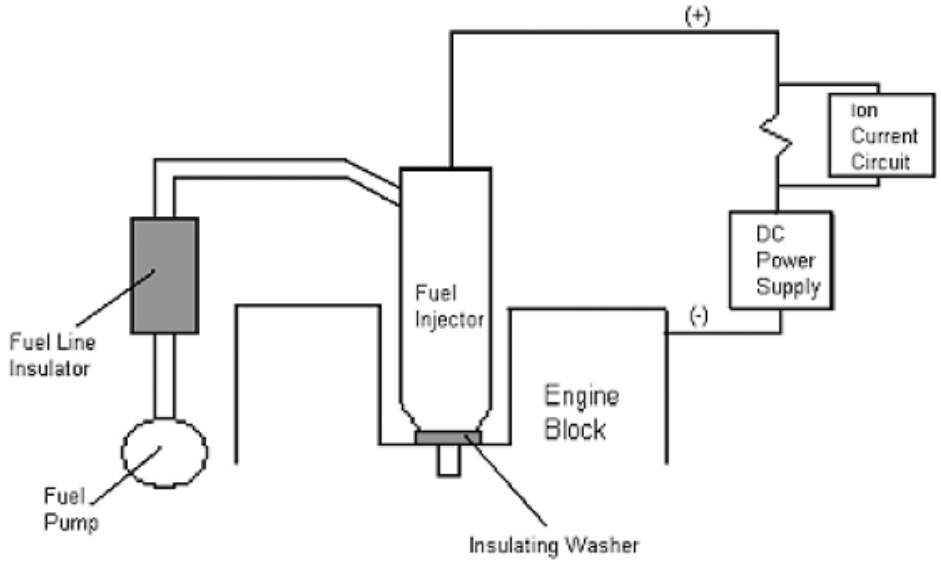

Figure 3-21 Schematic diagram of the Multi Sensing Fuel Injector (MSFI) system [29, 30]

CHAPTER 4

TEST PROCEDURE AND SAMPLE RESULTS

4.1 Introduction

This chapter explains the detailed test procedure used in this investigation along with the fuel specifications. It also presents the sample results at lower idling speed of 830 rpm and explains the traces obtained using a high speed data acquisition system. At the end, it describes the important definitions used in this research to analyze the test results.

The main purpose of this research is to understand the combustion instability by conducting a cycle to cycle analysis of auto-ignition, combustion and ionization characteristics during cold starting operation at an ambient temperature T_{amb} = 25˚C using two different fuels i.e. ULSD and JP8. The second objective of this investigation is to compare the ionization characteristics obtained from two different locations in the combustion chamber by using two ionization sensors at steady state low idling speeds. All the tests were conducted on a 4-cylinder, 4-stroke, Volkswagen 2.0L TDI engine using ULSD and JP8 with an OEM/industrial ECU.

These tests are mainly divided into two parts ⟶

1. Cold Starting at Ambient Temperature (T_{amb} = 25˚C)
2. Low Speed Idling at the speed of 830, 1000 and 1100 rpm

4.2 Fuel Specs

Table 4-1 Fuel Properties for ULSD and JP8 [5]

Fuel	ASTM	ULSD	JP8
Cetane Number	D613	42.3	49
Derived Cetane Number	D6890	42.1	49.3
Flash Point (˚C)	D93	69	49.5
Density kg/m^3 (@ 15˚C)	ASTM 85H	842	802
Viscosity (cSt,40°C)	D445	2.438	1.367
Heating Value (MJ/kg)	D3338	41.2	43.2
Aromatic Content	D2425	27.8	16.3

Table 4-1 shows some of the important fuel specifications for ULSD and JP8. Cetane number of the fuel indicates the auto-ignition quality of the fuel which plays a major role in determining the ignition delay under standard conditions. The derived cetane number of the fuels used in this investigation is 42.1 and 49.3 for ULSD and JP8 respectively. As compared to ULSD fuel, jet fuel is less dense and contains less aromatic content, but has a high heating value of 43.2 MJ/kg. The low flash point of JP8 explains its high volatility than ULSD, which can also be seen from the distillation curve shown in figure 4-1.

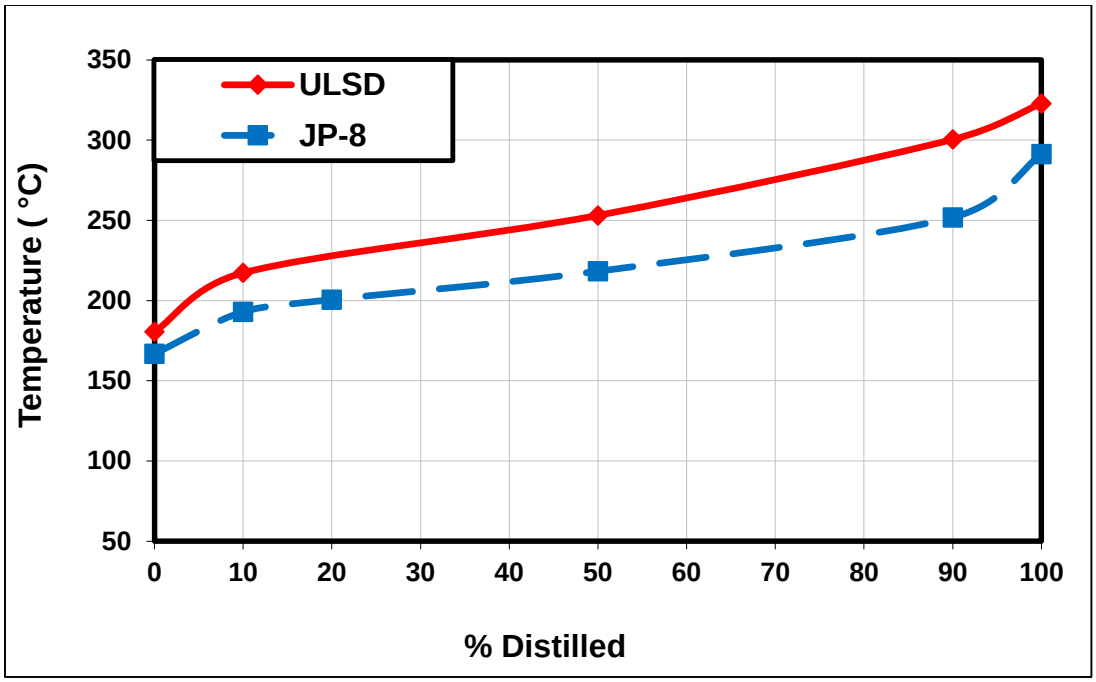

Figure 4-1 Distillation curve for ULSD and JP8 [5]

The distillation curves for the two fuels used in this research are given in figure 4-1 and show that JP8 is more volatile than ULSD. It is obtained by plotting boiling temperature of the fuel against percentage of the volume distilled. Volatility of the fuel affects fuel spray characteristics like liquid penetration lengths and fuel evaporation. At 50% recovery point, the difference between ULSD and JP8 is about 40˚C, which increases to 50˚C at 90% recovery point. At 100% recovery point, which is the final boiling point, temperature for ULSD and JP8 is 325˚C and 300˚C respectively.

4.3 Cold Starting at T_{amb} = 25˚C

For this research, first 200 consecutive cycles were recorded and a detailed cycle by cycle analysis was performed. A MATLAB code was used to separate out large data sets into individual cycles (2880 points per cycle). Coefficient of variation was calculated for all the key parameters in order to find the cycle to cycle variation and study its effect on combustion instability.

The cold starting investigation is further divided into two sections. The first section explains the variation of ion current characteristics by using two ionization sensors during cold starting at an ambient temperature of 25˚C. While the second part sheds a light on the cycle-to-cycle variation of various auto-ignition and combustion parameters and determine its effect on combustion instability during cold starting operation at the same temperature. All the tests were conducted at T_{amb} = 25˚C (77˚F); first using ULSD (DCN = 42.1) and then Jet Propulsion fuel, JP8 (DCN = 49.3) with an industrial/OEM ECU.

To carry out this investigation, an in-cylinder pressure transducer was placed in cylinder #1 and another pressure transducer was placed on the high pressure fuel injection line #1. A modified glow plug ion current sensor was placed in cylinder #4 to measure ion current characteristics whereas Multi-Sensing Fuel Injector was placed in cylinder #1. Moreover, a current probe was placed on injector #1 to obtain SOI, EOI, number of injection events and injection pulse width. An optical camshaft encoder with the resolution of 0.25 pulses/CAD was used to record the data with respect to crank angle degrees. A high speed 15-channel data acquisition system was used to obtain and process the data.

4.4 Idling Operation

The main focus of this section is to compare the ionization characteristics using two ion current sensors at different locations in the combustion chamber. For this purpose a modified glow plug ion current sensor and a newly instrumented MSFI sensor have been used. These tests were conducted at low idling speeds, i.e. 830, 1000 and 1100 rpm using ULSD and JP8. To conduct this investigation, the centrally instrumented Multi Sensing Fuel Injector (MSFI) was placed in cylinder #1 along with the in-cylinder pressure transducer and a modified flow plug ion current sensor was placed in cylinder #4, with all the other instrumentation kept unchanged. To reduce the effect of cycle-to-cycle variations, the average of 100 cycles was taken for analysis. An industrial/OEM ECU was used for all the tests in this section.

4.5 Sample Results

Figure 4-2 shows sample traces for engine operation at lower idling speed i.e. 830 rpm with ultra-low sulfur diesel. It displays the data for in-cylinder combustion pressure, rate of heat release, injection signal using current probe and ion current signals using modified glow plug and MSFI at an applied voltage of 100 V DC. Test was repeated twice in order to confirm the repeatability of the data at idling condition.

The injection signal shows the split injection strategy depicting two injection events. SOI #1 occurred at 4˚ bTDC which lasts for 3.5 CAD, while SOI #2 occurred at 2.5˚ aTDC and had duration of 4 CAD. The in-cylinder pressure trace shows one combustion event for cylinder #1 with a peak pressure of 42.87 bar at 11˚ aTDC. The rate of heat release has a peak value of 38.5 J/CAD. The Combustion phasing or LPPC occurs at 9.25 CAD. It also shows the ion current signal captured using two different sensors. The peak amplitude of ion current is 27.7 μA for modified

glow plug, whereas MSFI gives a lower peak of 2.7 μA, which is almost 10 times lower than the glow plug. MSFI picks up ion current at 7.75 CAD, while glow plug sensor has the SIC at 3.75 CAD.

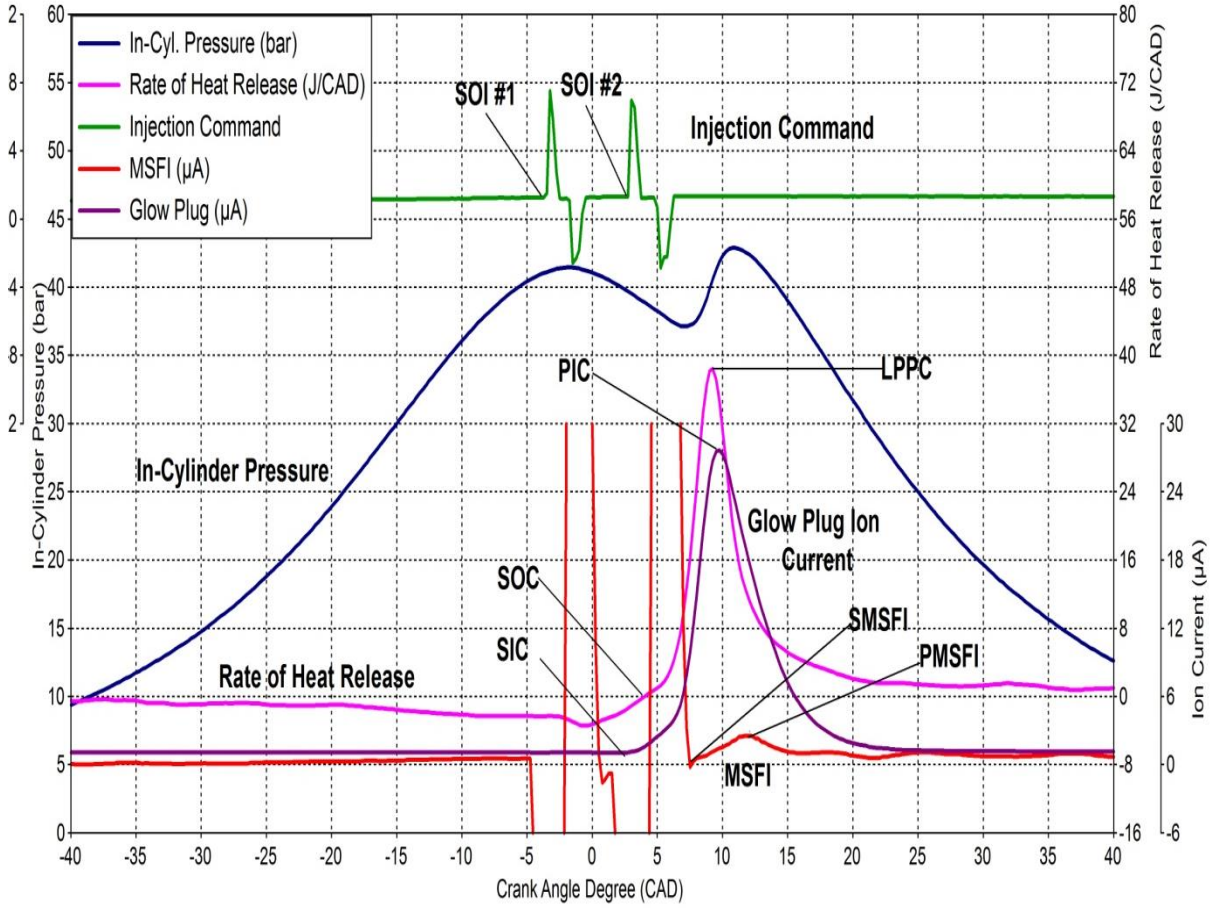

Figure 4-2 Sample traces showing cylinder pressure, rate of heat release, current probe, and ion current from glow and Multi-Sensing Fuel Injector for ULSD at 830 rpm

4.6 Definitions

In this investigation some key definitions were used to perform the analysis which can be seen in figure 4-2. They are listed as follows:-

- SOC: It is the point on the RHR trace where high temperature combustion starts.

- LPPC: The location of peak of premixed combustion is the location of the highest point on RHR trace produced early in the combustion process. The location of this point relative to TDC is used to identify combustion phasing in this investigation.
- SIC: Start of ion current measured by using modified glow plug in cylinder #4.
- SMSFI: Start of ion current measured by using MSFI in cylinder #1.
- SOI: Start of Injection measured by using current probe placed on Injector #1.
- ID: Ignition delay is defined as the period between SOI and SOC measured in crank angle degrees.

CHAPTER 5

COLD STARTING: IONIZATION ANALYSIS

5.1 Introduction

This chapter contains a comparison between the combustion and ionization characteristics of ULSD (DCN = 42.1) and Jet JP8 (DCN = 49.3) during the cold starting of the engine at an ambient temperature of 25˚C (77˚F). The main focus of this chapter is on the cycle-to-cycle variation. To reproduce the same engine conditions in different cold starting tests, the oil sump temperature and coolant temperatures were kept equal to the room temperature i.e. 25˚C. The first 200 consecutive cycles were recorded using a high speed 15-channel data acquisition system. Since the resolution of the camshaft encoder was 0.25 pulses/CAD, a total of 576,000 data points were obtained for the following signals: in-cylinder gas pressure, injection command, injection pressure, glow plug ion current and MSFI. A MATLAB code was thus used to obtain to each cycle (1 cycle = 2,880 data points). This is followed by an analysis of the changes of the different parameters from the first cycle to cycle number 200. Cylinder to cylinder variation was not considered in this investigation, since the engine is comparatively new and a previous investigation showed that the small variations between the cylinders are within the reading error.

The traces for the cylinder gas pressure and glow plug ion current were smoothed using a five point moving average filter.

5.2 Engine Speed and IMEP

This section describes the overall engine operation taking place during cold starting with engine speed variation for first 200 cycles with ULSD and JP8. It also shows cycle to cycle variation of IMEP for first 200 consecutive cycles which shows the behavior of combustion process taking place inside the cylinder #1.

Figure 5-1 is for engine speed in the first 200 consecutive cycles and figure 5-4 is for the first 50 cycles. Figure 5-2 is for the IMEP in the first 200 consecutive cycles and figure 5-5 is for first 50 cycles.

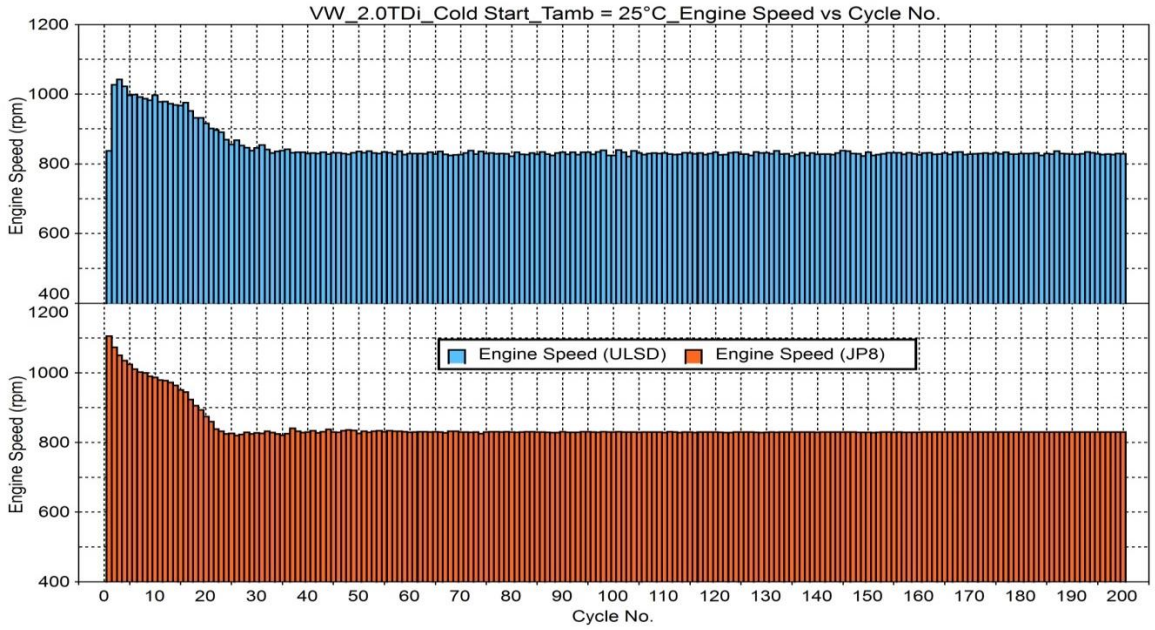

Figure 5-1 Engine Speed for first 200 cycles using ULSD (top) and JP8 (bottom)

It can be seen from figure 5-1 that, 1st cycle has an engine speed of 837 rpm for ULSD and a higher speed of 1106 rpm for JP8. Unlike JP8, the engine speed increases for ULSD from a low idling speed and then starts decreasing. Theses Similar trends were seen in the engine speed variation when the cold starting tests were repeated twice at same ambient conditions.

While operating on ULSD, as the engine operates further, it ramps up to a speed of 1042 rpm for cycle #3 and starts decreasing randomly reaching lower idling speed at cycle #33. On the other hand, when the engine operates on JP8 fuel the engine speed decreases smoothly reaching 832 rpm at cycle #23. It can be further observed that, after operating through cycle #50 for JP8, engine speed remains almost constant at its lower idling speed (830 rpm). On the contrary, it suffers some instabilities with less variations after it passes cycle #50 for ULSD. This instability in the engine speeds can be explained as the effect of cetane number of a fuel on obtaining a steady state, which improves with higher CN and minimizes the no. of cycles it takes to stabilize [10].

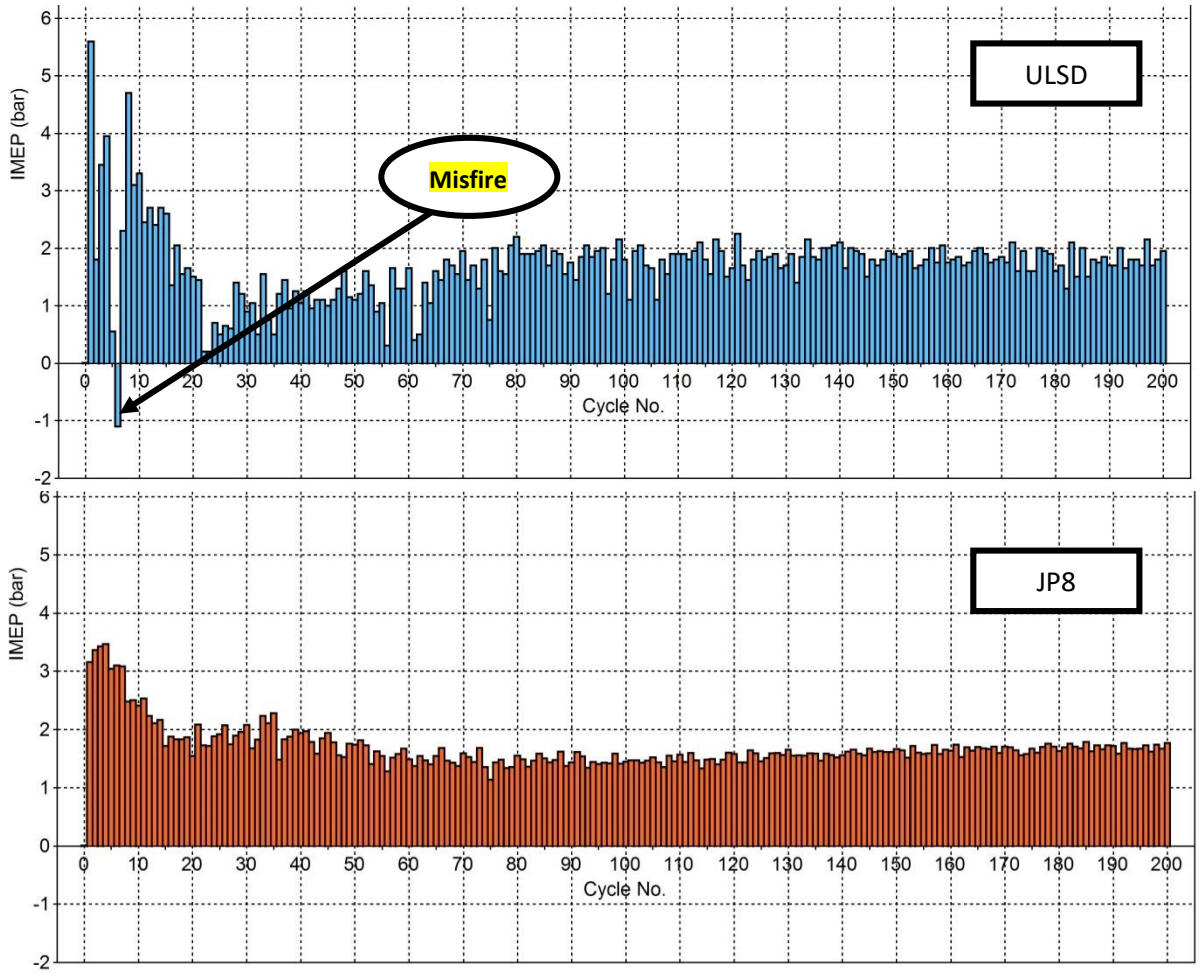

Figure 5-2 IMEP variation during cold starting for first 200 consecutive cycles using ULSD and JP8

Figure 5-2 shows the cycle to cycle variation of IMEP as the engine operates through first 200 cycles with ULSD and JP8. While operating on ULSD, maximum IMEP was observed at very first cycle which is equal to 5.6 bar followed by a complete misfire at cycle #6 (-1.1 bar). The IMEP randomly rises and falls, indicating higher amount of variation leading to combustion instability. It can be also seen from figure 5-3, some cycles having IMEP less than 1 bar indicating late combustion in the expansion stroke. The minimum IMEP occurs at cycle 22 and cycle 23, which is equal to 0.2 bar. Although IMEP for JP8 increases and decreases in a random pattern, it undergoes less fluctuations with most of the cycles being higher than 1.5 bar. The minimum IMEP is 1.48 bar at cycle 36, which is almost higher than the minimum value for ULSD by 1.28 bar.

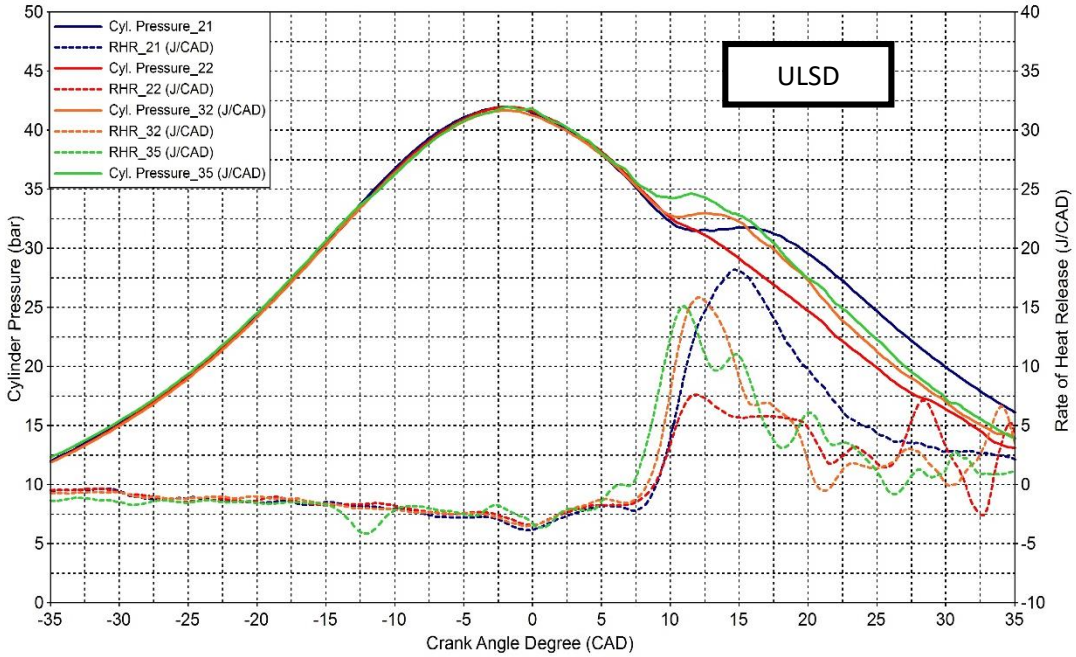

Figure 5-3 Cylinder Pressure and RHR traces for Cycles showing late or no combustion event for ULSD

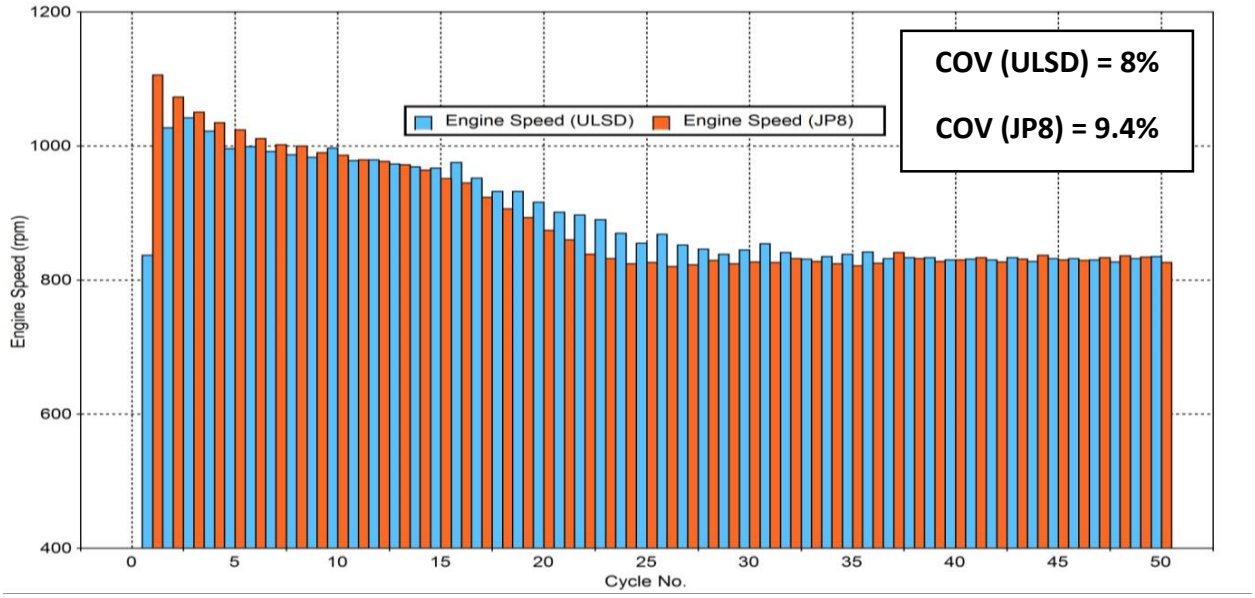

Figure 5-4 Engine Speed for first 50 cycles using ULSD (top) and JP8 (bottom)

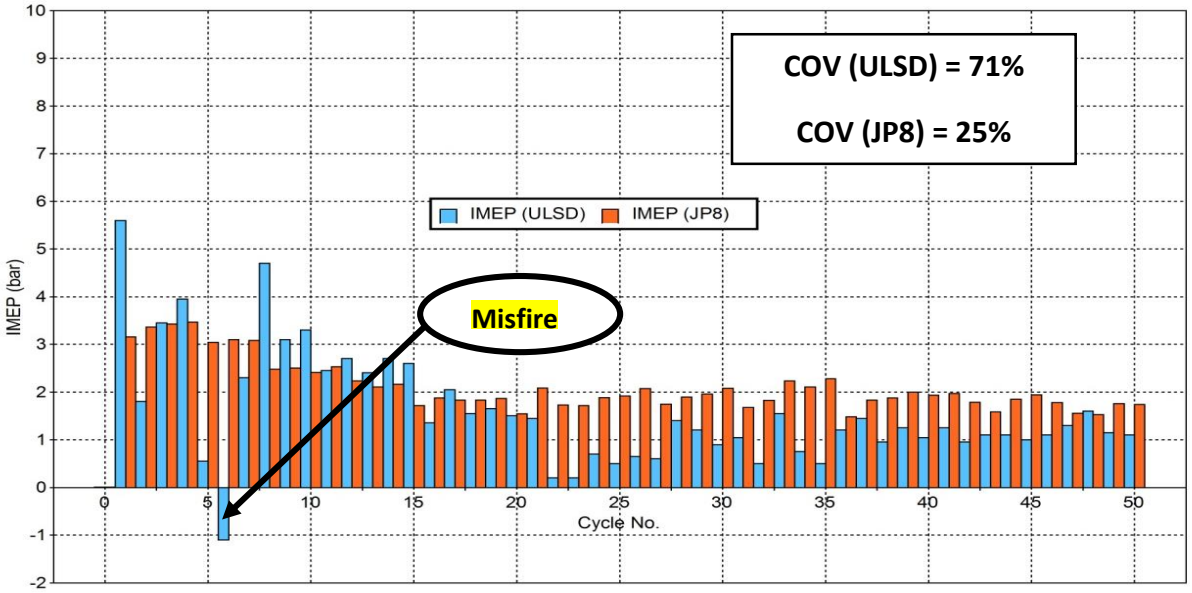

Figure 5-5 IMEP variations during cold starting for first 50 consecutive cycles using ULSD and JP8

Figure 5-4 and figure 5-5 show the cycle-to-cycle variation of first 50 cycles showing engine speed and IMEP respectively and compare the combustion instability of the engine. They also show the coefficient of variation (COV) calculated for first 50 cycles for engine speed and IMEP. It can be seen that, the COV for the engine speed is as low as 8% for ULSD and 9.4% for

JP8. On the other hand, the COV for IMEP is 71% for ULSD, which is almost 3 times higher than JP8. This shows that, engine suffers more cycle to cycle variation with ULSD in terms of IMEP which is a function of in-cylinder pressure. It further plays an important role in analyzing the combustion instability during cold starting operation. Thus, in order to determine the combustion instability during cold starting operation, all the in-cylinder parameters like combustion pressure, RHR, ion current etc. were analyzed further in chapter 5 and chapter 6.

5.3 Misfiring and Misdetection of Ion Current

The main purpose of this subsection is to explain the development of combustion process taking place during misfiring in the case of ULSD. It also shows the comparison between ion current signals captured by modified glow plug and MSFI. In order to achieve this goal, first 9 combustion cycles are displayed operating with ULSD where a high amount of cycle to cycle variation was observed. It explains the combustion events taking place inside cylinder #1 when it undergoes complete misfiring after having normal combustion event and again regains its stability. It also further explains the impact of injection strategy and rail pressure on detection of ion current by glow plug for first 50 cycles where most of the combustion was observed.

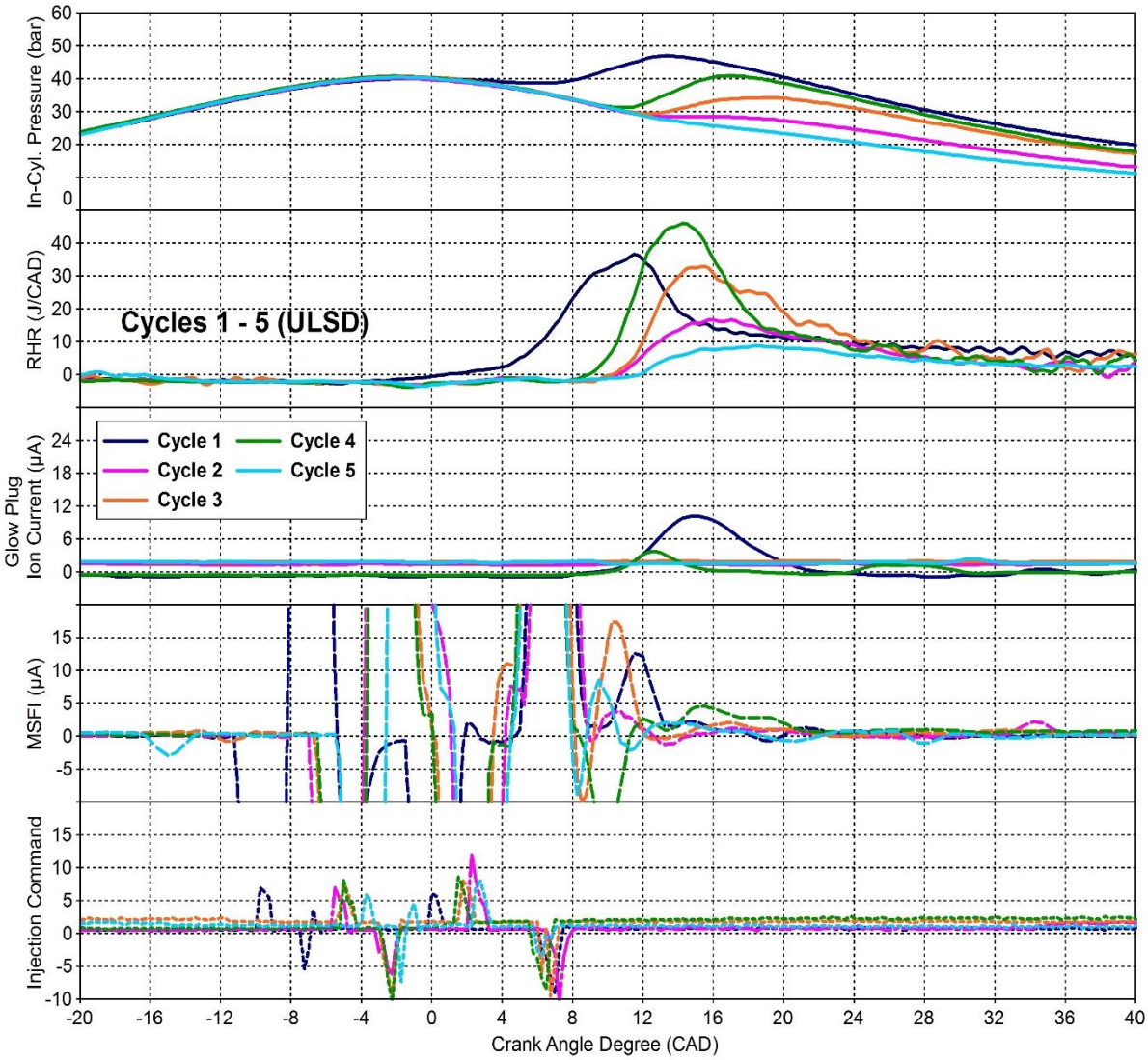

Figure RHR, Ion current with glow plug and MSFI and Injection Command for first 5 consecutive cycles with ULSD 5-6 Cylinder Pressure

Figure 5-6 shows in-cylinder pressure, RHR, ion current signal with glow plug and MSFI and injection command for first 5 consecutive cycles with ULSD. It can be seen that cycle #1 starts with the most advanced SOI #1 at 10˚ bTDC which also has an earliest SOC at 4˚ aTDC. This cycle also ends up with the highest IMEP of 5.62 bar. The following cycle #2 has retarded SOI #1 at 6˚ bTDC which undergoes late combustion event while the peak firing pressure decreases by almost 20 bar. Also, the amplitude of PPC for cycle #2 shows a huge fall of 10 J/CAD with a 5 deg. retarded combustion phasing than cycle #1. In this course, the pulse separation between two

injections reduces from 6.5 CAD to 4 CAD with an increase in rail pressure (Table 5-1). Hence, this large shift in the combustion phasing and SOC can be explained by a shift in start of injections and the difference in the pulse separation between EOI #1 and SOI #2. Cycle #3 and #4 undergo normal combustion events while trying to regain the stability by increasing firing pressure and the rate of exothermic reactions. After regaining the combustion stability, the combustion degrades further for cycle #5 where no combustion is detected by pressure transducer, showing very less amount of heat release. The cylinder further undergoes complete misfiring at cycle #6, which can be evident from figure 5.2, where no distinct combustion event was detected by RHR trace. This nature of combustion from cycle #4 to #6 can be explained with the values indicated in Table 5-1. It is important to ensure that an appropriate combination of SOIs and Rail Pressure along with the pulse separation is used in order to have strong pilot flame close to the glow plug tip [15]. This will help in initiating the combustion process and achieve normal combustion. During this operation, glow plug shows a single peak of ion current for cycle #1 and #5, while it's undetected or misdetected for other cycles. On the other hand, MSFI shows peaks of high amplitude following the end of 2nd injection event. As compared with glow plug, the ionization signal from MSFI shows a high amount of noise signal which can be also seen in further analysis.

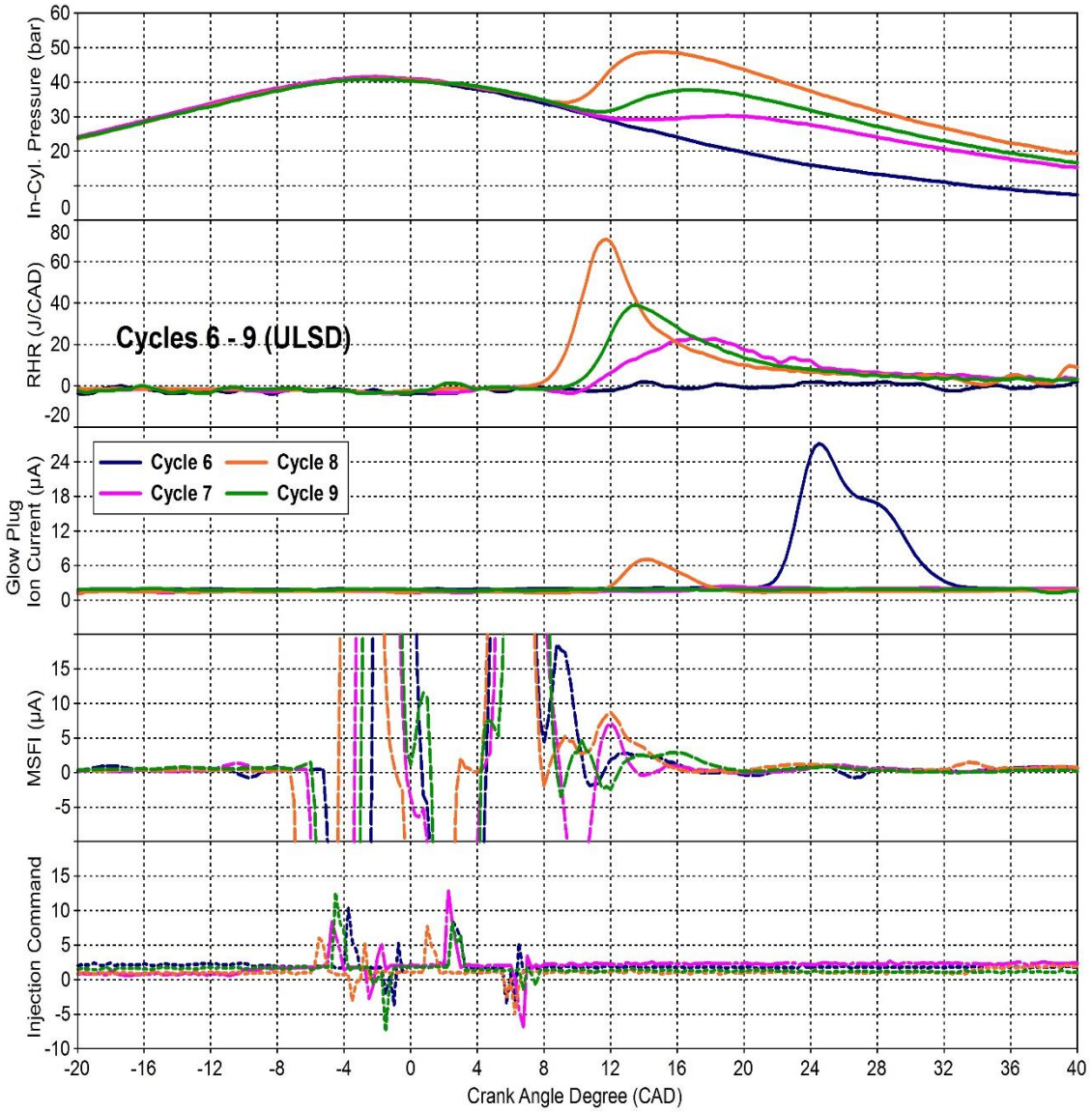

Figure 5-7 Cylinder Pressure, RHR, Ion current with glow plug and MSFI and Injection Command for cycles 6-9 with ULSD

Figure 5-7 shows in-cylinder pressure, RHR, ion current signal with glow plug and MSFI and injection command for cycles 6 to 9 with ULSD. Cycle #6 undergoes a complete misfiring event which can be evident from both cylinder pressure and RHR traces. On the other hand, glow plug shows late bump of ion current indicating a late combustion cycle with higher IMEP in cylinder #4. In-spite of having complete misfiring, MSFI shows a sharp peak after the end of 2nd

injection event. As the combustion proceeds further, cycle #7 shows late/incomplete combustion event having a low firing pressure of 30 bar. In the process of regaining the stability, cycle #8 undergoes a normal combustion cycle with an advanced SOC of 8˚ aTDC with a high amount of heat release. As compared with the misfiring cycle, SOIs for both the injection events advances by 1.5 to 2 CAD with a reduction of rail pressure by 25 bar. Cycle #8 is quiet similar to cycle #1 apart from injection timings. At the end, cycle #9 achieves normal combustion event similar to cycle #4. It can be noticed that, combustion stabilizes as SOI #1 advances while increasing the pulse separation.

It can be seen from figure 5-6 and figure 5-7 that MSFI signal has more discrepancy which can be misleading at times and needs further conditioning to eliminate the noise. Hence, in the further analysis for cold starting, ionization signal from glow plug is analyzed and its characteristics have been studied for 200 cycles. In this course of high instability, both injection events have been distinctly detected by the current probe.

Table 5-1 shows the detailed combustion and injection parameters for first 9 consecutive cycles with ULSD. It also indicates the nature of the combustion for each of the 9 cycles. The only completely misfired cycle has been indicated by red box which has the most retarded SOI #1 with lowest pulse separation of 2.5 CAD and a high rail pressure of 350 bar. Misfiring can be caused due to the failure of transporting the fuel spray close to the glow plug as a result of high rail pressure [15]. This in turn decreases the temperature near the vicinity of glow plug as well as increases the leanness of fuel-air mixture provoking the initiation of pilot flame. Thus, a proposed combination of SOI#1 with rail pressure and pulse separation is indicated by green box, where a normal combustion is achieved. This also shows that irrespective of fuel quantity or IMEP an appropriate combination of SOIs and rail pressure can avoid misfiring.

Table 5-1 Detailed combustion and injection characteristics for first 9 cycles with ULSD

Cycle No.	Nature of Combustion	IMEP (bar)	SOI 1/ DOI 1 (bTDC/ CAD)	SOI 2/ DOI 2 (aTDC/ CAD)	Pulse Separation (CAD)	Rail Pressure (bar)
1	Highest IMEP/Early SOC	5.62	10/3.5	0/7	6.5	250
2	Late/Incomplete Combustion	1.83	6/4	2/6	4	290
3	Regaining Stability	3.45	5.5/4	1.5/6	3.5	325
4	Normal Combustion	3.95	5.5/4	1/5.5	3	325
5	No Combustion	0.56	4/3.5	2.5/4.5	3.5	330
6	**Complete Misfire**	**-1.1**	**4/3.5**	**2.5/4**	**2.5**	**350**
7	Late/Incomplete Combustion	2.3	5/3.5	2/5	3.5	350
8	Regain Stability with High IMEP	4.75	6/3.5	1/6	3.5	325
9	Normal Combustion	3.12	5/4	2.5/6	3.5	325

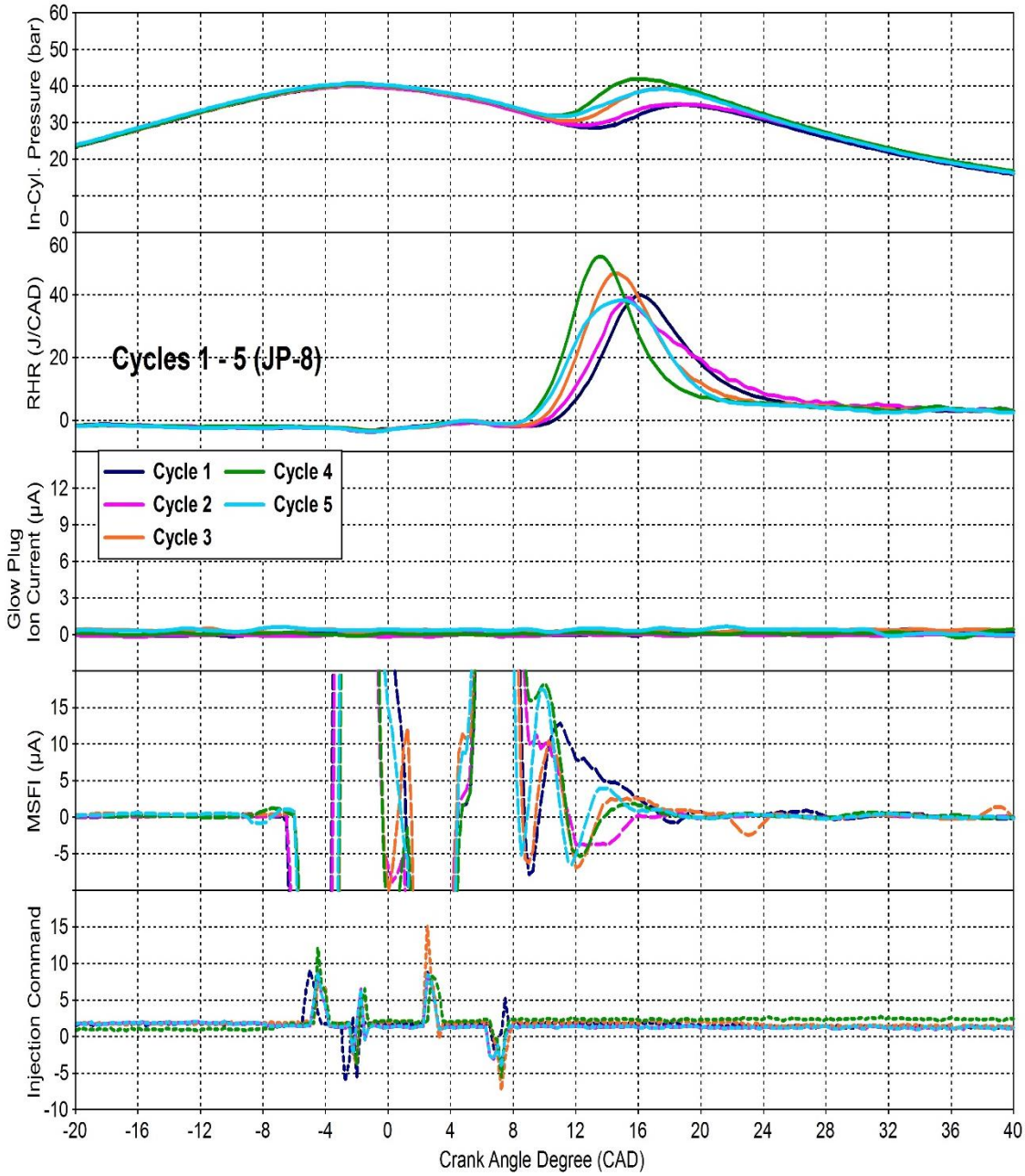

Figure 5-8 Cylinder Pressure, RHR, Ion current with glow plug and MSFI and Injection Command for first 5 consecutive cycles with ULSD

Figure 5-8 shows in-cylinder pressure, RHR, ion current signal with glow plug and MSFI and injection command for first 5 consecutive cycles with JP8. It shows much better combustion stability than ULSD as compared to figure 5-6, which is evident from in-cylinder pressure and RHR trace. In contrast to ULSD operation, Cycle #1 for JP8 undergoes late combustion event with

the peak firing pressure of 35 bar. Its SOC is located at 11˚ aTDC, 7 CAD retarded than that of ULSD. The LPPC for this cycle is located at 16˚ aTDC which is around 4.5 CAD later than ULSD. As the combustion develops further, SOC advances by 3 CAD with the peak pressure rises to 41 bar. The combustion phasing also advances by the same amount while the amplitude of peak of premixed combustion reaches 50 J/CAD. It can be seen that, unlike ULSD operation both the injection events remain almost constant, where SOI #1 = 5.5˚ bTDC and SOI #2 = 2.5˚ aTDC. It is also evident that, none of these cycles detect ion current signal from glow plug in-spite of having a healthy and stable combustion.

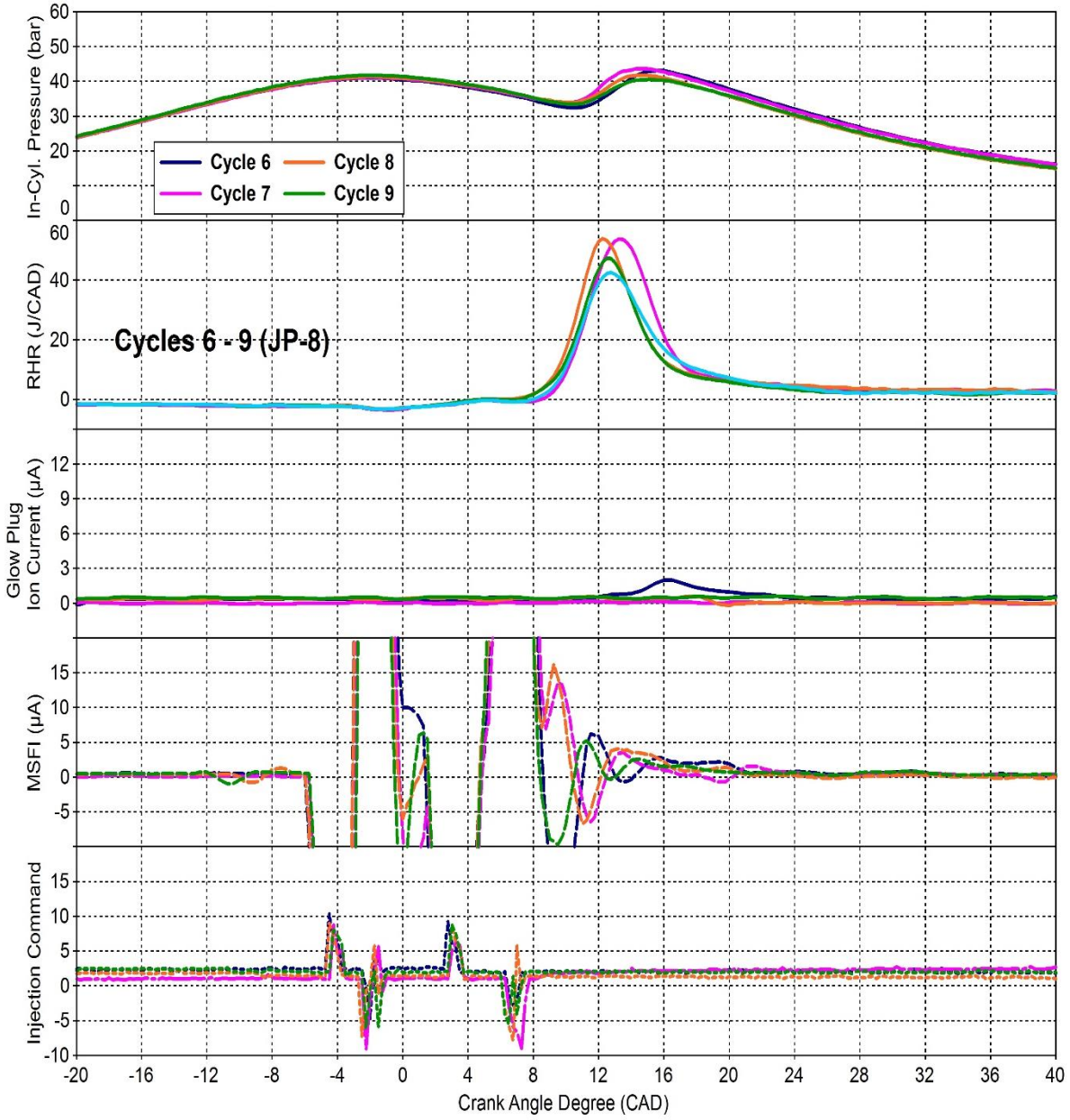

Figure 5-9 Cylinder Pressure, RHR, Ion current with glow plug and MSFI and Injection Command for cycles 6-9 with JP8

Similar behavior can be seen for cycle #6 to cycle #9, which is displayed in figure 5-9. In this case, the peak firing pressure as well as the combustion phasing along with the injection events remain constant. These cycles show more stability than the cycles shown in figure 5-7 for ULSD. An unaltered start of injection for both the injection events with a constant injection duration with

a 10-15 bar fall in rail pressure give a good stability to the combustion for JP8 during the initial phase of cold starting cycles. On the other hand, none of the cycles detect a distinct point of ion current from glow plug which can be further explained in figure 5-9. Here, similar nature of signals are detected by MSFI as can be seen from figure 5-6 through figure 5-8. It consists of a sharp rise after the end of second injection showing a higher amount of noise and vibration than glow plug. This shows that, glow plug can be used to detect a noiseless ionization signal for transient engine operation. Therefore, for further ionization analysis in this chapter glow plug signal is used and a detailed cycle to cycle analysis for first 200 cycles is performed.

Table 5-2 Detailed combustion and injection characteristics for first 9 cycles with JP8

Cycle No.	Nature of Combustion	IMEP (bar)	SOI 1/ DOI 1 (bTDC/ CAD)	SOI 2/ DOI 2 (aTDC/ CAD)	Pulse Separation (CAD)	Rail Pressure (bar)
1	Late Combustion	3.15	5.5/4	2.5/5.5	4	320
2	Late Combustion	3.36	5.5/4	5/5.5	3.5	320
3	Normal Combustion	3.43	5/3.5	2.5/5.5	3.5	320
4	Normal Combustion	3.46	5/4	2.5/5.5	4	325
5	Normal Combustion	3.05	5/3.5	2/5.5	3.5	310
6	Normal Combustion	3.1	5/3.5	2.5/5	4	310
7	Normal Combustion	3.1	4.5/3.5	3/5	4.5	310
8	Normal Combustion	2.5	5/4	3/5	4.5	300
9	Normal Combustion	2.5	5/4	3/5.5	4	305

Table 5-2 shows the injection and combustion characteristics for JP8 for first 9 consecutive cycles. Unlike the engine operation with ULSD, most of the injection parameters remain unchanged or show very less deviation for JP8. A major change is spotted in case of rail pressure which only decreases by 15 bars through cycle #9, whereas it rises by almost 100 bars for ULSD (Table 1). This plays an important role in maintain stability of the engine and detecting ion current irrespective of fuel used, which is further explained with the help of figure 5-10.

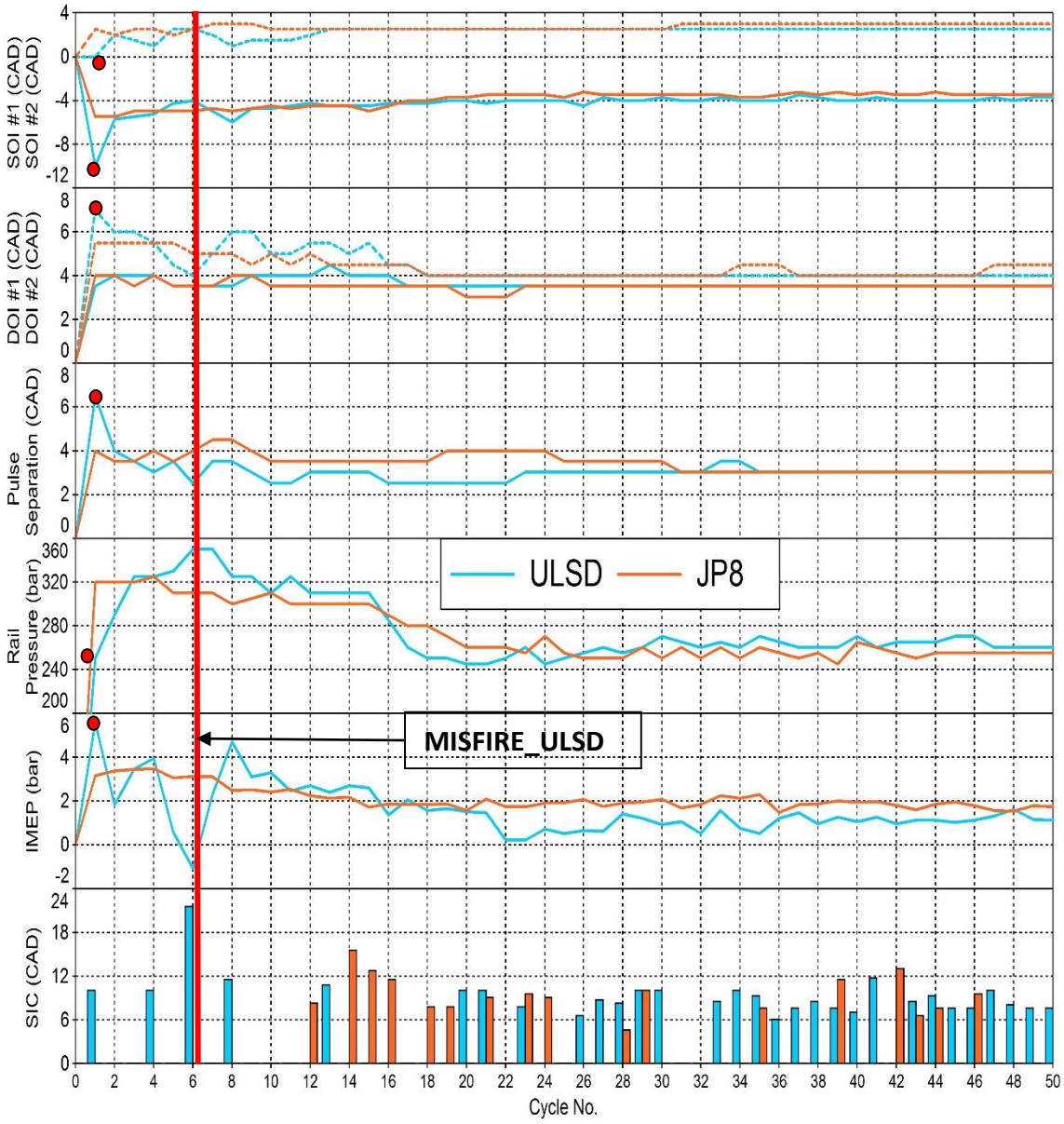

Figure 5-10 Cycle to cycle variation for Start of injection, Duration of Injection, Pulse separation, IMEP, Rail Pressure and SIC of first 50 consecutive cycles with ULSD and JP8

It is important to further analyze the cycles in details to find the reason for misdetection of ion current for the initial cycles shown in figure 5-6 through figure 5-9. In order to achieve this goal, figure 5-10 displays the injection strategy along with the IMEP, rail pressure and SIC for the first 50 consecutive cycles with ULSD and JP8. In this figure solid lines indicate the SOI and DOI for first injection event while dotted lines are used for second injection. A completely misfired cycle for ULSD is indicated by a red solid line (cycle #6). As stated earlier, detection of ion current depends mainly on the temperature and equivalence ratio near the vicinity of the glow plug. It also depends upon the area of exposure of the glow plug tip in the combustion chamber, applied voltage and its location in the combustion chamber [4]. Apart from these factors, the appropriate combination of injection timings, duration and rail pressure play a key role in determining the mixture strength near glow plug tip. Thus, even if the combustion is detected by pressure and RHR trace, it can be misdetected by glow plug. It can be noticed that the SOI #2 and DOI #1 remain almost unchanged for the first 50 cycles at 2.5˚ aTDC and 3.5 CAD respectively. A sharp retardation in SOI #1 can be seen for ULSD while operating for first 4 to 5 cycles. After that, it remains constant at around 3.75˚ bTDC. Here, a major deviation in the DOI #2 and injection pulse separation is seen for first 14 to 16 cycles for both the fuels. In case of ULSD, very first cycle (denoted by red dot) has a very advanced injection than rest of the cycles at 10˚ bTDC with a highest pulse separation of 6.5 CAD. This particular cycle also does have the longest duration for 2^{nd} injection with a very low rail pressure of 250 bar. This cycle detects a distinct point for start of ion current with the highest IMEP. It shows that, low rail pressure along with highest pulse separation gives a sufficient time for pilot spray to reach near glow plug tip. This further helps in enhancing the mixture strength and increases the temperature which creates a strong pilot flame. In addition to this, a longer duration for 2^{nd} injection further helps increasing the gas temperature

and thus detects ionization signal. As the engine operates further, DOI #2 as well as pulse separation decreases while rail pressure has a significant rise. At the same time, glow plug fails to detect ionization signal for first consecutive 11 cycles for JP8, while only 4 cycles detect ion current for ULSD. Here, DOI #2 decreases by 4 CAD for ULSD while it remains unaltered for JP8. Thus, DOI # along with the rail pressure play a deciding factor to maintain a better fuel transport irrespective of IMEP. From cycle #15, rail pressure starts to decrease and settles down around 260 bar while the pulse separation and DOI#2 also falls down and stays constant. It is evident from figure 5-10 that detection of ion current improves as the rail pressure decreases.

It can be further seen that in-spite of having an almost constant rail pressure, there are very less occurrences of detection of ion current for JP8. This can be further explained with the difference in the volatility of the two fuels, being higher for JP8. As can be explained from figure 4-1 and table 4-1, JP8 consists of lower density and viscosity than ULSD. Thus, it will require lower rail pressure than ULSD to atomize the fuel while other injection parameters remain constant. With the same rail pressure as of ULSD (260 bar in this case), it will have a higher momentum and might vaporize before even reaching near the glow plug area. This can explain the less detection of ionization signal for JP8 in-spite of having a stable and a normal combustion throughout.

5.4 Ionization Analysis with Glow Plug

A detailed ion current analysis using glow plug sensor is presented in this section. It describes cycle to cycle variation of ionization characteristics such as start of ion current (SIC), peak of ion current (PIC), location of peak of ion current (LPIC), ion current delay (ICD) was carried out for ULSD and JP8. In addition, different combustion parameters such as start of combustion (SOC), combustion phasing/location of peak premixed combustion (LPPC) and peak premixed combustion (PPC) were analyzed. The main goal of this section is to build a correlation between combustion and ionization characteristics obtained in two different cylinders with two different sensors, namely pressure transducer and glow plug. For this analysis, all the definitions described in section 4.6 were used.

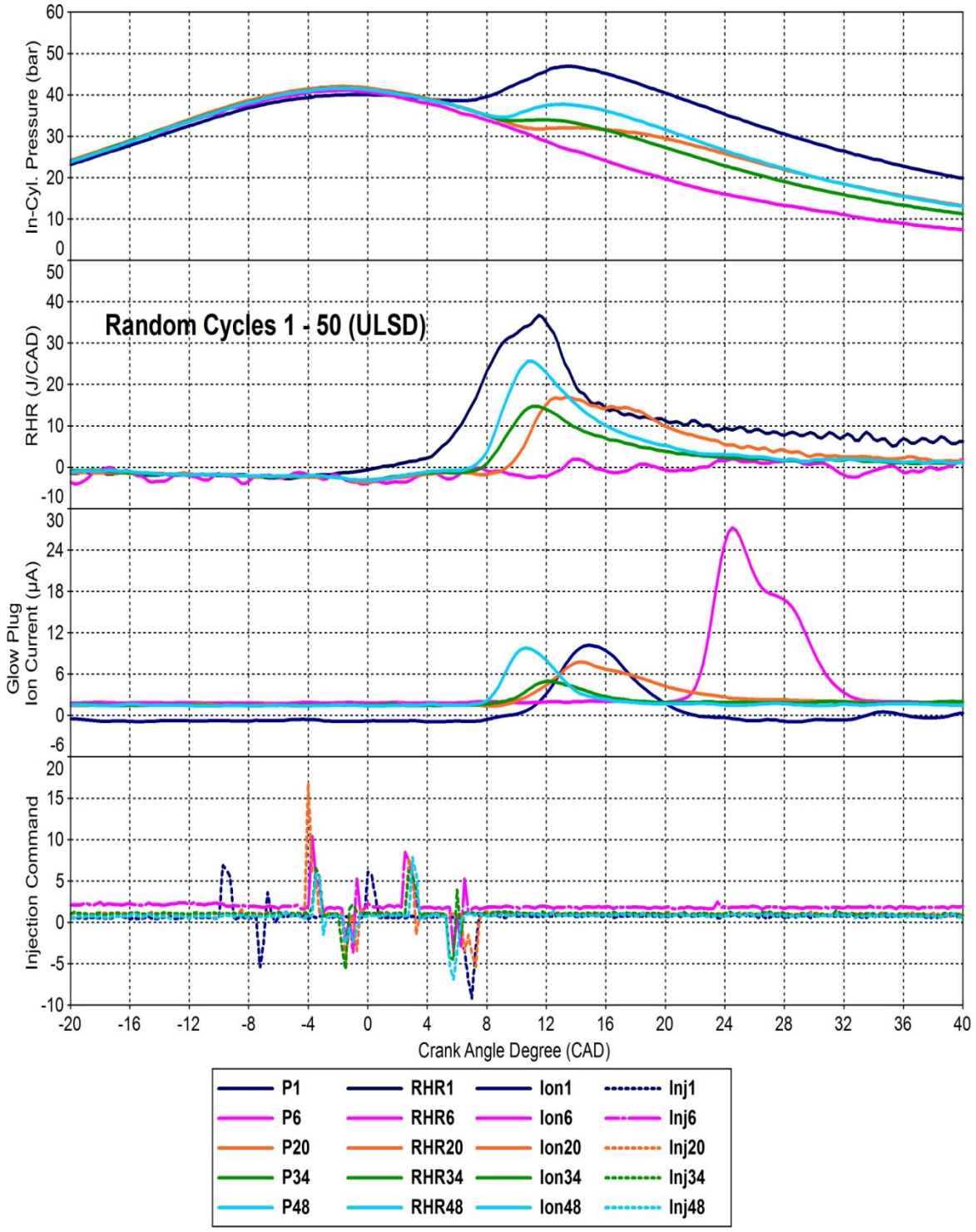

Figure 5-11 Random Cycles (1-50) showing in-cylinder pressure, RHR, glow plug ion current and injection command for ULSD

Figure 5-11 displays the 5 random cycles from the first 50 cycles for engine operation with ULSD. It mainly shows the traces for in-cylinder pressure, rate of heat release, injection signal and glow plug ion current plotted against crank angle degrees. It can be clearly seen that, cycle #1 has an early injection event (SOI #1) at 10˚ bTDC and 2nd injection (SOI #2) at 1˚ bTDC. It also ends up being the cycle with highest peak pressure 49 bar among all 200 cycles. As compared to other cycles, it has an early SOC at 4˚ bTDC. This particular cycle also has high amount of rate of heat release equal to 38.5 Joules/CAD. From figure 5-2 and figure 5-5, it is also evident that, cycle #1 has the highest IMEP equivalent to 5.6 bar. The amplitude of peak of ion current is 11 μA and the start of ion current occurs at 9˚ aTDC. While operating on ULSD, cylinder # 1 misfires at cycle #6, which can be seen from in-cylinder pressure and RHR traces. At the same time, it can be predicted that cylinder #4 undergoes late combustion event from ion current signal, which has SIC at 21˚ aTDC. It has the highest amplitude of 27 μA, indicating high amount of heat release and higher peak pressure for cylinder #4. Except cycle #1, all the other cycles have almost same injection timing for both injection events, i.e. SOI #1 = 4˚ bTDC and SOI #2 = 2.5˚ aTDC. It can be observed that, after misfiring, cylinder #1 undergoes late combustion with some low IMEP cycles which can be seen in figure 5-3 and figure 5-5 further indicating lower peak firing pressures.

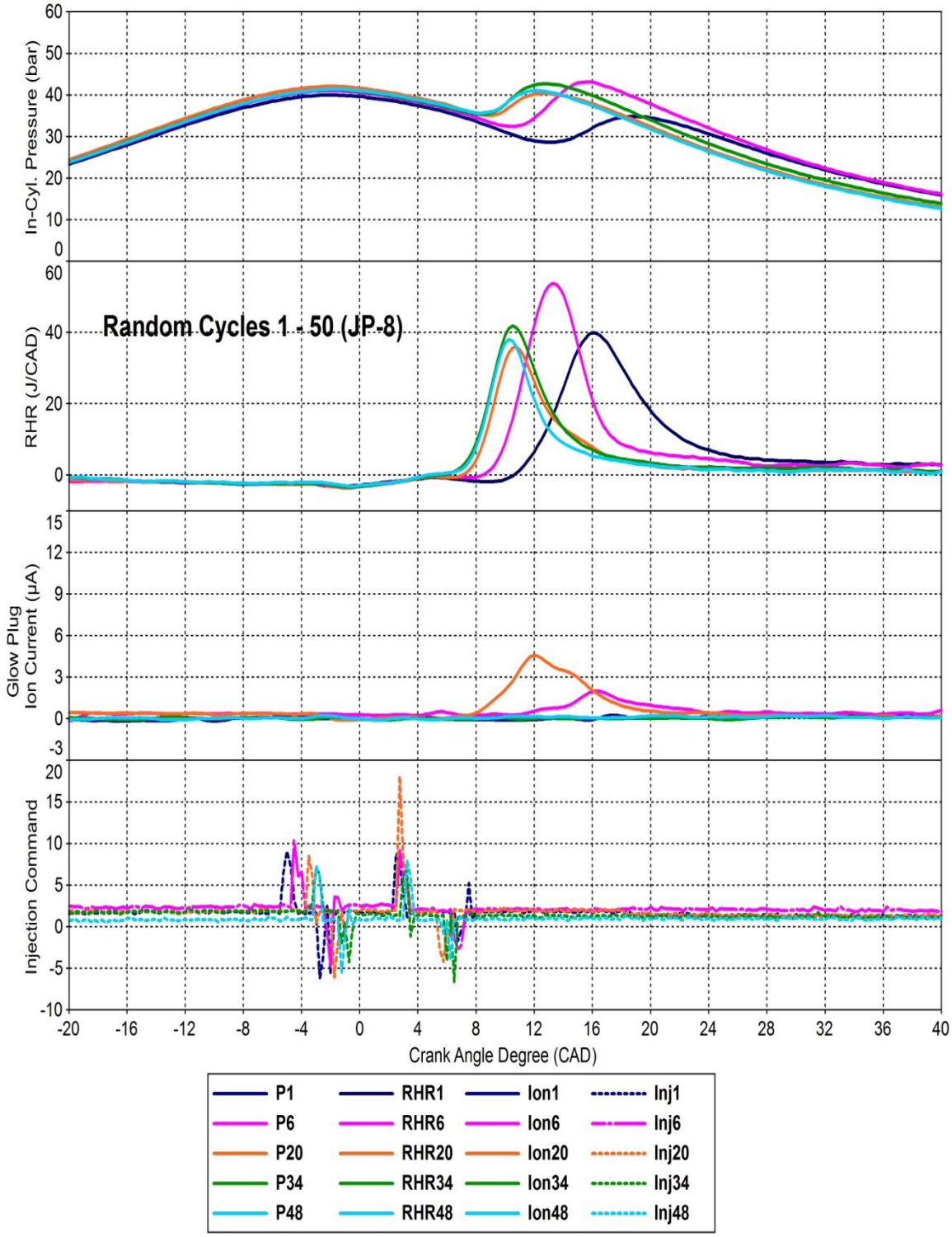

Figure 5-12 Random Cycles (1-50) showing in-cylinder pressure, RHR, glow plug ion current and injection command for JP8

Figure 5-12 shows 5 random cycles from the set of first 50 cycles for engine operation with JP8. It displays the traces for in-cylinder pressure, rate of heat release, injection signal and glow plug ion current plotted against crank angle degrees. It can be observed that, the very first cycle undergoes late combustion having SOC at 11˚ aTDC, which is 7 CAD later than cycle #1 operated with ULSD. It also has the lowest peak pressure of 35 bar and late combustion phasing at 16˚ aTDC. It could not detect ion current signal, indicating a misfired cycle or a sensor failure for cylinder #4. It can be seen that, unlike the operation with ULSD, the location of peak pressure, SOC and combustion phasing advances steadily as the combustion progresses through cycle #50. This is further explained in detail in later parts of chapter 5 and 6. It basically reduces the cycle to cycle variation and helps in minimizing the combustion instability. While operating on JP8, glow plug fails to detect ion current for some cycles which can be seen in figure 5-12 and later in figure 5-15. Cycle #20 shows the maximum value for PIC which is 5 μA. On the other hand, the amplitude of PPC is comparatively greater in this case and remains almost constant at 40 J/CAD except cycle #6 Both the injection events occur at almost same time i.e. SOI #1 = 6˚ bTDC and SOI #2 = 2˚ aTDC, where SOI 1 being advanced by 2 degrees for JP8.

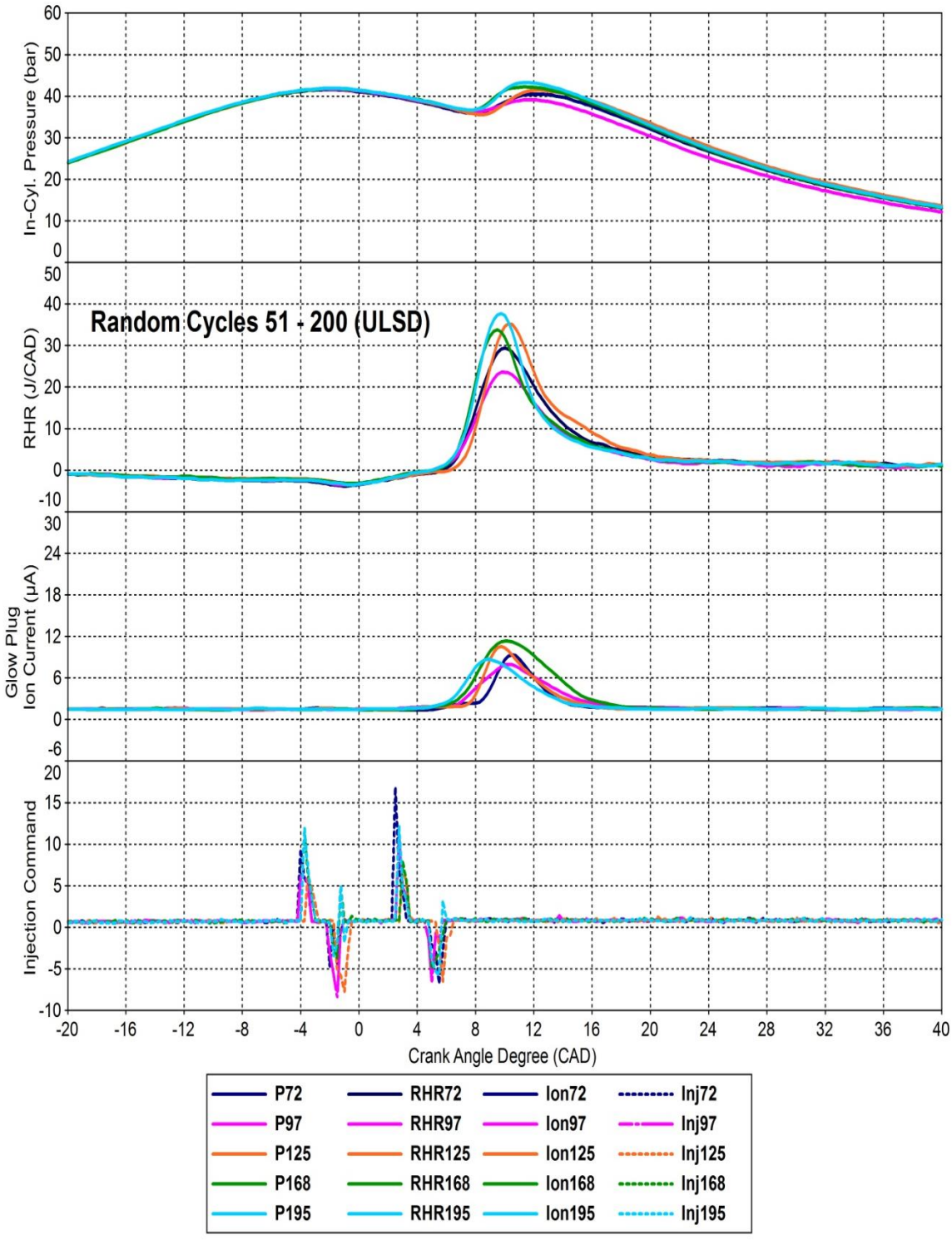

Figure 5-13 Random Cycles (51-200) showing in-cylinder pressure, RHR, glow plug ion current and injection command for ULSD

Figure 5-13 demonstrates a set of 5 random cycles between cycles #51 to #200 for the engine operation with ULSD. It shows more stable engine operation than cycle 1-50 shown in figure 5-5. As the combustion progresses from cycle #51 to cycle #200, the start of combustion and start of ion current both advance with less fluctuation. In addition to that, as the combustion takes place further, the amplitude of peak pressure as well as PPC keeps on increasing. Moreover, a less variation in combustion phasing and the peak of premixed combustion is observed. Both the injections occur at their same respective timings, 4˚ bTDC and 2.25˚ aTDC. No misfiring or late combustion event was observed between cycles 51-200.

Similar features are displayed in figure 5-14, where a set of 5 random cycles between cycle #51 and #200 is shown. Similar to figure 5-13, not only the location for SOC and combustion phasing advances but also undergoes very less variation. During this course, the amplitude of peak pressure as well as PPC increases step by step. This behavior of combustion process with JP8 is quite similar to the engine operation with ULSD. In contrast, the value for peak of ion current is almost 2-3 times higher than the one obtained with ULSD. On the contrary, cycle #72 fails to detect ion current.

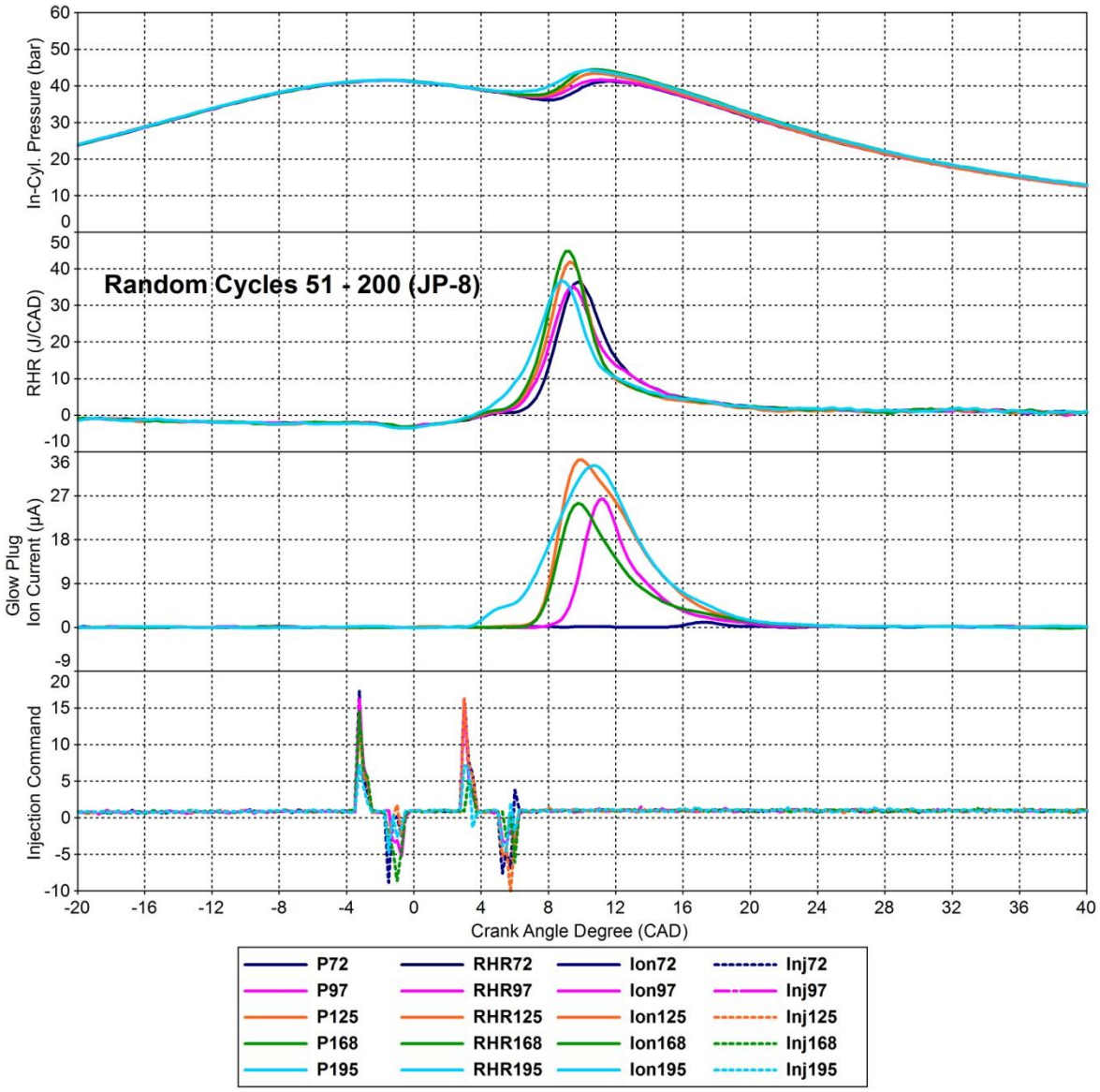

Figure 5-14 Random Cycles (51-200) showing in-cylinder pressure, RHR, glow plug ion current and injection command for JP8

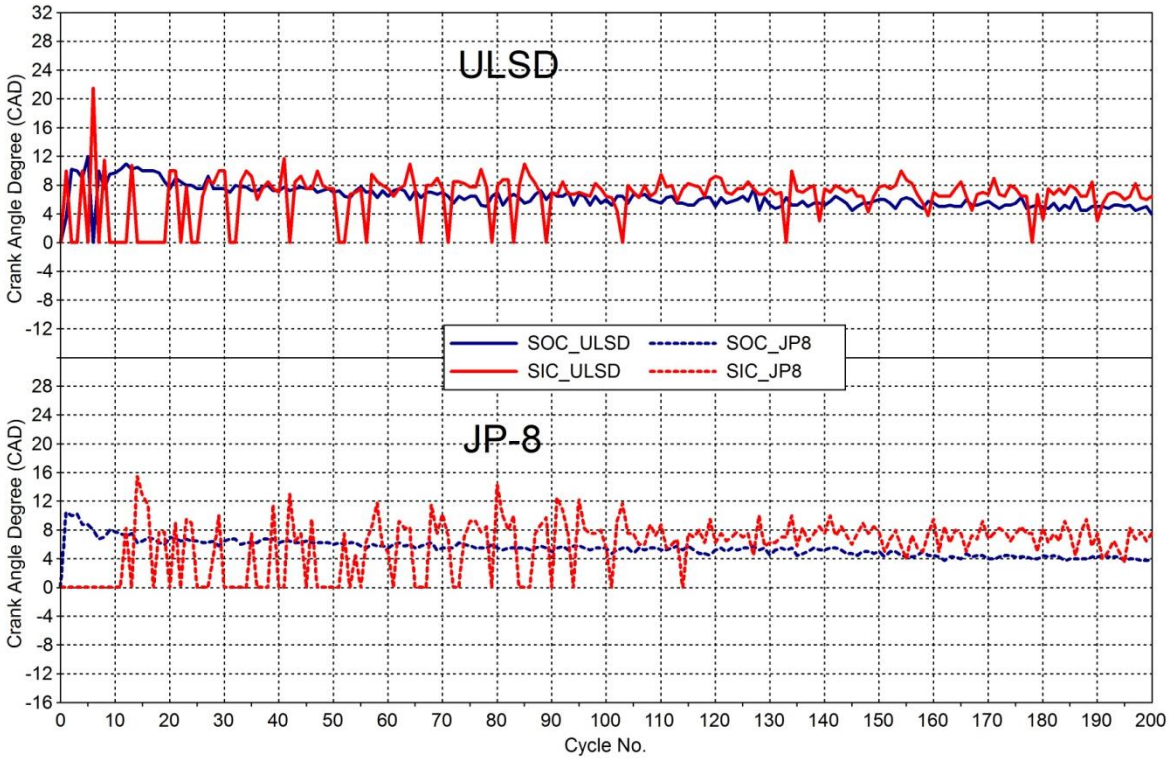

Figure 5-15 Correlation between SIC and SOC

Figure 5-15 shows the correlation between start of ion current and start of combustion with ULSD and JP8 for the first 200 cycles during cold starting operation. Even if the a distinct point for SOC was detected, it can be seen that the glow plug could not detect ion current for some of the cycles for both the fuels. As a matter of fact, glow plug was unable to detect ion current for 28 cycles for ULSD and 50 cycles JP8. For both ULSD and JP8, SOC advances from cycle 1 to 200 and stabilizes near 4˚ aTDC. It is clear that, SIC always lags SOC by 1 to 1.5 degrees for ULSD, whereas it lags by 3 to 4 degrees for JP8. It is also observed that, glow plug could not detect ion current for first 11 consecutive cycles when operating on JP8. There are certain occasions where ion current was detected very late for both ULSD and JP8. While operating on ULSD, cycle # 6 detects ion current very late in the expansion stroke at 21˚ aTDC, whereas it is 16˚ aTDC for JP8.

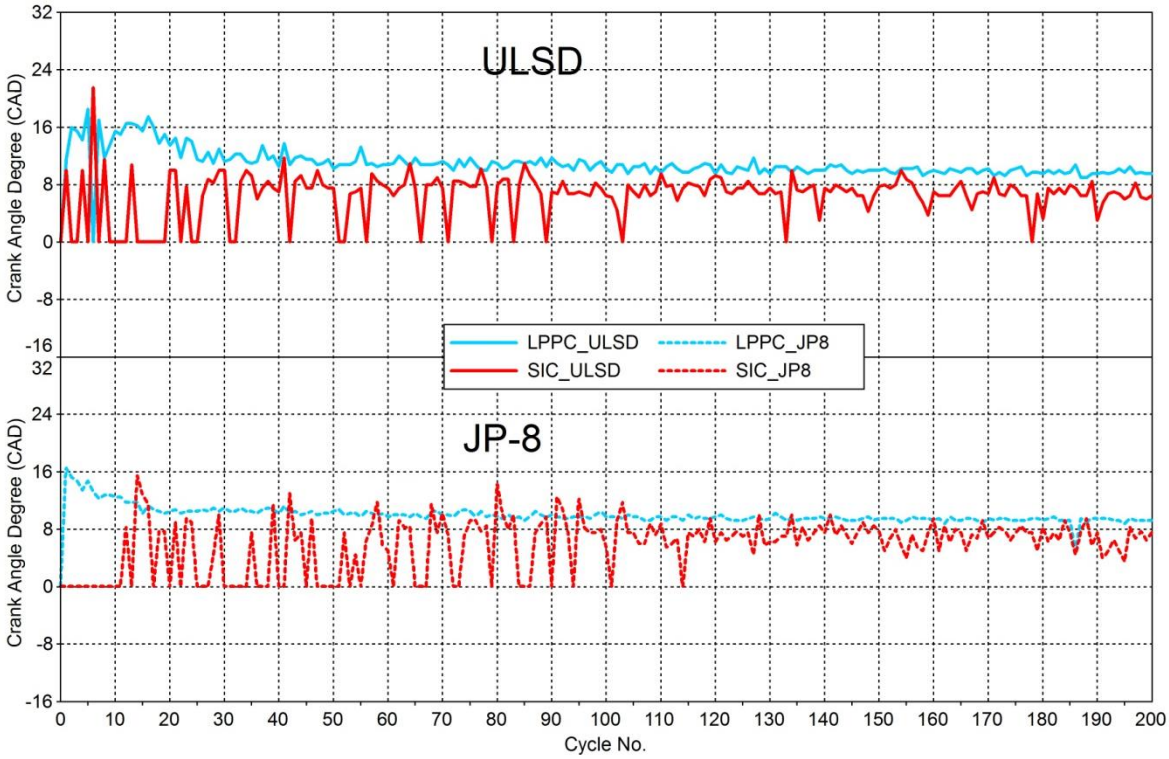

Figure 5-16 Correlation between LPPC and SIC

Figure 5-16 shows the correlation between start of ion current and location of peak of premixed combustion (combustion phasing) for first 200 consecutive cycles with ULSD and JP8. It can be seen that LPPC always lags the start of ion current for ULSD and JP8 with few exceptions. While operating on JP8, ion current was detected 1 to 2 crank angle degrees later than the combustion phasing for fewer cycles. On the other hand, for ULSD cycle #6 is the only event where SIC lags the combustion phasing by almost 4.5 CAD. Cycle to cycle variation for combustion phasing shows that, it advances from 16˚ aTDC to 8.5˚ aTDC, as the combustion progresses from cycle #1 to #200. Unlike JP8, combustion phasing for ULSD first advances, then it retards from cycle #9 to #17 and finally it continues to advance further till it reach steady state.

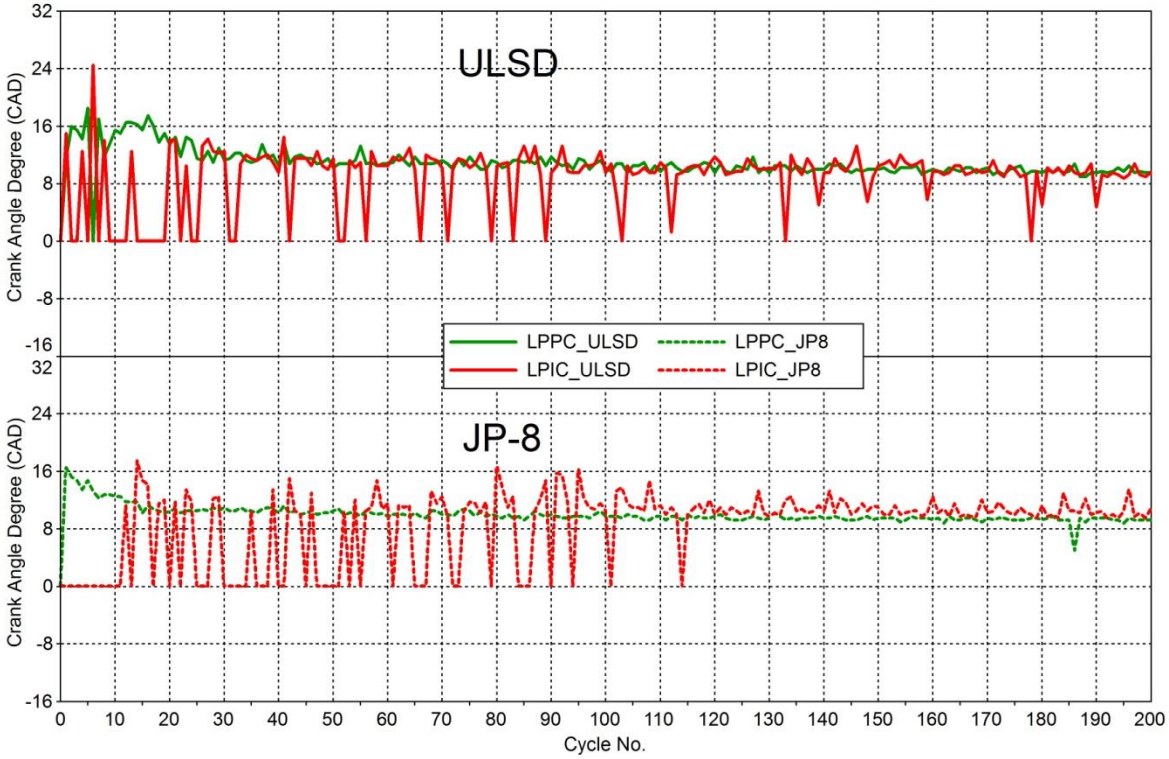

Figure 5-17 Correlation between LPPC and LPIC

Figure 5-17 shows the correlation between LPPC (combustion phasing) and location of peak of ion current for first 200 consecutive cycles with ULSD and JP8. A close correlation can be observed between LPPC and LPIC for all the cycles irrespective of fuel used. For JP8, LPIC lags LPPC more than 3 CAD for some cycles. Combustion phasing and LPIC both steadied down at 8.5˚ aTDC as the engine reaches its steady state. It can be observed from figure 5-15 through figure 5-17 that, ion current takes lesser time to reach its peak than RHR trace. In other words, ion current has a higher slope than the RHR trace when reaching its peak value. This in turn helps in predicting the combustion phasing with the help of ion current and develop a strong feedback system during cold starting operation at ambient room temperature.

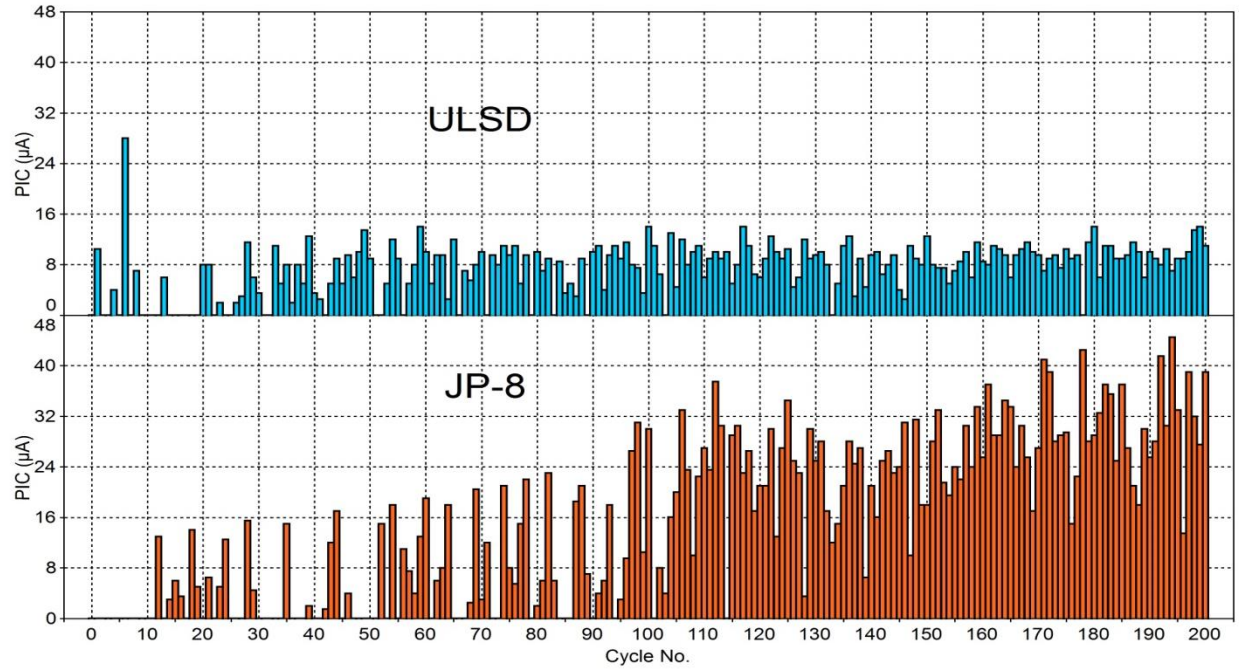

Figure 5-18 Comparison between Peak of Ion Current using ULSD and JP8

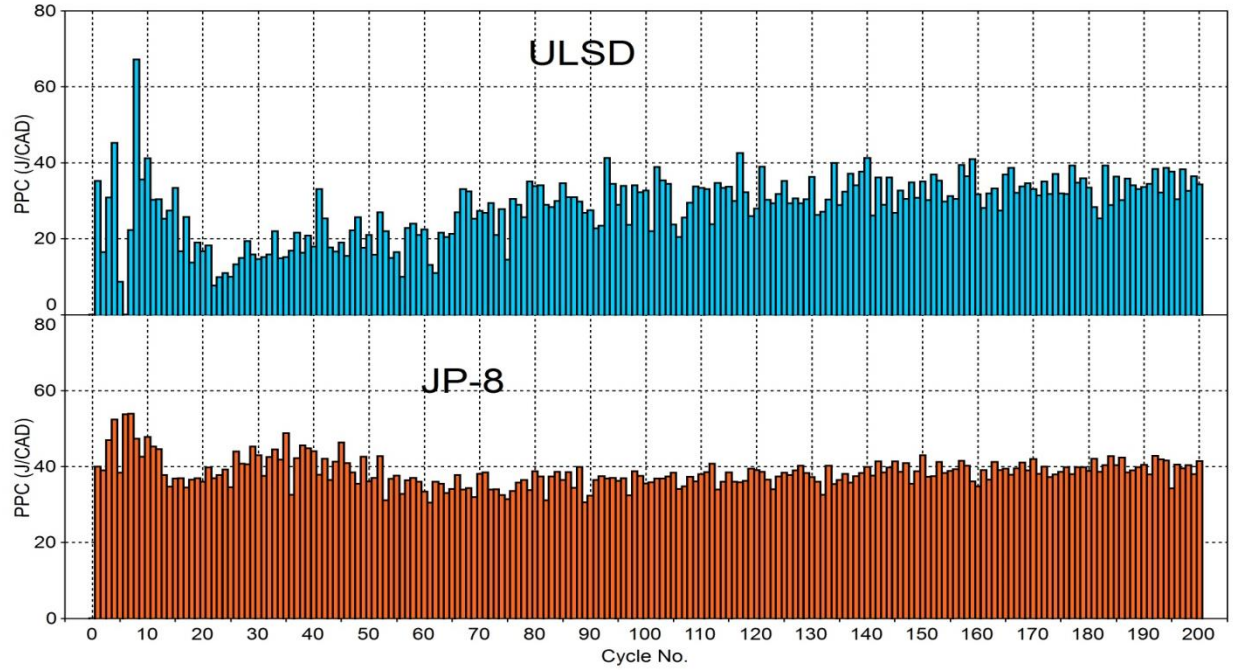

Figure 5-19 Comparison between Peak of Premixed Combustion using ULSD and JP8

Figure 5-18 displays the comparison between peak values of ion current obtained with glow plug ion current sensor for first 200 consecutive cycles with ULSD and JP8 fuel. In spite of the fact that, the appearance of ion current signal is more for ULSD, the amplitude of PIC for JP8 is greater than that for ULSD for most of the cycles. This can be further explained with figure 5-19 which shows the cycle to cycle variation for peak of premixed combustion for first 200 consecutive cycles. In the case for JP8, the mean value of PPC remains higher than that of ULSD throughout the course of cold starting operation. The average value of PIC is 7.3µA and 15.6µA for ULSD and JP8 respectively. It can be seen that, the highest value of PIC using ULSD is 28µA for cycle #6, while it is less than 16µA for all the remaining cycles. This can be caused due to the partial or late combustion cycles contribute during the cold starting operation with ULSD, which in turn causes amplitude for PPC to have a sudden drop as can be seen from figure 5-19. On the other hand, the amplitude for PIC with JP8 is almost greater than 24µA for more than 100 cycles.

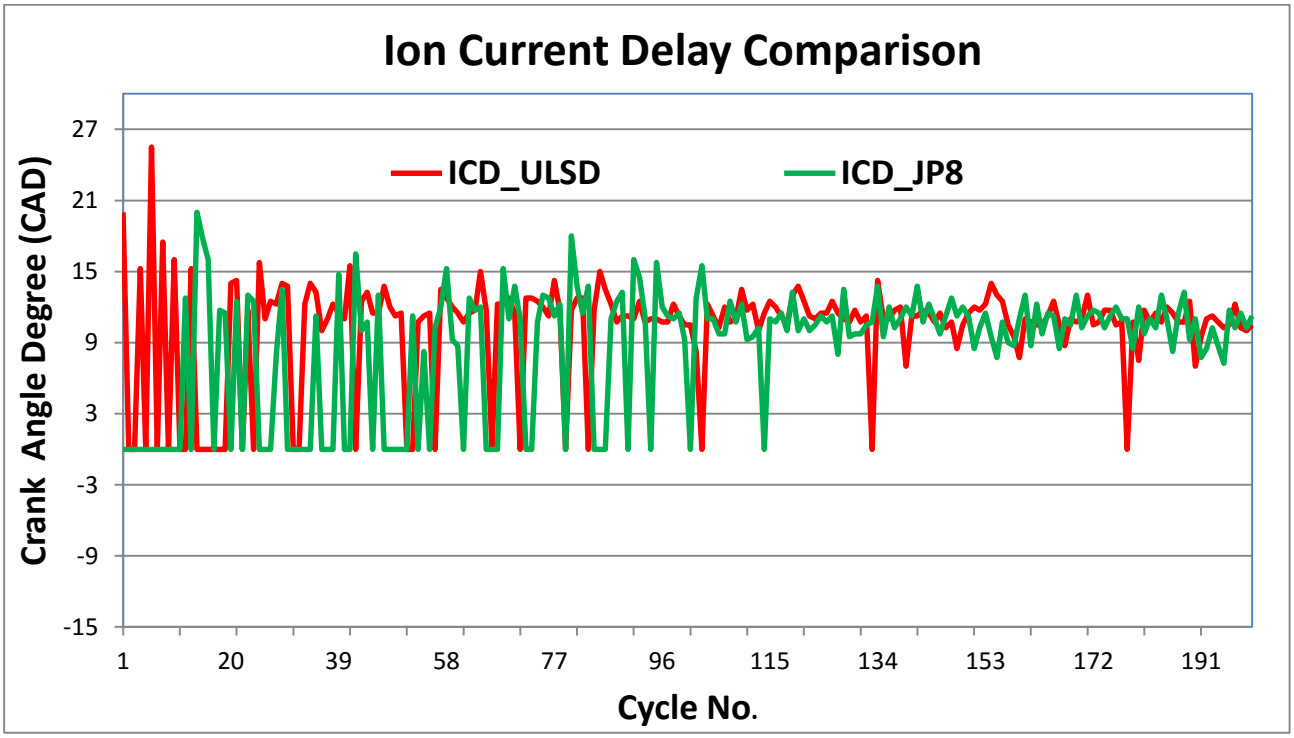

Figure 5-20 Comparison between Ion Current Delays

Figure 5-20 shows the comparison between ion current delays for first 200 consecutive cycles obtained by using ULSD and JP8 fuels. ICDs are defined as the duration between start of first injection (i.e. SOI #1) and start of ion current. ICD = 0 is used for the cycles where a distinct point for SIC was not detected. The highest ICD is 25.5 CAD for cycle #6 operated with ULSD, while it is 20 CAD for cycle #14 for JP8. It can be seen that, the average value of ICD for both the fuels is around 10 to 12 CAD, for all the cycles where ion current is detected. In other words, ICDs for both the fuels follow close to each other, which also explain the same COV shown in table 5-3 for both ULSD and JP8.

The following Table 5-3 shows the coefficient of variation for all the vital parameters within first 50 cycles, where most of the combustion instability was observed. It can be observed that, COV for SOC with JP8 is less than ULSD by 7.4% while the variation in SOI is almost 5% more in ULSD. A difference of 3.5% is seen in the case of combustion phasing, where COV for LPPC is more for ULSD than that of JP8. On the other hand, the variation in ionization characteristics for the first 50 cycles is very less, especially for SICs and ICDs. But in the case of LPIC, the COV is 21.2% for ULSD which is almost 6 % higher than JP8 fuel.

Table 5-3 Coefficient of variation for first 50 cycles with ULSD and JP8

Combustion/Ionization Characteristics	COV_ULSD	COV_JP8
SOI	22.3	17
SOC	22.8	15.4
SIC	28.84	28.58
LPPC (Combustion Phasing)	16.5	13
LPIC	21.2	15.2
ICD	22.4	22.4

5.5 Chapter Summary

This chapter describes the cycle to cycle variation of ionization characteristics and different combustion parameters from two different cylinders during cold starting at 25˚C with ULSD and JP8. The overall engine operation during cold starting is shown by the cycle to cycle variation of engine speed and IMEP which further helps in determining the combustion instability. The ionization characteristics were measured by using a modified glow plug sensor (cylinder #4) and compared with various combustion parameters (cylinder #1) where cylinder to cylinder variation was considered as negligible. It shows that glow plug fails to capture ionization signal for some cycles for both the fuels, even if for those having a distinct point of start of high temperature combustion (SOC). The misdetection of ion current was explained with the help of different operating parameters such as SOI, pulse separation, DOI and rail pressure and fuel properties. In spite of having higher peak values for PPC and PIC, there are more number of occasions where ion current was not detected while operating on JP8. It is found that, LPIC and LPPC have a closer correlation when engine reaches steady state. Finally, it displays the calculated coefficient of variation for various combustion and ionization characteristics using both the fuels, which in turn plays a vital role in determining the combustion instability. This also shows that, the detection of ion current more depends on energy density of a particular fuel.

CHAPTER 6

COLD STARTING: EFFECT OF FUEL PROPERTIES

6.1 Introduction

This chapter explains the effect of physical and chemical fuel properties on various auto-ignition and combustion parameters which contribute to combustion instability during cold starting operation at an ambient temperature $T_{amb} = 25^{\circ}C$. This investigation was carried out on a 4-stroke, 4-cylinder Volkswagen 2.0L TDi engine by using Ultra Low Sulfur Diesel and Jet Aviation JP8 fuel. All the tests were completed using an industrial/OEM ECU and data was acquired using a high speed 15-channel data acquisition system. Similar procedure was implemented for recording the data as explained in chapter 5, where first 200 consecutive cycles were recorded. The engine instrumentation was kept the same as explained in chapter 5.

The first part of this chapter deals with the effect of fuel properties on various combustion parameters like peak pressure, location of peak pressure, formation of LTC and NTC regimes and their contribution towards the combustion instability. It also further explains its effect on cycle to cycle variation of combustion phasing as the combustion progresses through cycle #200 for both ULSD and JP8 fuels. The second part takes through the effect of fuel properties on various delays during cold starting transient operation for the first 50 consecutive cycles, where instability was observed the most. To achieve this goal, physical and chemical delays were compared for first 50 cycles for both the fuels. The main focus of this sub-section is to investigate the effect of "**volatility**" and "**cetane number**" on combustion instability by analyzing RHR traces for ULSD and JP8.

6.2 In-Cylinder Pressure

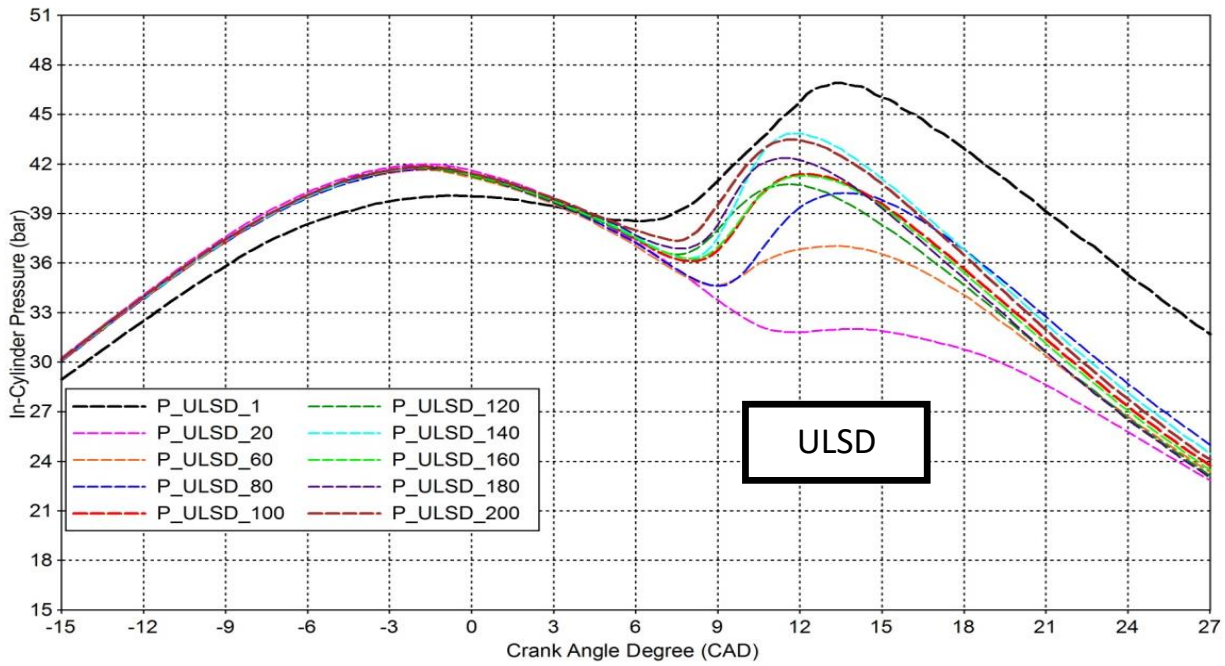

Figure 6-1 Comparison of In-Cylinder Pressure for random cycles with ULSD

Figure 6-1 shows the variation of in-cylinder combustion pressure for 10 random cycles as engine operates through cycle #200 using ULSD. It can be seen that, cycle #1 has the highest peak pressure close to 48 bar with an advanced combustion. In addition to that, it also ends up having a highest IMEP (5.6 bar) among all the cycles. As the combustion progresses further to cycle #20, a late or incomplete combustion is observed. As it goes past cycle #20, the start of pressure rise keeps on advancing along with the location of peak firing pressure. In this course of combustion events, the magnitude of peak firing pressure keeps on rising and reaches a steady value of 43.5 bar at 11.75˚ aTDC. This shows a higher amount of variation in combustion phasing which is explained later in section 6.4.

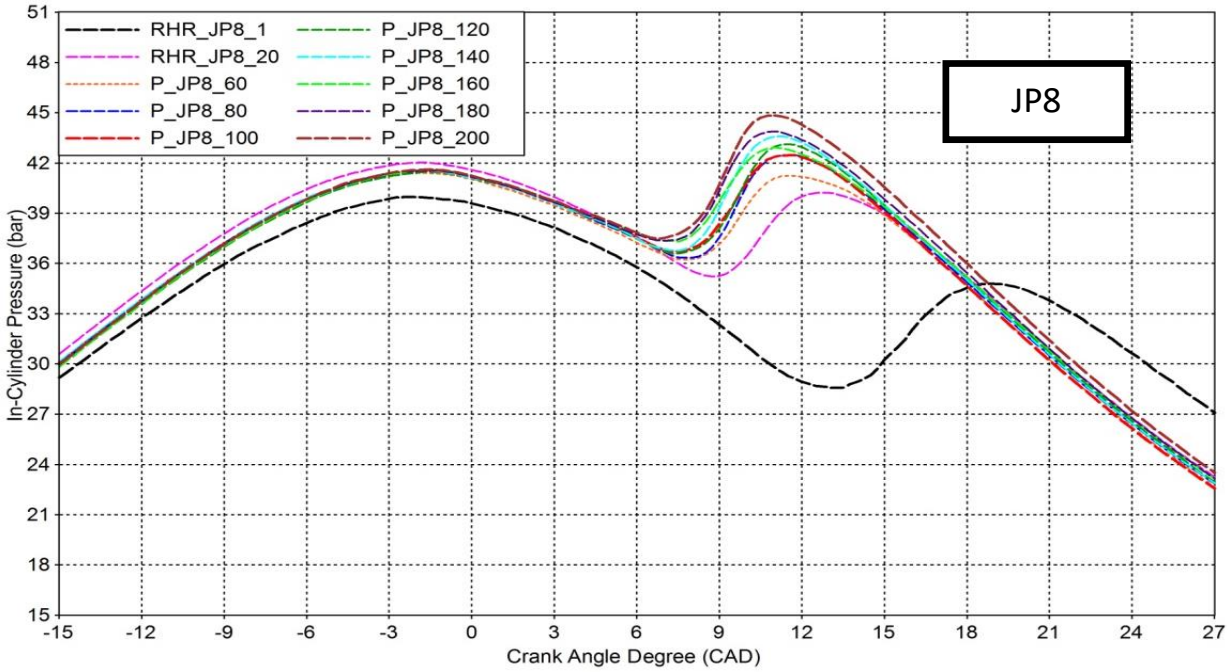

Figure 6-2 Comparison of In-Cylinder Pressure for random cycles with JP8.

Figure 6-2 displays the cycle to cycle variation of in-cylinder combustion pressure for 10 random cycles as the engine operates through cycle #200 for JP8. An exactly opposite behavior is seen here with JP8 as compared to figure 6-1. Cycle #1 has the lowest peak firing pressure of 34.5 bar and the most retarded combustion among all the cycles. When the engine operates further to cycle #20, combustion process advances with greater variation. The amplitude and location of peak firing pressure then stabilizes as the engine operates from cycle #60 through cycle #200. This adds up into better stability in the engine operation with JP8. Therefore, a less amount of cycle to cycle variation is observed in location of peak firing pressure and its amplitude with JP8, which is evident from figure 6-1 and figure 6-2. As compared to the engine operation with ULSD, the average value for peak firing pressure is higher with JP8 along with and advanced LPP.

6.3 LTC and NTC regimes

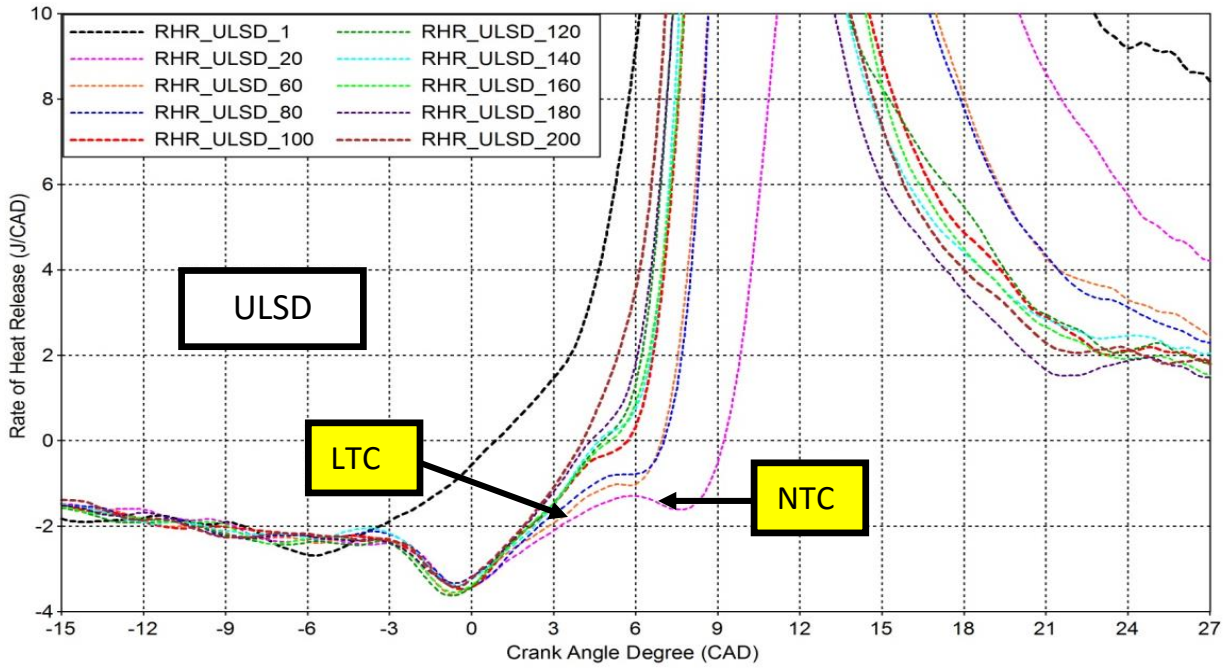

Figure 6-3 Comparison of Rate of heat release (magnified) for random cycles with ULSD.

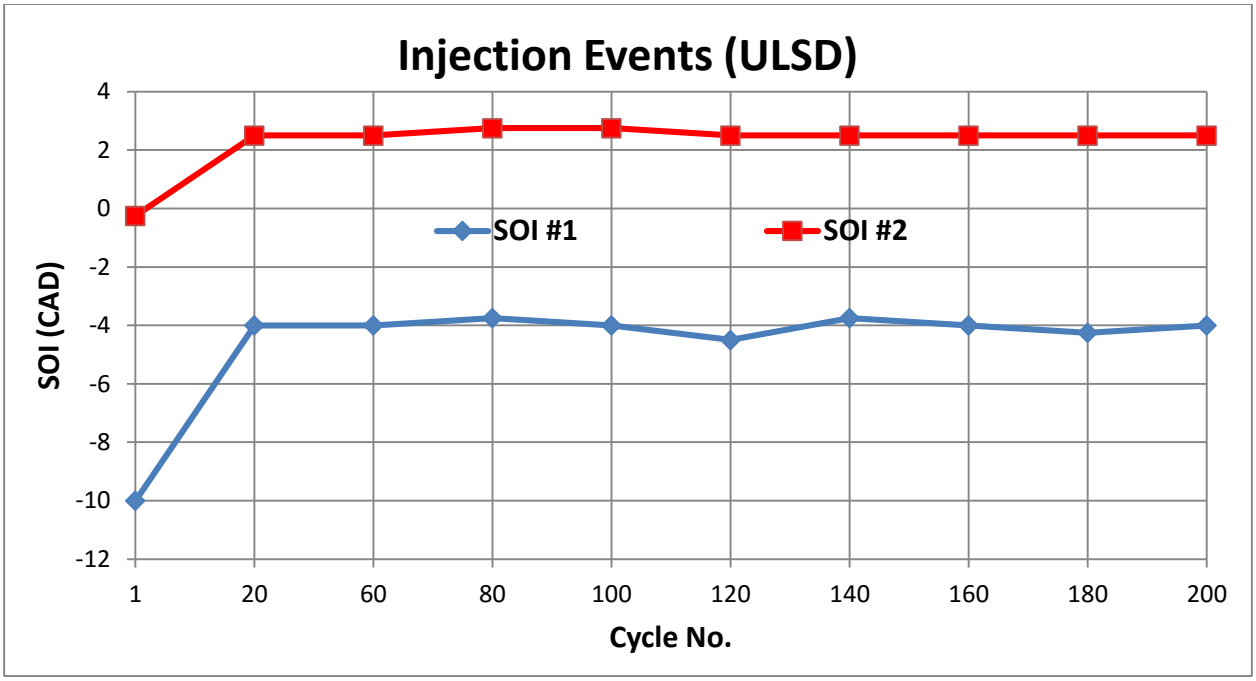

Figure 6-4 Injection Events for random cycles with ULSD

Figure 6-3 shows a magnified version of rate of heat release traces, while figure 6-4 shows the injection events for 10 random cycles between cycle #1 and #200 (same cycles as demonstrated in figure 6-1) for engine operation using ULSD. It also displays the formation of LTC and NTC regimes followed with the high temperature combustion. It can be observed that, cycle #1 has an early injection (SOI #1 = 10˚bTDC) and the highest IMEP = 5.6 bar (figure 5-2), a high temperature combustion zone was observed with no appearance of LTC and NTC regimes. At cycle #20 a large shift in the injection timing is seen along with the formation of LTC and NTC regimes. As the engine operates further, SOI #1 and SOI #2 remain unchanged which can be observed from figure 6-4. It can be noticed that, as the engine operation move on, both LTC and NTC regimes start to disappear and merge into the high temperature combustion zone. This is due to the fact that the continuous increase in combustion temperature reduces the duration of NTC which further causes the LTC regime to merge. This in turn helps to achieve good high temperature combustion and reducing the combustion instability which can be observed post cycle #100 in figure 6-3.

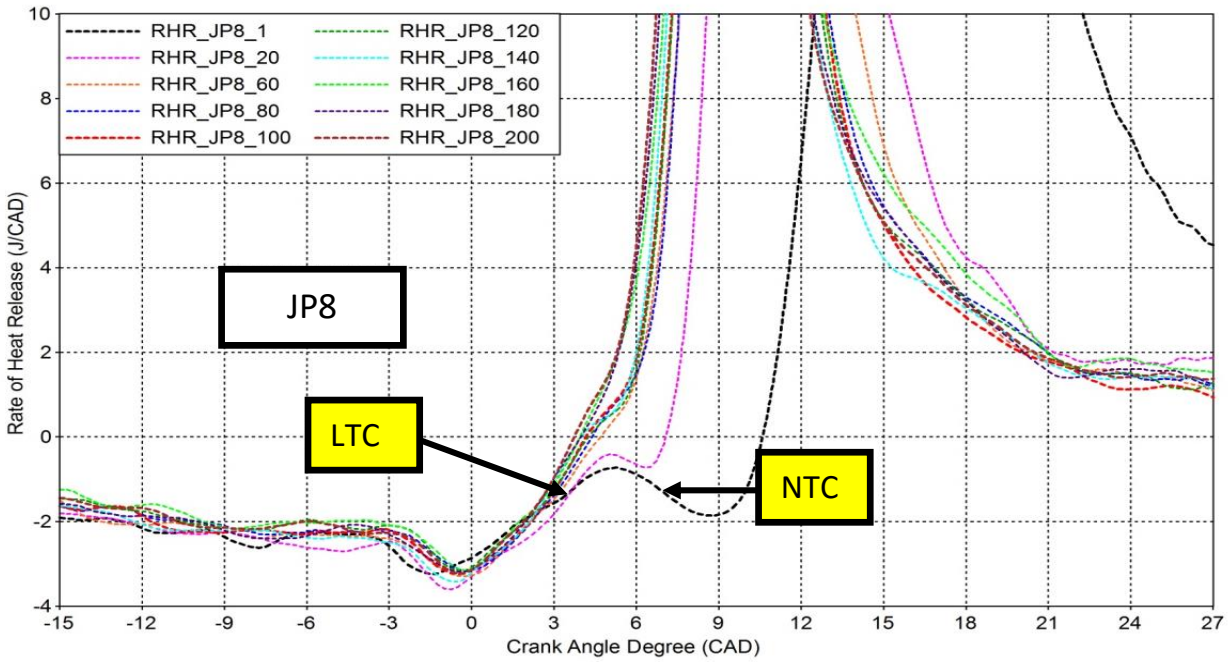

Figure 6-5 Comparison of Rate of heat release (magnified) for random cycles with JP8.

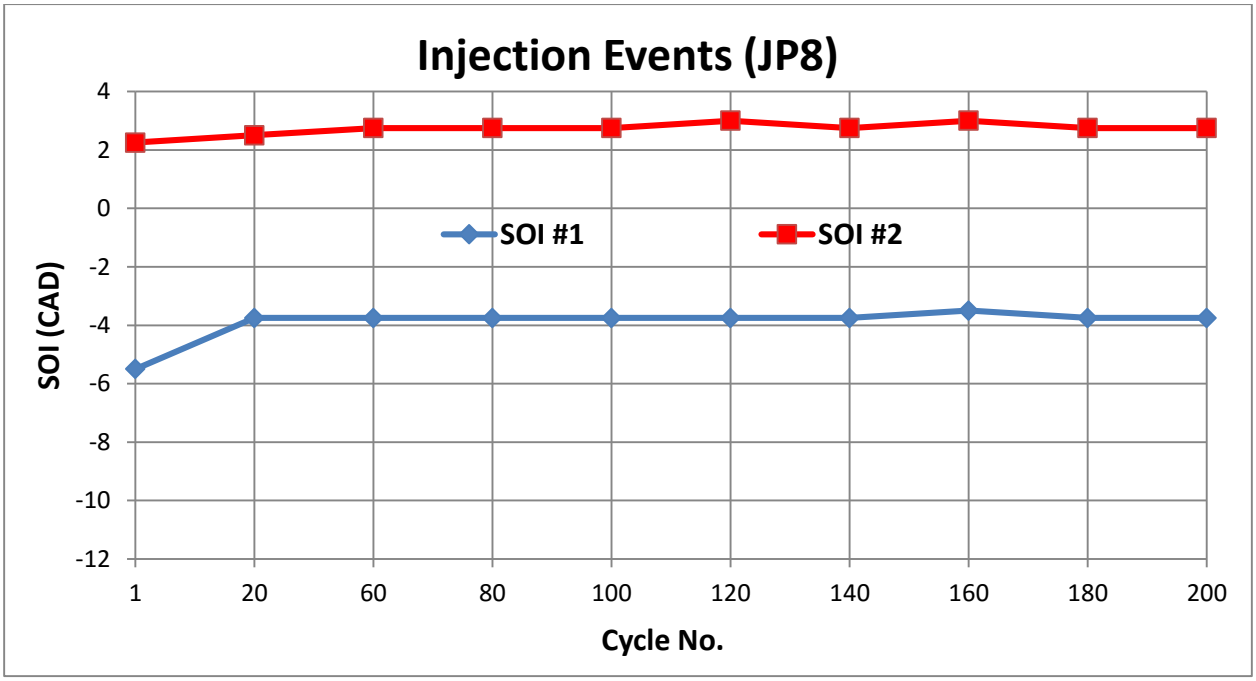

Figure 6-6 Injection Events for random cycles with JP8

Figure 6-5 shows a magnified version of rate of heat release traces, while figure 6-6 shows the injection events for 10 random cycles between cycle #1 and #200 (same cycles as demonstrated in figure 6-2) for the engine operation using JP8. Like figure 6-3, formation of LTC and NTC regimes can be seen for initial cycles after the fuel evaporation phase. SOI #1 retards by 2 CAD as the engine operates form cycle #1 to #20 and then remains unchanged at 4.25˚ bTDC throughout. These two cycles show LTC and NTC regimes distinctly, after which they merge to continue as a high temperature combustion zone. As compared to figure 6-3, the occurrence of these two regimes is less and thus merges quickly into a high temperature combustion zone. Unlike the operation with ULSD, the duration of NTC zone reduces to a greater extent between cycle #1 and #20 which further helps in keeping the combustion phasing almost unchanged and minimizing the combustion instability while operating with JP8.

It can be seen that, the variation of injection timing, especially SOI #1 plays a vital role in the formation and elimination of LTC and NTC regimes. It contributes in cycle to cycle variation of combustion phasing and thus combustion instability. It is further explained with the help of figure 6-7 and figure 6-8.

6.4 Combustion Phasing

Figure 6-7 displays the effect of cycle to cycle variation of combustion phasing (LPPC) on combustion instability for a set of 10 random cycles (same cycles as figure 6-3) from cycle #1 to cycle #200 as the engine operates on ULSD. Since it is evident from figure 6-3 and figure 6-4 that cycle #1 undergoes an early combustion with an advanced SOI #1, the combustion phasing first retards in the beginning with a fall in the amplitude of peak of premixed combustion. As the engine runs further, it advances and stabilizes at around 10˚ aTDC. The highest value of PPC is 43.5 J/CAD, which is witnessed for cycle #140 at 10.5˚ aTDC. It also shows the calculated COV for first 50 cycles which is 16.5% which is also shown in table 5-3.

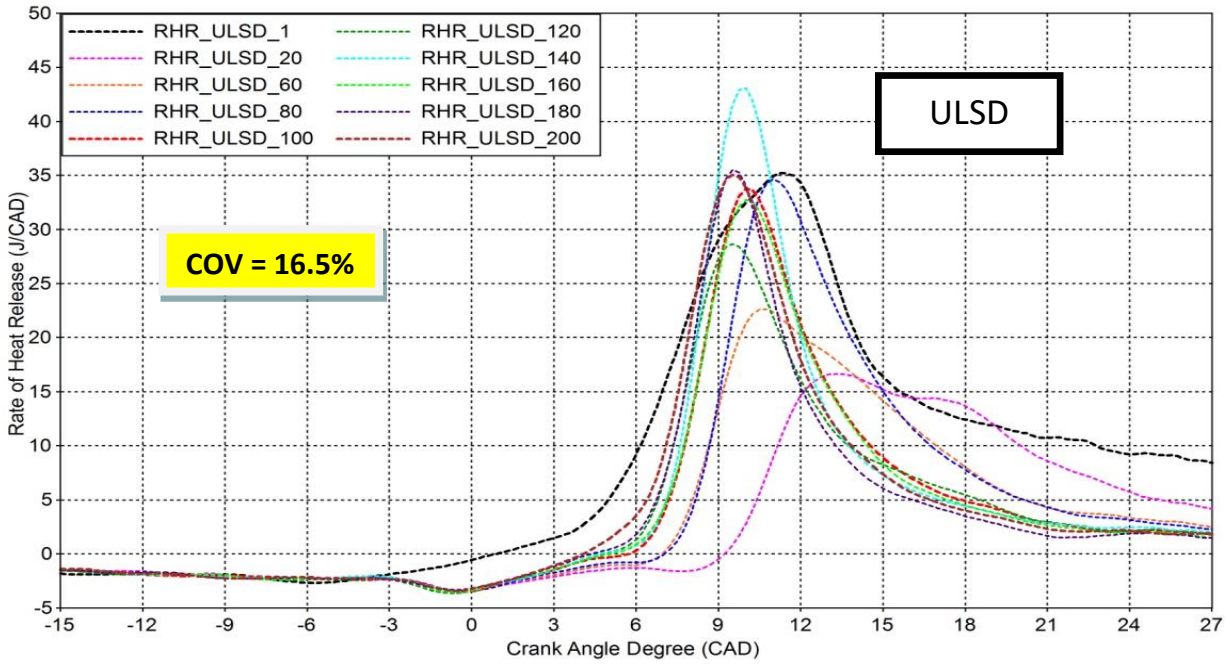

Figure 6-7 Comparison of Rate of heat release for random cycles with ULSD.

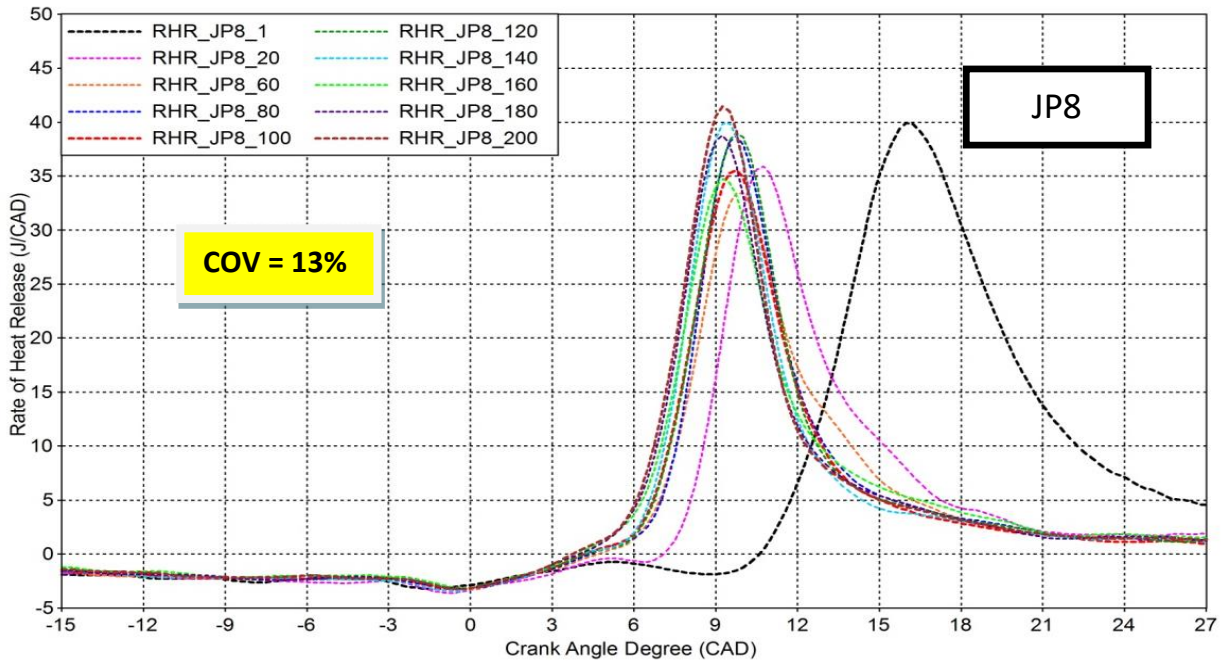

Figure 6-8 Comparison of Rate of heat release for random cycles with JP8.

On the other hand, at the initial stages, the combustion phasing for JP8 test advances to a greater extent, while the amplitude of PPC reduces by 5 J/CAD. As the combustion develops, the location of peak of premixed combustion reaches 9˚ aTDC with very minute variation. While reaching a steady state, it re-gains the amplitude of PPC to 40 J/CAD. It can be observed that, the amplitude of peak of premixed combustion varies between 35 J/CAD to 41 J/CAD, which is very less as compared to ULSD. This further explains a stable and continuous high temperature operation of the engine, which helps in reducing LTC and NTC regimes as explained earlier. For the transient operation, COV for combustion phasing with ULSD is more than JP8, which compares the combustion instability between two fuels.

6.5 Effect of delays

In order to analyze and study the cold starting operation, it is important to understand which of the fuel properties has more contribution and impact on combustion instability. This subsection explains the effect of fuel properties like volatility and cetane number on physical and chemical delays respectively during the transient engine operation. As these delay periods are greatly impacted by fuel volatility and Cetane number [31], a detailed cycle to cycle analysis is carried out in order to determine its effect on combustion instability. At the end, the combined effect of ignition delay is demonstrated during the transient engine operation.

6.5.1 Physical Delay

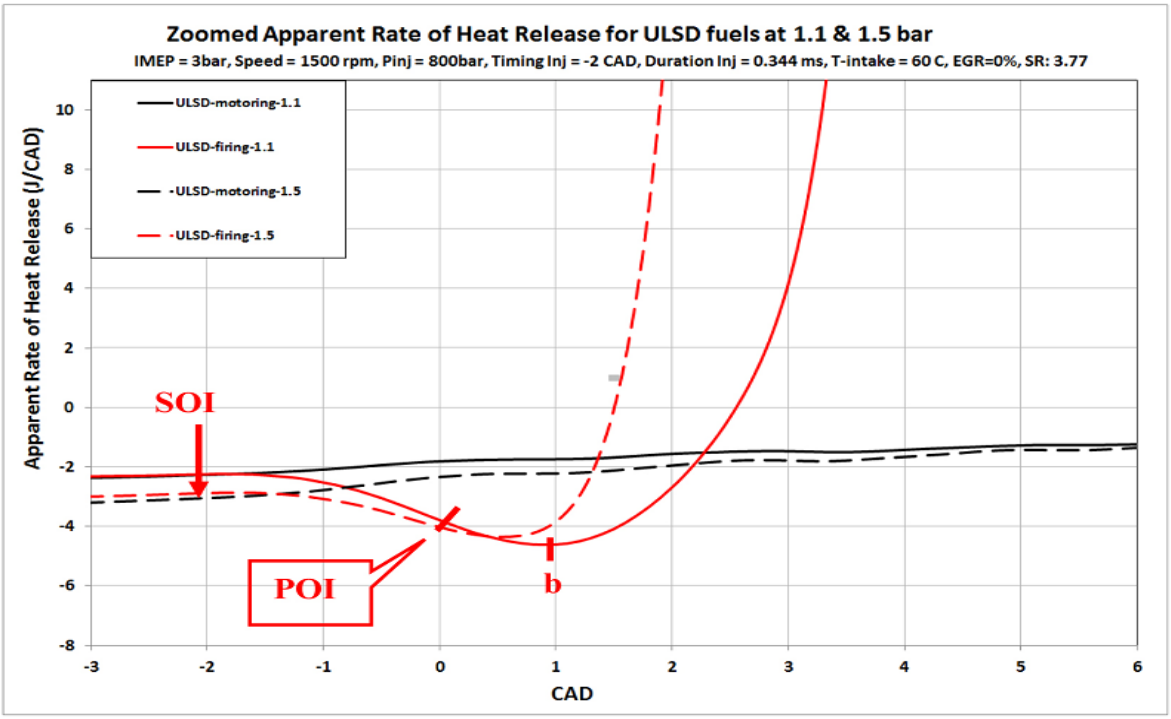

Figure 6-9 Definition for Point of Inflection [31]

The physical delay period is the duration between start of injection and point of inflection in crank angle degrees. Point of inflection (POI) is defined as the point on the RHR trace where exothermic reaction starts [31]. Figure 6-9 displays the location of point of inflection on the RHR trace. It can be also calculated by taking the second derivative of RHR trace, which is zero after SOI and then becomes positive indication the start of exothermic reactions [31].

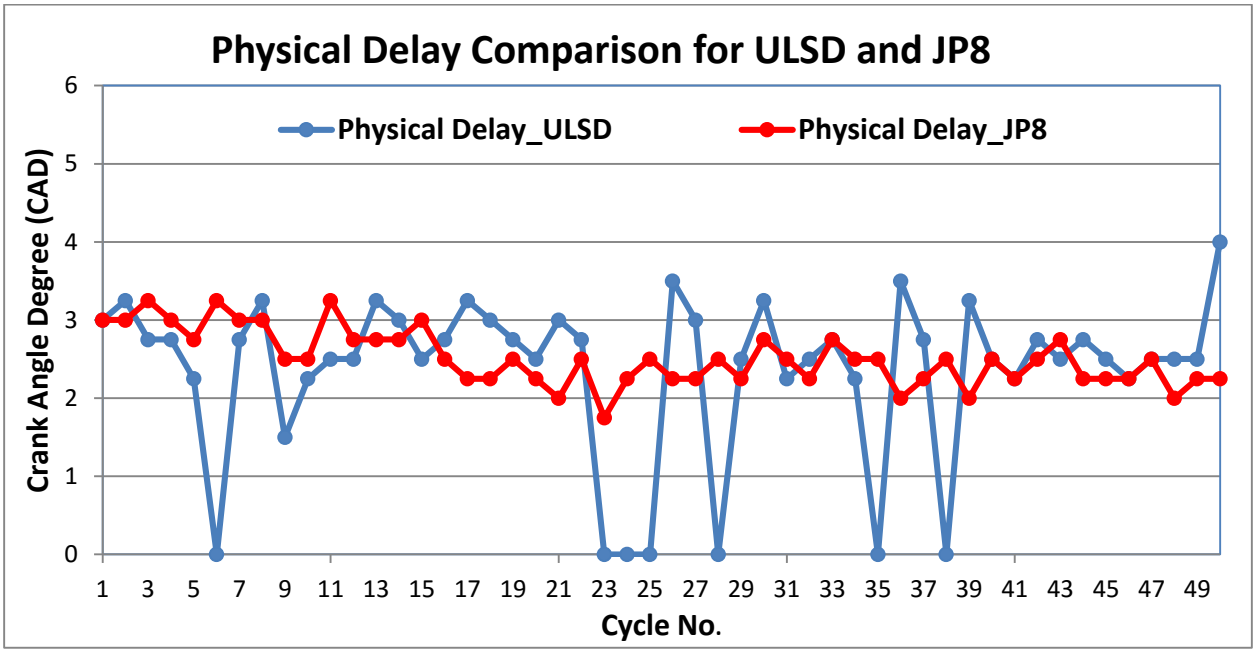

Figure 6-10 Cycle to cycle variation of physical delay for ULSD and JP8

Figure 6-10 shows the comparison for cycle to cycle variation for the physical delay period during cold starting transient state for first 50 cycles with ULSD and JP8. While operating on ULSD, cycle #6 could not detect a distinct point of inflection, as the engine undergoes complete misfiring. When the engine continues to operate in a transient state for ULSD, it gives rise to more number of vibrations, which in turn makes it difficult to detect POI for some of the later cycles. Physical delay is considered as 0, where a distinct POI is not detected. On the other hand, point of inflection was detected for all the 50 cycles, when the engine runs on JP8 fuel. It can be seen that, the physical delay for JP8 is less than 1 to 1.5 CAD than ULSD for most of the cycles. On the other hand, for the few initial cycles operating on ULSD, physical delay shortens, as the

combustion starts very early with a high IMEP (figure 5-2). This phenomenon can also be explained with a greater variation of rail pressure for initial cycles with ULSD (table 5-1).

6.5.2 Chemical Delay

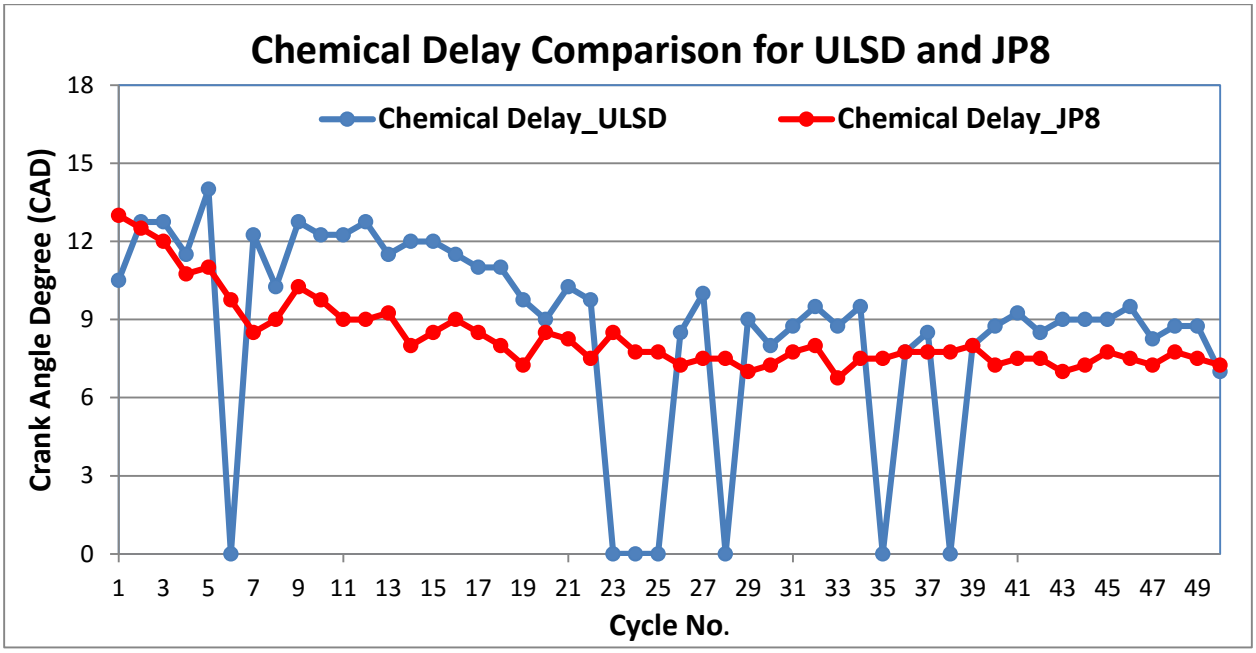

Figure 6-11 Cycle to cycle variation of chemical delay for ULSD and JP8

Figure 6-11 shows the comparison cycle to cycle variation for the chemical delay period when the engine operates through a transient state for ULSD and JP8. The duration between the point of inflection and start of combustion is termed as chemical delay period in crank angle degrees. As explained in section 6.5.1, no distinct POI was detected due to misfiring and vibrations in the RHR signal, which in turn makes it difficult to compute the chemical delay period for such cycles. Those cycles are denoted by duration of 0 CAD. It is evident from figure 6-11, except for cycle #1, the chemical delay period for JP8 fuel is always less than ULSD, which also helps to reduce the ignition delay during the transient engine operation.

6.5.3 Ignition Delay

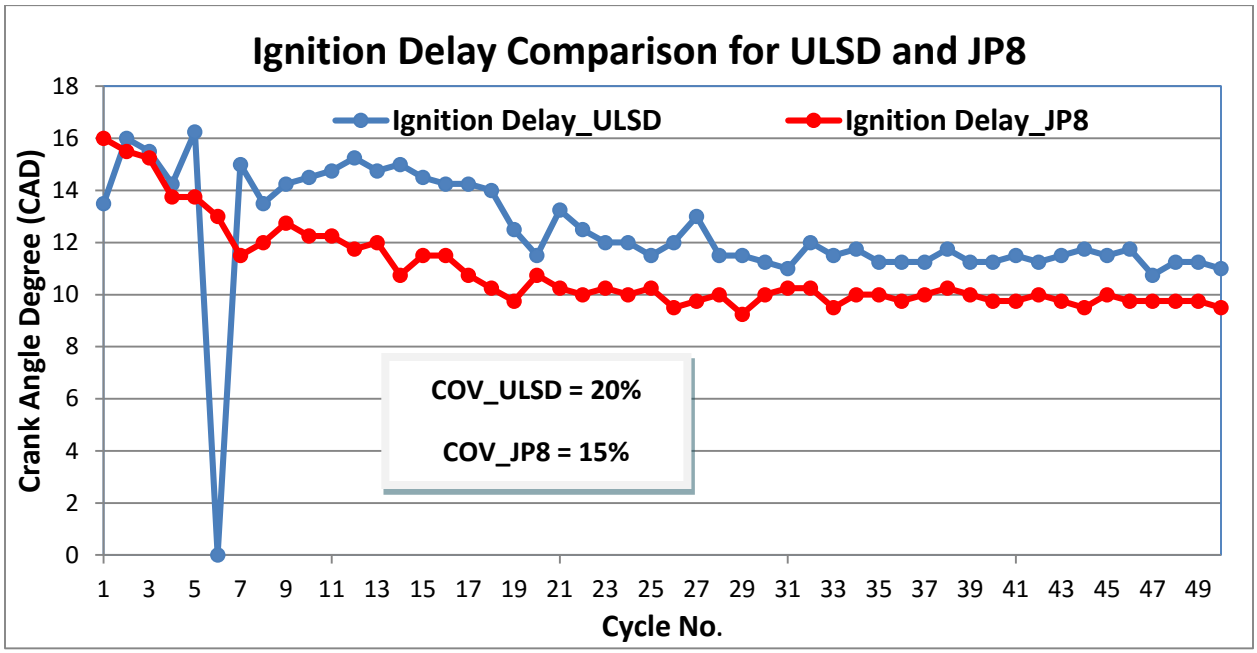

Figure 6-12 Cycle to cycle variation of ignition delay for ULSD and JP8

Figure 6-12 displays the comparison of ignition delay during cold starting transient operation for first 50 cycles with ULSD and JP8. It is defined as duration between start of injection and start of high temperature combustion in the RHR [4]. It is clear that, the ignition delay period is always less for JP8 fuel, with the exception of cycle#1, where it's higher than 2 CAD. This difference occurs due to a high IMEP start for ULSD causing advanced and high temperature combustion. This effect stays in the initial stages till the engine misfires, in which ignition delay for both the fuels is almost same. As the engine operates further, ID for both ULSD and JP8 decreases, which in turn advances the combustion event and helps in securing the stability. COV for ignition delay is 20% and 15% for ULSD and JP8 respectively, which is also indicated in figure 6-12. This also shows more variation and instability when engine operates with ULSD.

6.6 Chapter Summary

This chapter explains the effect of physical and chemical properties of fuel on combustion instability during cold starting transient state. It is explained with the help of cycle to cycle variation of various auto-ignition and combustion parameters and their contribution towards combustion instability. It deals with various parameters such as in-cylinder pressure, rate of heat release, combustion phasing, formation of LTC and NTC regimes as the engine operates through 200 cycles. In addition to that, it also sheds a light on the effect of physical and chemical delays for both the fuels on combustion instability. The causes of combustion instability are identified after a detailed analysis during cold starting transient period. The high amount of shift in the combustion phasing increases the combustion instability for ULSD. Also the formation of LTC and NTC regimes affects the combustion process, which also plays a major role in deciding the instability when the engine operates on ULSD. At the end, it can be seen that chemical delay has a greater impact in reducing the ignition delay, which also helps in minimizing the combustion instability for JP8 fuel.

CHAPTER 7

COMPARISON OF IONIZATION SENSORS

7.1 Introduction

This chapter explains the combustion and ionization characteristics using two ionization sensors at steady state lower idling speeds of 830 rpm, 1000 rpm and 1100 rpm with two fuels; ULSD (42.1) and JP8 (DCN = 49.3). For this investigation, a centrally instrumented multi-sensing fuel injector (MSFI) sensor was placed in cylinder #1. It is constructed by insulating the piezo injector from the engine body. It is compared with a modified glow plug sensor which is placed in cylinder #4. All the other engine instrumentation kept unchanged and average of 100 cycles was recorded using a high speed 15-channel data acquisition system. All the low speed idling tests were performed on a 4-cylinder, 4-stroke Volkswagen 2.0L TDi engine with an industrial/OEM ECU.

The main focus of this chapter is to compare ionization characteristics obtained using two sensors placed in different cylinders and at different locations in the combustion chamber. It not only does explain the nature of the signal but also demonstrates its strength at two different locations. This ultimately gives a brief idea of the development of the heterogeneous diesel combustion during low speed idling operation with two different fuels. The location of two sensors in the combustion chamber is shown in figure 3-5 and figure 3-6. It also shows the comparison of ion current delays from two different sensors with the ignition delay. At the end, it shows the emissions such as NOx and %Opacity at various idling conditions for both the fuels.

7.2 Idling with ULSD

This section covers the data analysis of the idling operation at the speeds of 830 rpm, 1000 rpm and 1100 rpm with ULSD. Figure 7-1 shows the traces for in-cylinder pressure, rate of heat release, ion current signal obtained from both the sensors and injection signal. It shows two injection events for all the tested speeds. With increase in speed, SOI #1 advances by a short duration of 1 CAD, whereas SOI #2 retards by almost same amount. As the speed increases from 830 rpm to 1100 rpm, two combustion events can be seen from in-cylinder pressure trace. The peak of premixed combustion for SOI #1 can be seen at 1000 and 1100 rpm. The amplitude of peak of premixed combustion is 40 J/CAD for 830 rpm which occurs at 9˚ aTDC. It then decreases to 30 J/CAD at 11˚ aTDC while showing PPC for each of the injection.

The ion current signal obtained from glow plug shows a distinct location for SIC and PIC. As the speed increases, it shows a small peak after the end of first injection, which also corresponds to RHR trace. The maximum amplitude of PIC is 32μA for engine operation at 1000 rpm. A centrally instrumented MSFI sensor shows comparatively smaller peak for ion current signal. The start of MSFI signal retards as the speed increases with a rise in its amplitude to 4μA. This shows that the strength of ion current signal is weaker at the center than the periphery. Also, with the increase in the speed, some vibrations in the MSFI signal can be observed. For all the tested speeds, both the injection events were detected by MSFI sensor which is explained later in detail.

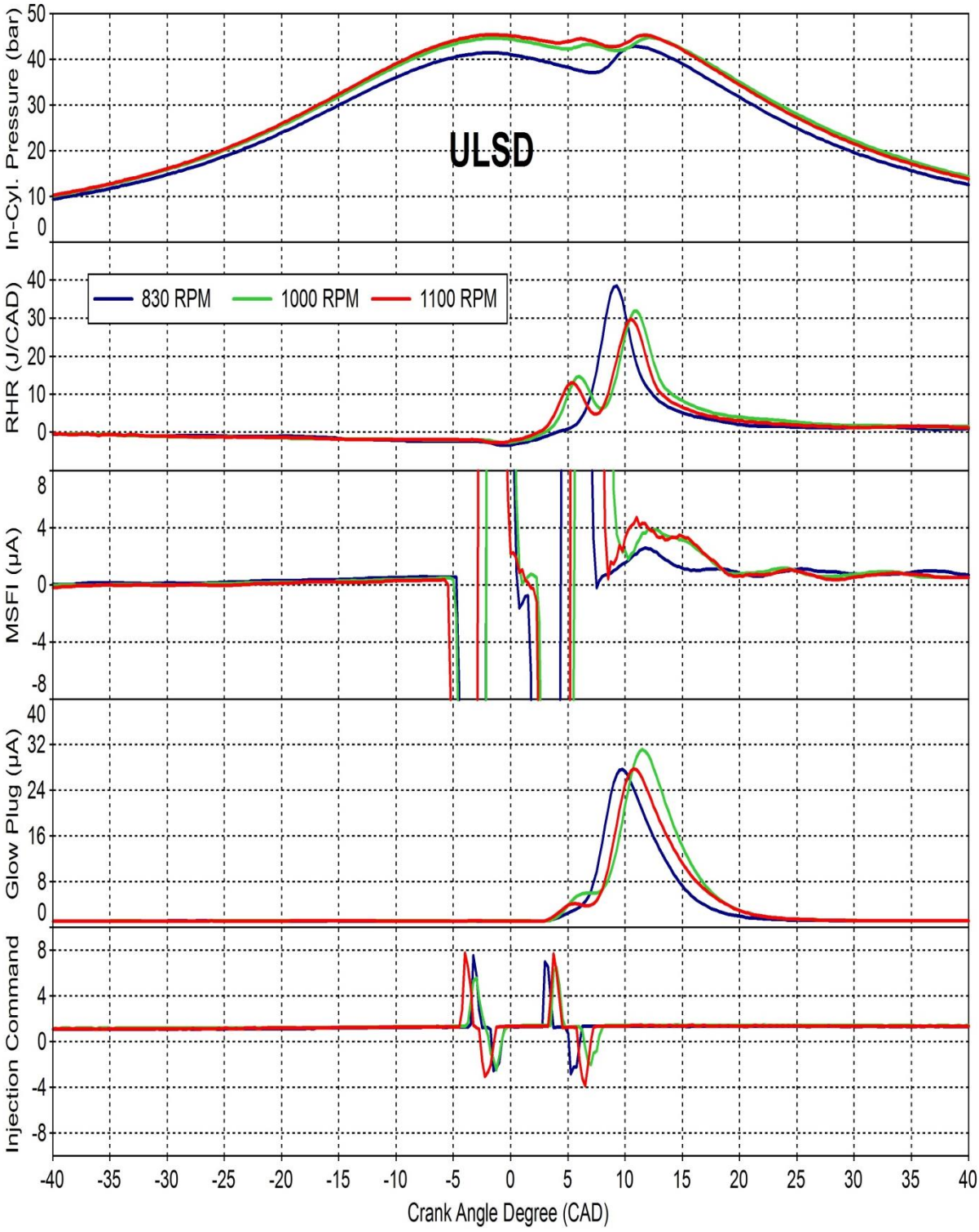

Figure 7-1 Traces showing In-Cylinder Pressure, RHR, Ion Current and injection signal at Idling Operation for ULSD

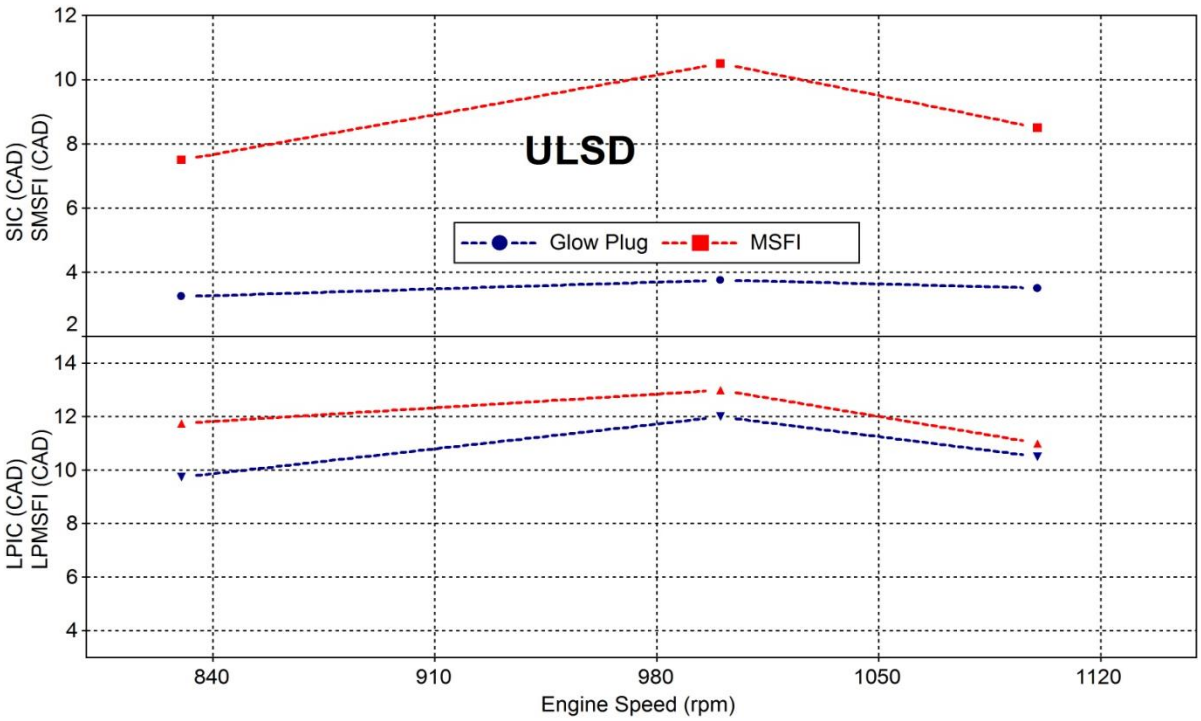

Figure 7-2 Comparison of two ionization sensors for idling speeds with ULSD

Figure 7-2 and figure 7-3 compare the ionization characteristics and ion current delay between glow plug and MSFI sensor. Figure 7-2 shows that, the start of ion current for glow plug (SIC) always advances by 4 to 4.5 CAD, when compared with MSFI. In spite of having a considerable amount of lag between SIC and SMSFI, the lag between location of peak of ion current is less than 2 CAD and becomes almost concurrent as the speed increases. This shows the strength of ion current signal detected by glow plug which clearly has a longer duration than MSFI. When the engine operates at 1000 rpm, a difference of 6 CAD is observed in the start of ion current, where SMFI equal to 10.5˚ aTDC. It further advances for 1100 rpm by 2 CAD. At the end, it can be observed that, the LPMSFI follows with LPIC irrespective of the start of ion current.

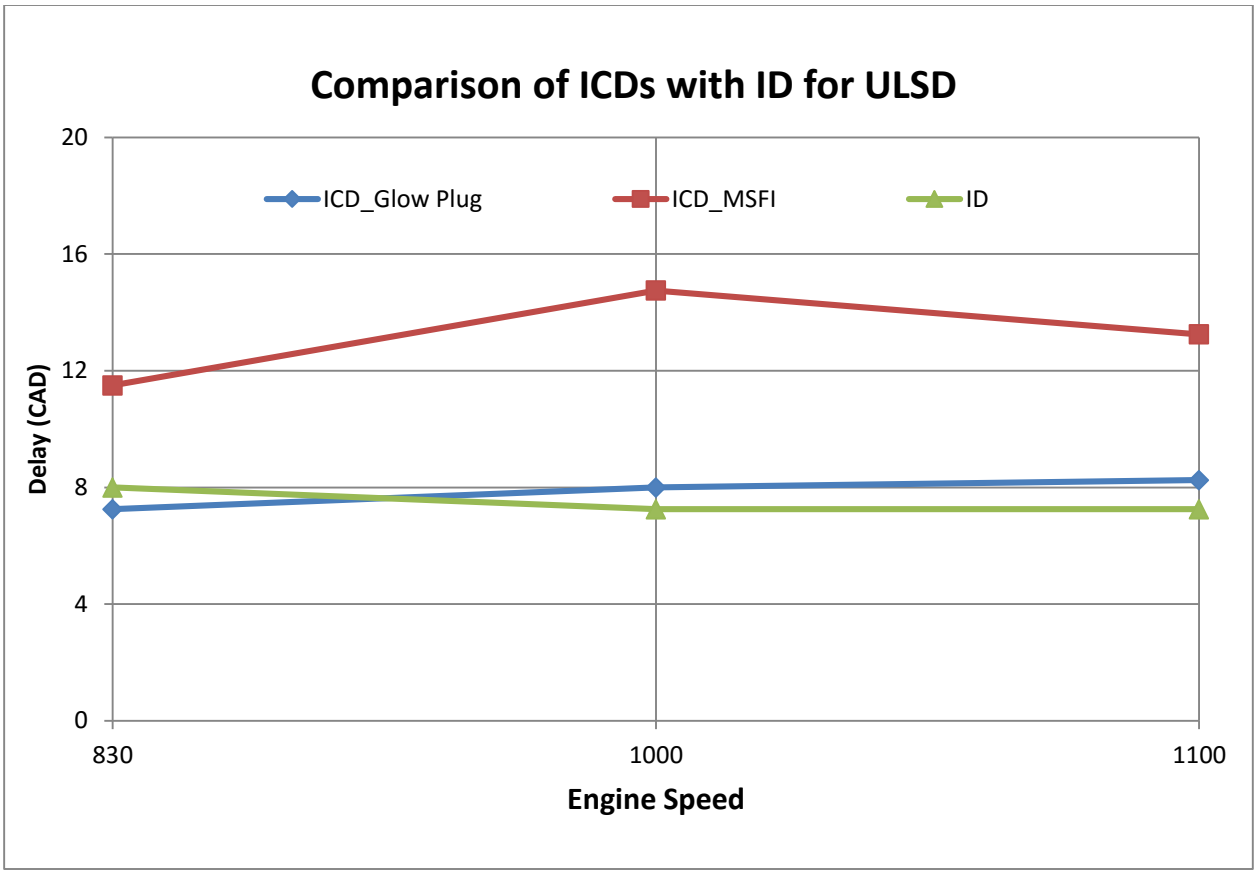

Figure 7-3 Comparison of ion current delays with ignition delay for low idling speeds using ULSD

Figure 7-3 compares the ion current delays with the ignition delay for all the tested speeds using ULSD. Ion current delays are calculated as the duration between SOI #1 and SIC, whereas ignition delay is computed as the duration between SOI#1 and start of high temperature combustion in RHR. It can be seen that ion current obtained from glow plug has a close correlation with ignition delay, where the difference between the two is very less. On the other hand, the difference between the ICD acquired from MSFI is as high as 7 CAD when compared with ID. It shows that, for all the tested speeds, glow plug not only does detect ion current earlier than MSFI sensor, but also has a close trend with SOC.

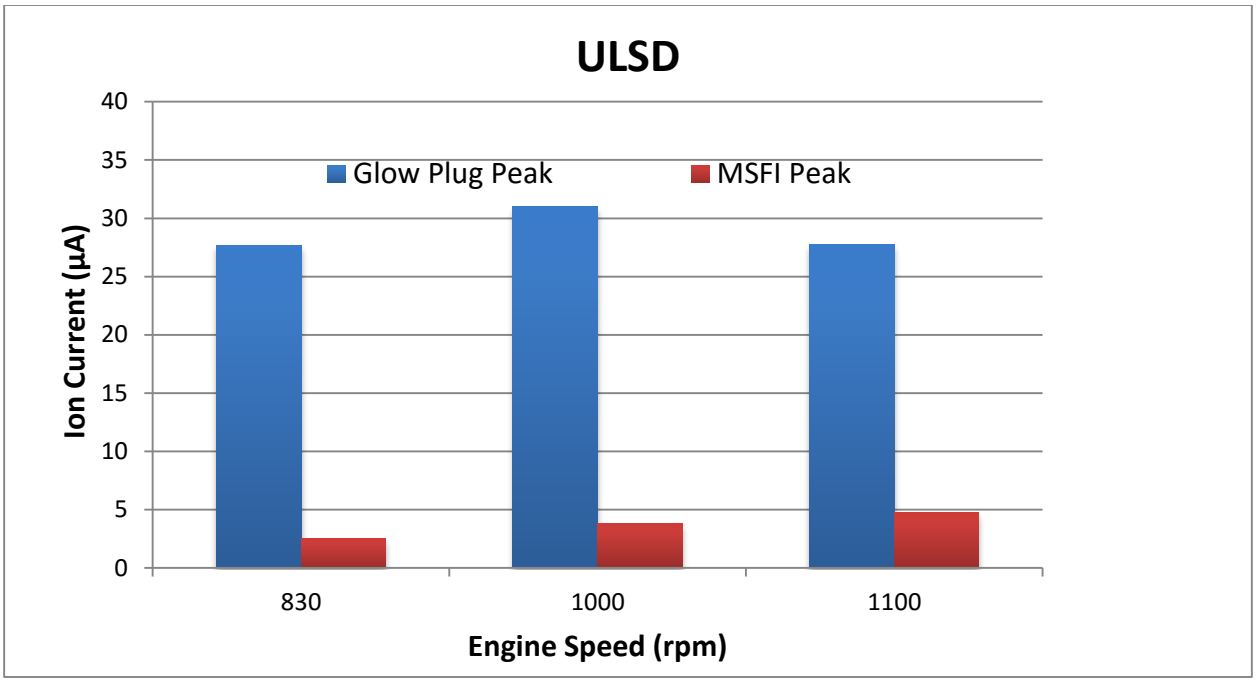

Figure 7-4 Comparison of amplitude of peak of ion current for low idling speeds using ULSD.

Figure 7-4 shows the comparison of the peak values of ion current obtained from two sensors at low idling speeds using ULSD. It can be seen that, ion current detected by the glow plug is always higher than almost 10 times than MSFI. Ion current detected from glow plug ranges between 25 to 30 µA, whereas with MSFI it varies from 2 µA to 4 µA. This shows that, the strength of ion current is very much less at the centre of the combustion chamber. This in turn helps in understanding the distribution of equivalence ratios and the combustion temperature across the combustion chamber when combustion occurs in a diesel engine.

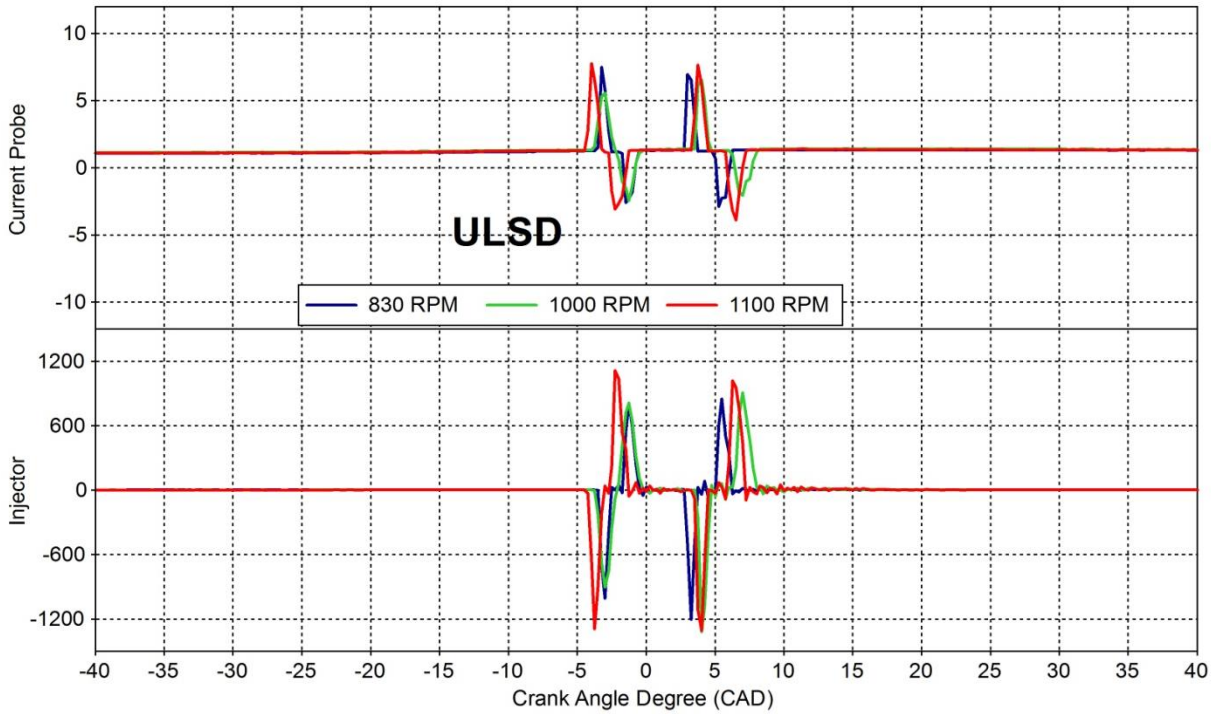

Figure 7-5 Injection signals obtained from current probe and MSFI for lower idling speeds using ULSD

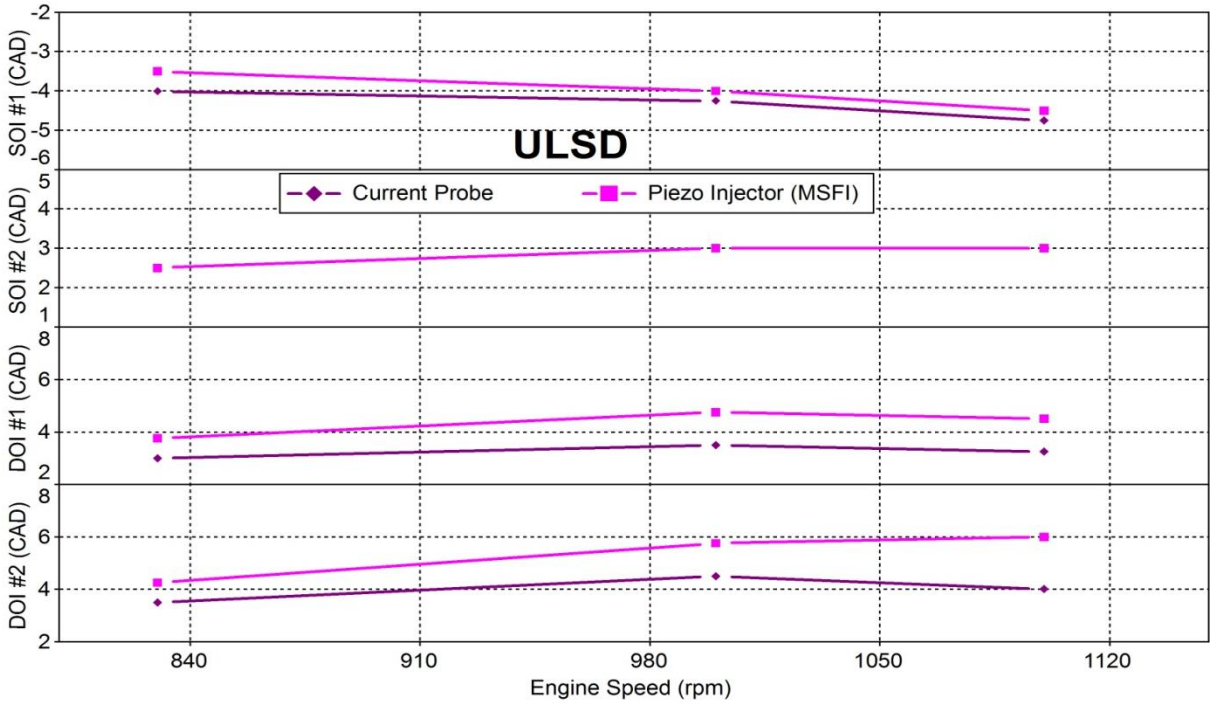

Figure 7-6 Comparison of SOI and DOI from current probe and MSFI for low idling speeds using ULSD.

Figure 7-5 and figure 7-6 show the injection signals obtained by using current probe and MSFI sensor and compare start and duration of injection events respectively, for low idling speeds using ULSD. It can be seen from figure 7-5 that, the injection signals obtained from current probe and MSFI flow in the opposite direction of each other. The method of instrumentation of the MSFI sensor and its polarity setting causes this phenomenon. Since the piezo injector requires high voltage (100V) to operate the stacks and deliver the fuel, the amplitude of the injection signal is very high for MSFI sensor than the current probe. This might cause overlapping of any ion current signal which could have been detected by MSFI.

The injection delays for both the injection event between the two sensors have been plotted in figure 7-6. It shows that, there is a lag of 0.25 to 0.5 CAD for MSFI sensor, when it detects SOI #1. On the other hand, in case of SOI #2, both the sensors have the same injection timing. This shows that, both current probe and MSFI can detect multiple injections with very less lag.

7.3 Idling with JP8

This section covers the data analysis for the combustion and ionization characteristics for idling operation at 830 rpm, 1000 rpm and 1100 rpm using JP8 (DCN = 49.3) fuel. Figures 7-7 through 7-12 cover a detailed analysis for various signals such as in-cylinder pressure, RHR, injection command and ion current from glow plug and MSFI. It also compares the ionization signals obtained using the two sensors. And in the end, it sheds a light on comparison of injection signals using current probe and MSFI.

Figure 7-7 shows the traces for in-cylinder pressure, rate of heat release, ion current and injection signal at low idling speeds using JP8. It shows two combustion events captured by the in-cylinder pressure signal as the speed increases from 830 rpm to 1000 rpm. It is also evident from the RHR trace, where premix combustion is detected for both the injection events for 1000

rpm and 1100 rpm. At 830 rpm, the peak of premix combustion occurs at 11 CAD with its amplitude being 49 J/CAD. It then decreases to 31 J/CAD, while the PPC1 is equal to 14 J/CAD at 5 CAD for 1100 rpm. As the speed increases, SOI #1 advances by 1 CAD, whereas SOI #2 gets retarded by 0.5 CAD.

Both the sensors detect ion current for all the tested speeds operating with JP8. The peak and the duration of ion current for glow plug as well as MSFI increases as the speed increases from 830 to 1100 rpm. The location of ion current detected by both the sensors advances as the speed increases. Like the engine operation with ULSD, the peak amplitude of ion current is much higher for glow plug, while it also detects ion current 5 to 6 CAD earlier than MSFI. As explained in previous section, amplitude of the injection signal obtained from MSFI is higher than the average value of ion current which might overshadow the ion current signal captured earlier.

Figure 7-8 through figure 7-10 compares the ionization characteristics obtained by using glow plug and MSFI sensors for low idling speeds using JP8. A comparison of start of ion current and location of peak of ion current is shown in figure 7-8. It shows that, the SIC (glow plug) advances by almost 4 CAD as the engine speed increases, while a very less change is observed in LPIC (glow plug). Similar to the engine operation with ULSD (figure 7-2), SIC (MSFI) lags SIC (glow plug) by 2 to 5 CAD as the speed increases. In contrast to SICs, the LPIC for both glow plug and MSFI have very less delay, 1 CAD being the maximum at 1000 rpm at 1100 rpm, LPIC (glow plug) is same as LPIC (MSFI) which is equivalent to 11.5 deg. aTDC. This shows that, even if there is a large delay in SICs detected by both the sensors, they have almost same phasing (LPIC) at all the tested speeds, which is also similar to ULSD operation. This also displays that, the duration of ion current detected by glow plug is more than that of MSFI as it takes more time to

reach its peak, which in turn demonstrates that the strength of ion current for glow plug is much higher, which is explained further in detail.

Figure 7-9 shows the correlation between ion current delay and ignition delay for low idling speeds using JP8. Same definitions were used to compute ICDs and ID, as explained in section 7.2. It can be observed that, ICD (glow plug) decreases as the engine speed increases which follows a close trend with ID. An opposite trend was seen for ICD (MSFI), which slightly increases as engine speed rises.

The amplitude for peak value of ion current for glow plug and MSFI is displayed in figure 7-10 and compared for all the tested idling speeds operating with JP8. Similar to engine operation with ULSD (figure 7-4), the peak of ion current for glow plug is almost 6 to 8 times higher than MSFI for all the speeds. PIC for MSFI is 5μA for 1100 rpm, which is being the highest among all, while the highest PIC for glow plug is 30μA for 1000 rpm engine speed.

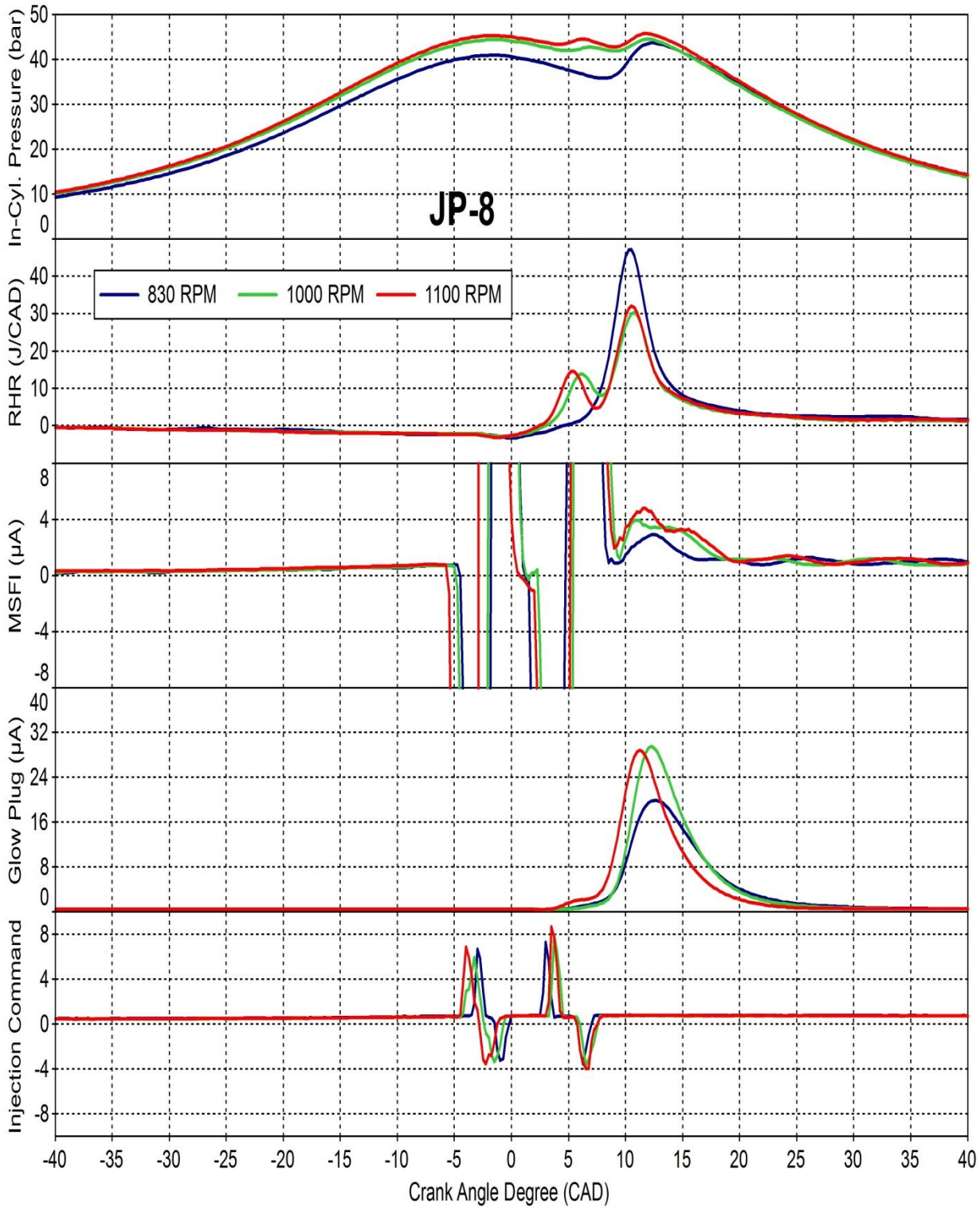

Figure 7-7 Traces showing In-Cylinder Pressure, RHR, Ion Current and injection signal at Idling Operation for JP8.

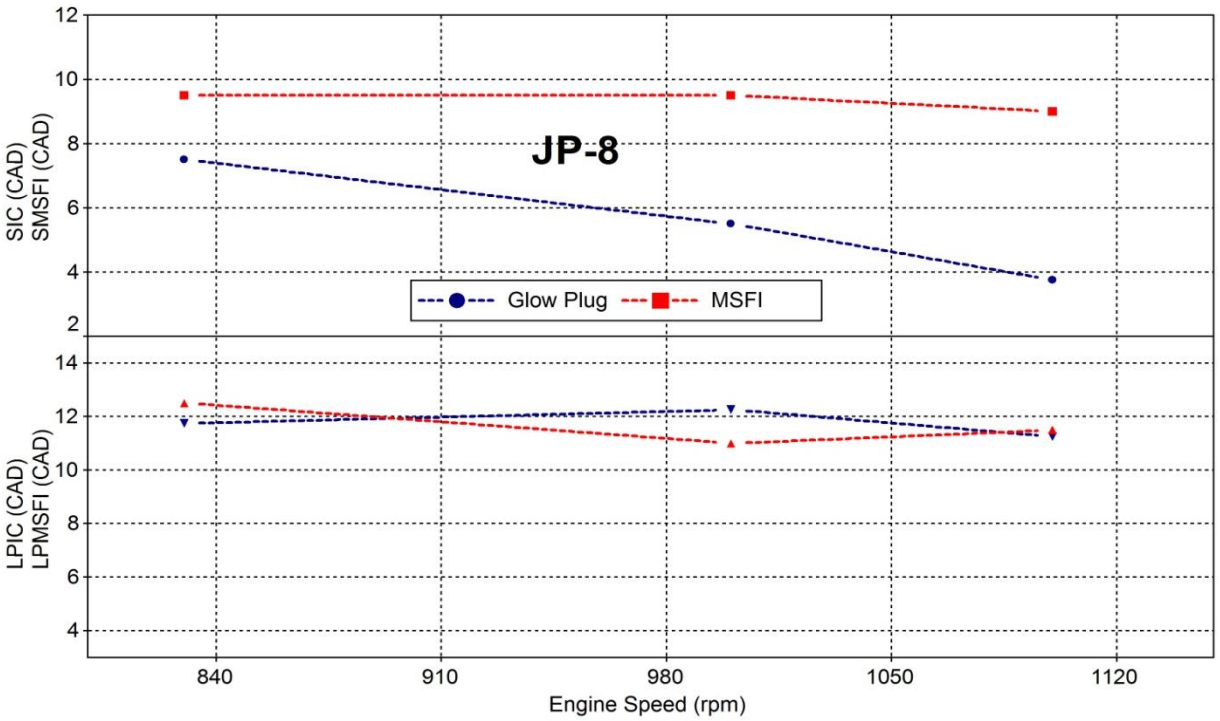

Figure 7-8 Comparison of two ionization sensors for idling speeds using JP8

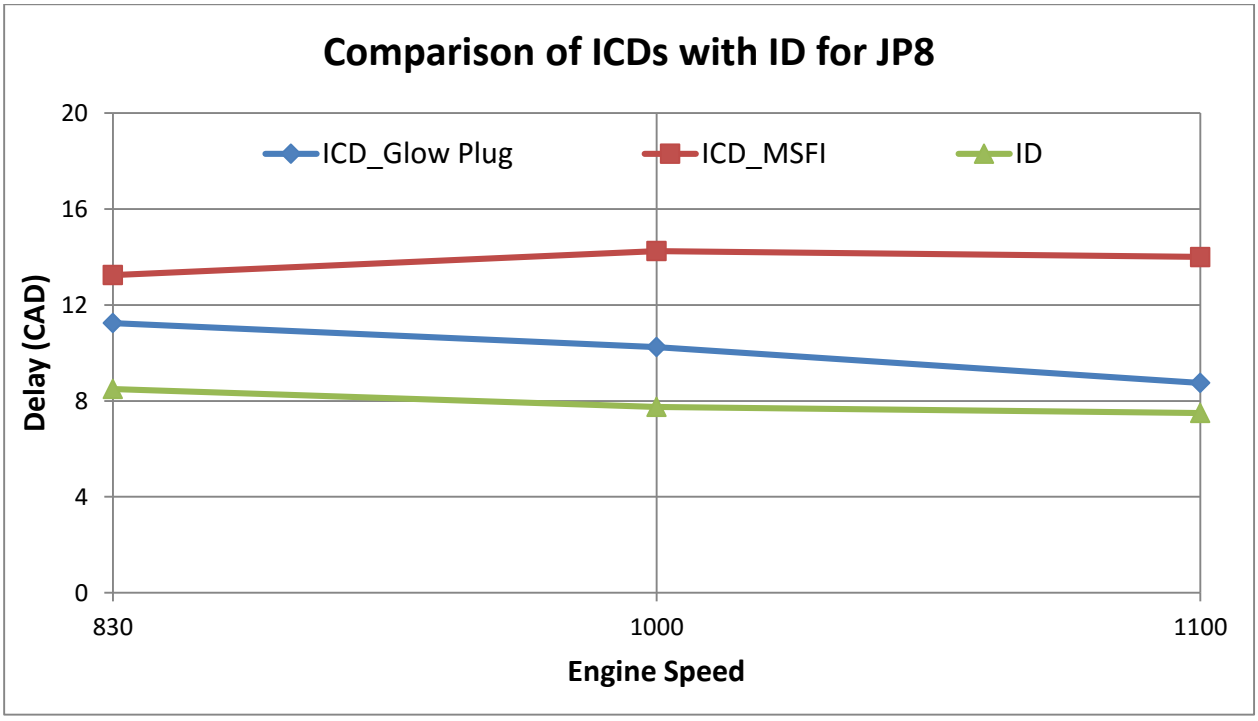

Figure 7-9 Comparison of ion current delays with ignition delay for low idling speeds using JP8.

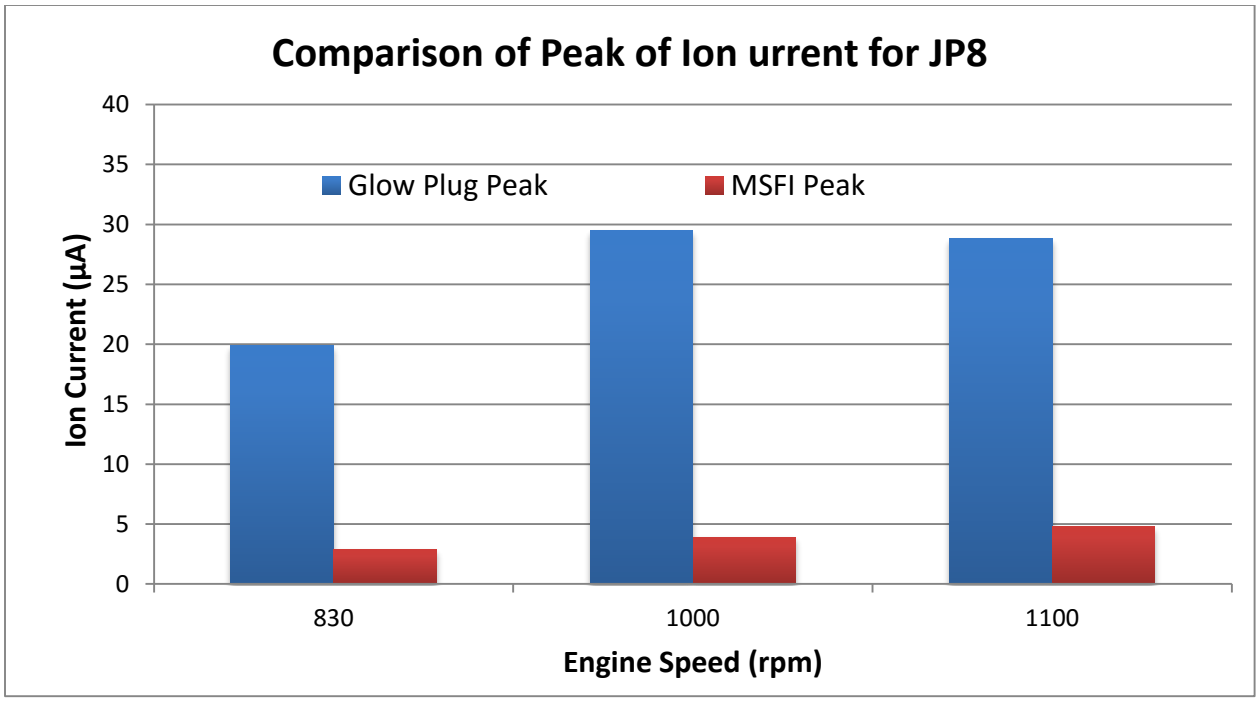

Figure 7-10 Comparison of amplitude of peak of ion current for low idling speeds using JP8.

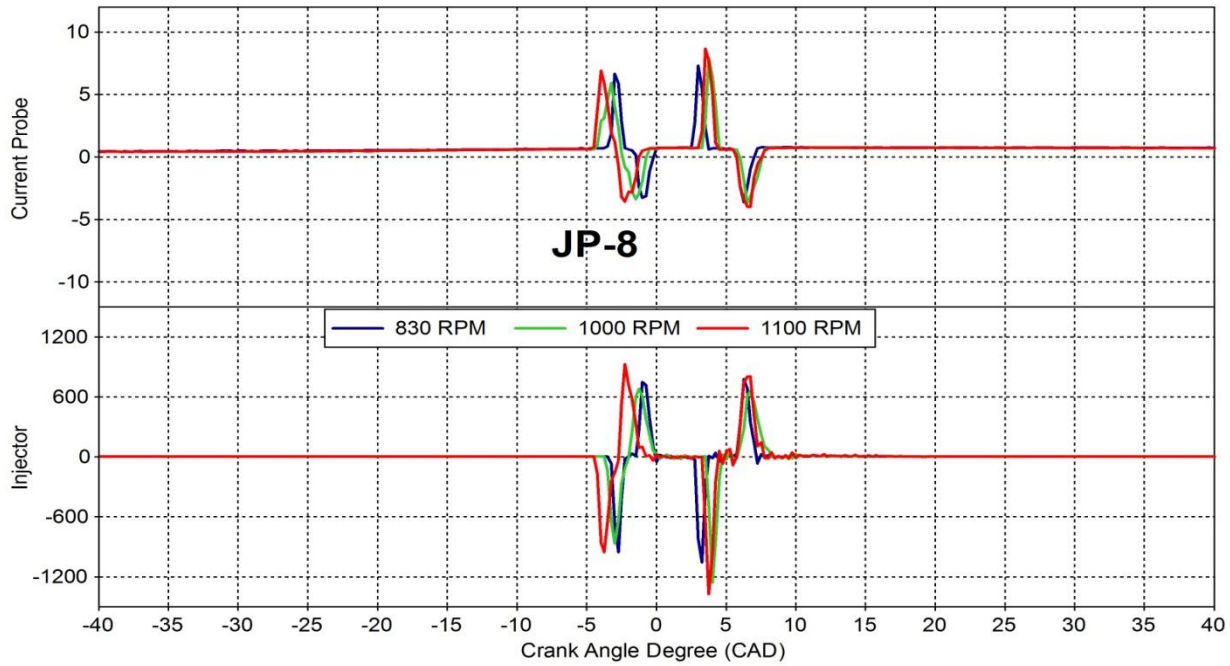

Figure 7-11 Injection signals obtained from current probe and MSFI for lower idling speeds using JP8.

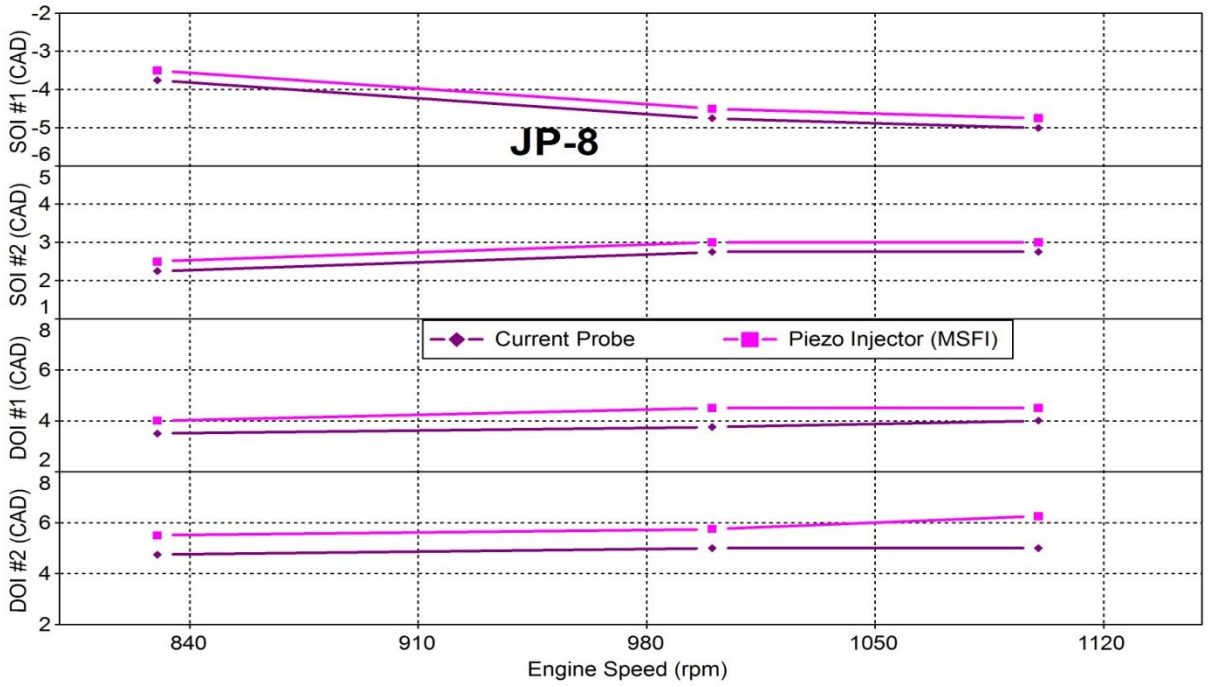

Figure 7-12 Comparison of SOI and DOI from current probe and MSFI for low idling speeds using JP8.

Figure 7-11 and figure 7-12 display the injection signals obtained from current probe and MSFI and compare the SOI and DOI for both the injection events for low idling speeds using JP8. As can be seen from figure 7-11, both the injection events were detected by current probe as well as MSFI. As explained in section 7.2, the injection signals oppose each other in the direction for the two sensors used. SOI #1 advances by 1 to 1.5 CAD as the engine speed increases, whereas SOI #2 retards by 0.5 CAD detected by both current probe and MSFI. SOI #1 as well as SOI #2 captured by piezo injector always lags by 0.25 CAD with the one detected by current probe. On the other hand, both DOI #1 and DOI #2 is more than 1 CAD for the one detected by the injector. This clearly shows that, like the engine operation with ULSD, EOI detected by the injector for both the injections is 1 CAD later than current probe.

7.4 Exhaust Emissions

This section shows the results for exhaust NO (ppm) and % opacity for the low idling speeds using ULSD and JP8. Figure 7-13 shows the comparison for exhaust NO for both the fuels, while % opacity is plotted in figure 7-14.

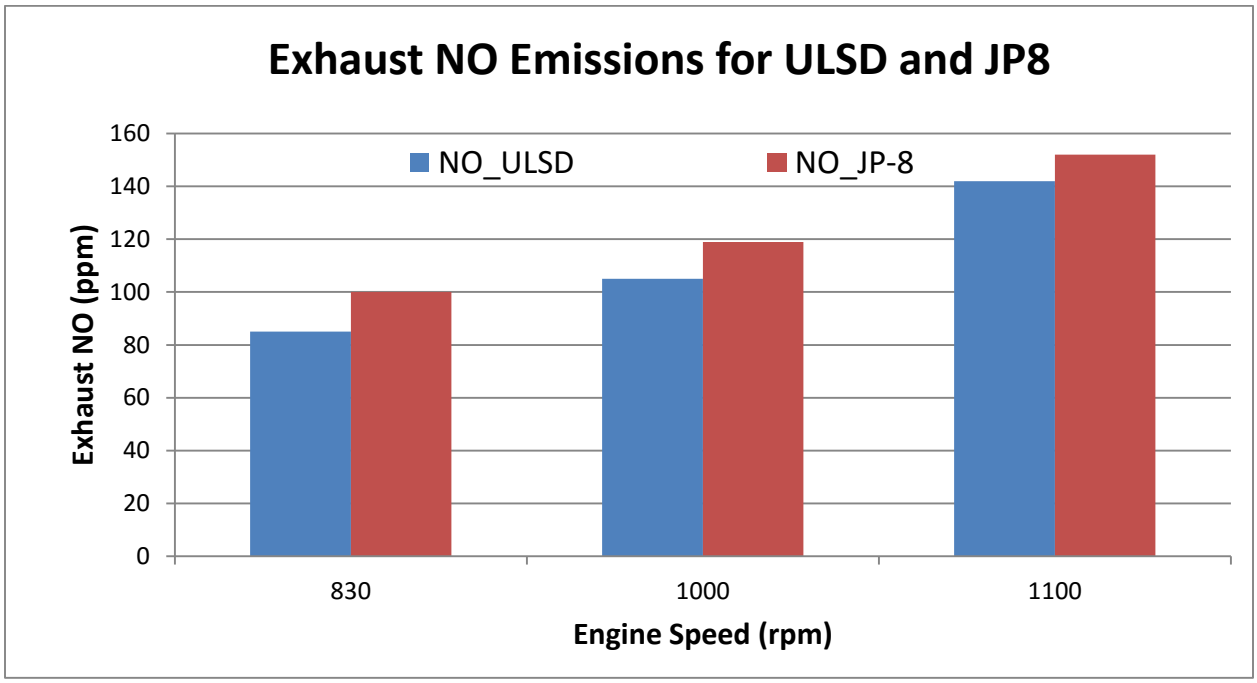

Figure 7-13 Comparison of exhaust NO emissions for low idling speeds using ULSD and JP8

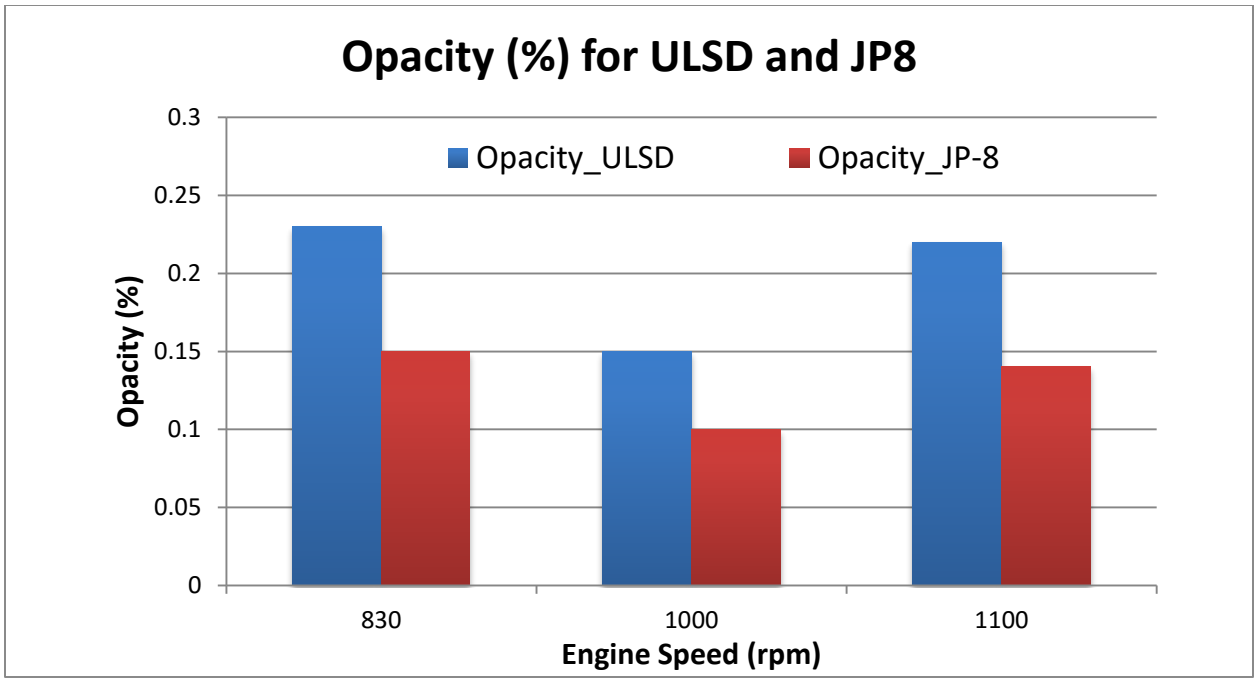

Figure 7-14 Comparison of % opacity for low idling speeds using ULSD and JP8

It can be observed that, exhaust NO for ULSD is lower than that obtained with JP8 by 5 to 10 ppm for all the tested speeds. This difference decreases as the engine speed increases from 830 rpm to 1100 rpm. On the other hand, opposite trend is seen for % opacity, which is plotted in figure 7-14. It is higher than 0.05% for JP8 as compared with that of ULSD for all the tested speed. It decreases as the engine operates through 1000 rpm for both the fuels and then increases by same amount at 1100 rpm. This mainly occurs due to lower volatility and high density for ULSD fuel which causes a difference in NO and % opacity as can be seen from figures 7-13 and 7-14 respectively.

7.5 Chapter Summary

This chapter explains the auto-ignition, combustion and ionization characteristics and exhaust emissions for low idling speeds of 830 rpm, 1000 rpm and 1100 rpm using ULSD and JP8. It shows the comparison of ion current characteristics for two ionization sensors, glow plug and MSFI at all the tested speeds using ULSD and JP8. It further explains the injection signals obtained by using current probe and MSFI. It shows that ion current detected by glow plug is stronger than that of MSFI at all the low idling speeds. In addition to that, it also detects ion current earlier than MSFI. This basically helps in explaining the nature of combustion and the distribution of the air-fuel ratios inside the combustion chamber. In addition to this, MSFI sensor detects both the injection events with a very little lag.

CHAPTER 8

CONCLUSIONS

For this investigation, all the tests were conducted on a 4-stoke, 4-cylinder, 2.0 L Volkswagen turbocharged direct injection diesel engine for cold starting at an ambient temperature T_{amb} = 25˚C by using ULSD and JP8. Another set of tests were carried out at steady state low idling speeds of 830, 1000 and 1100 rpm using ULSD and JP8. The engine is equipped with a high pressure common rail injection system and piezo operated injectors. The main objective of the cold starting tests is to study cycle to cycle variation of auto-ignition, combustion and ionization characteristics and determine their contribution towards combustion instability. The purpose of steady state idling is to compare ion current signal by using two different sensors in two different cylinders. All the tests were performed using an OEM/industrial ECU and following conclusions were obtained and following conclusions are drawn.

8.1 Cold-Starting

Cycle to cycle analysis of various auto-ignition, combustion and ionization characteristics during cold starting at an ambient temperature extracts following conclusions:

- Engine operation with ULSD undergoes more instability than JP8, in which a complete misfiring occurs followed by late combustion events. Misfiring can be avoided by using an appropriate combination of rail pressure and injection timing.
- Glow plug fails to detect ion current for 28 and 50 cycles while operating on ULSD and JP8 respectively. It could not detect ion current for first 11 consecutive cycles operating with JP8 with a repetitive trend.

- Detection of ion current by using glow plug mainly depends on rail pressure and duration of injection along with fuel density which in turn control the spray momentum and mixture strength near the vicinity of glow plug.
- MSFI signal for cycle to cycle basis has more noise and requires further conditioning. Hence, in-spite of being undetected or misdetected, glow plug has a better tendency to detect ion current under cold starting conditions.
- Combustion phasing (LPPC) has a close correlation with LPIC for ULSD, while it always lags SIC by 1 to 2 crank angle degrees.
- Peak value of ion current mostly depends on the consistency of peak of premixed combustion, which is quite consistent for JP8.
- Prolonged presence of LTC and NTC regimes contributes towards more combustion instability, further adding high amount of variation in combustion phasing.
- Chemical delay of a fuel is a key factor during transient engine operation which decreases with ID. This implies that, combustion instability is most affected by quality of fuel (CN).

8.2 Ionization Sensors

Comparison of two ionization sensors at steady state operating condition derives following conclusions:

- Glow plug sensor generates a stronger ionization signal than MSFI at all the low idling speeds. This indicates that, ion current has a weaker strength at the center of the combustion chamber, which also has closer correlation with ID.

- Detection of ion current by MSFI sensor always occurs after the EOI and lags the one detected by glow plug sensor. Ionization signal might be overlapped by a high amplitude of injection signal detected by MSFI, which could make it undetected in the earlier stages.
- MSFI sensor not only does detect ionization signal, but also detect both the injection events and their respective duration which closely matches with current probe.
- NO emissions increase with the speed and remain higher for JP8, whereas opacity has an opposite trend being maximum for ULSD.

APPENDIX

ABBREVIATIONS

CAD: Crank Angle Degree

aTDC: After Top Dead Center

bTDC: Before Top Dead Center

OEM: Original Engine Manufacturer

ECU: Electronic Control Unit

DAQ: Data Acquisition System

CN: Cetane Number

ULSD: Ultra Low Sulfur Diesel

JP8: Jet Propellent 8

MSFI: Multi Sensing Fuel Injector

IMEP: Indicated Mean Effective Pressure

RHR: Rate of heat release

SOC: Start of combustion

SOI: Start of injection

DOI: Duration of injection

EOI: End of injection

ID: Ignition Delay

ICD: Ion current delay

SIC: Start of ion current (Glow Plug)

SMSFI: Start of MSFI ion current

LPIC: Location of peak of ion current (Glow Plug)

PIC: Peak of ion current (Glow Plug)

LPMSFI: Location of peak of MSFI ion current

PMSFI: Peak of MSFI ion current

LPPC: Location of peak premixed combustion

PPC: Peak of premixed combustion

LTC: Low Temperature Combustion

NTC: Negative Temperature Coefficient

COV: Coefficient of variation

REFERENCES

1. Heywood, J., 1988, Fundamentals of Internal Combustion Engines, McGraw-Hills and Hall, London.

2. Self-study program 826803, 2.0 Liter TDi Common Rail BIN5 ULEV Engine.

3. "Specifications for Volkswagen Industrial Engine." Volkswagen AG Engine Manual, 2009.

4. Gujarathi, S., Badaway, T., Henein, N., "Ion current during cold starting and idling in diesel engines," ASME ICEF2012-92093.

5. George, R., Badawy, T, Henein, N., "Experimental study of fuel properties on ion current, combustion, and emission in a high speed diesel engine," SAE Technical Paper 2014-01-1263.

6. Zahdeh, A., Henein, N., Bryzik, W., "Diesel cold starting: Actual cycle analysis under border line conditions," SAE Technical Paper 900441.

7. Henein, N., Zahdeh, A., Yassine, K., Bryzik W., "Diesel engine cold starting: Combustion Instability," SAE Technical Paper 920005.

8. Osuka, I., Nishimura, M., Tanaka, Y., and Miyaki, M., "Benefits of New Fuel Injection System Technology on Cold Startability of Diesel Engines-Improvement of Cold Startability and White Smoke Reduction by Means of Multi Injection with Common Rail Fuel System (ECDU2)," SAE International, 940586.

9. Yassine M., Tagomori, M., Henein, N, Bryzik, W., "White smoke emissions under cold starting of diesel engines," SAE International 960249.

10. Hara, H., Itoh, Y., Henein, N. A., and Bryzik, W., "Effect of Cetane Number with and without Additive on Cold Startability and White Smoke Emissions in a Diesel Engine," SAE International, 1999-01-1476.

11. Han, Z., Henein, N., Nitu, B., and Bryzik, W., "Diesel Engine Cold Start Combustion Instability and Control Strategy," SAE International, 2001-01-1237.

12. Lippert, A., Stanton, D., Reitz, R., Rutland, C., Hallet, W., "Investigating the effect of spray targeting and impingement on diesel engine cold start," SAE 2000-01-0269.

13. Liu, H., Henein, N., Bryzik, W., "Simulation of diesel engine cold start," SAE 2003-01-0080.

14. Pastor J , Bermúdez, V., García-Oliver, J., Ramírez-Hernández, J., "Influence of spray glow plug configuration on cold start combustion for high speed direct injection diesel engines," Energy 36 (2011) 5486-5496.

15. Pastor, J., García-Oliver, J., Pastor, J., Ramírez-Hernández, J., "Ignition and combustion development for high speed direct injection diesel engines under low temperature cold start conditions," Fuel 90 (2011) 1556-1566.

16. Payri, F., Broatch, A., Salavert, J., Martín, J., "Investigation of Diesel combustion using multiple injection strategies for idling after cold start of passenger-car engines," Experimental Thermal and Fluid Science 34 (2010) 857–865.

17. Desantes, J., García-Oliver, J., Pastor, J., Ramírez-Hernández, J., "Influence of nozzle geometry on ignition and combustion for high-speed direct injection diesel engines under cold start conditions" Fuel 90 (2011) 3359-3368.

18. Antonino La Rocca, MacMillan, D., Shayler, P., Murphy, M., Pegg, I., "CFD Investigation on the Influence of In-Cylinder Mixture Distribution from Multiple Pilot Injections on Cold Idle Behaviour of a Light Duty Diesel Engine," SAE 2014-01-2708.

19. Henein, N., M-C. Lai, M-C, Singh, I., Zhong, L., Han, J., "Characteristics of a Common Rail Diesel Injection System under Pilot and Post Injection Modes," SAE 2002-01-0218.

20. Magno, A., Mancaruso, E., Vaglieco, B., "Optical Investigation of Injection and Combustion Phases of a Fouled Piezoelectric Injector in a Transparent CR Diesel Engine," SAE 2013-01-1591.

21. Oki, M., Matsumoto, S., Toyoshima, Y., Ishisaka, K. et al., "180MPa Piezo Common Rail System," SAE Technical Paper 2006-01-0274.

22. Oh, B., Oh, S., Lee, K., and Sunwoo, M., "Development of an Injector Driver for Piezo Actuated Common Rail Injectors," SAE Technical Paper 2007-01-3537.

23. Caika, V., Kammerdiener, T., Dorr, N., "Operation of Piezoelectric Common Rail Injector with Diesel and FT-Kerosene," SAE 2007-24-0070.

24. Kubach, H., Velji, A., Spicher, U., and Fischer, W., "Ion Current Measurement in Diesel Engines," SAE Technical Paper 2004-01-2922.

25. Henein, N., Bryzik, W., Abdel-Rehim, A., and Gupta, A., "Characteristics of Ion Current Signals in Compression Ignition and Spark Ignition Engines," SAE Int. J.Engines 3(1):260-281, 2010.

26. Abdel-Rehim, A., Henein, N., VanDyne, Ed, "Impact of A/F Ratio on Ion Current Features Using Spark Plug with Negative Polarity," SAE 2008-01-1005.

27. Henein, N. A., Badawy, T., Rai, N., and Bryzik, W., "Ion Current, Combustion and Emission Characteristics in an Automotive Common Rail Diesel Engine," Journal of Engineering for Gas Turbines and Power, 134(4), pp. 042801-042807, 2012.

28. Badawy, T., Henein, N., and Bryzik, W., "Closed Loop Control Using Ion Current Signal in a Diesel Engine," SAE Technical Paper 2011 -01-2433, 2012.

29. Estefanous, F., Henein, N., "Multi Sensing Fuel Injector for Electronically Controlled Diesel Engines," SAE 2011-01-0936.

30. Estefanous, F., “Multi-Sensing Fuel Injection System and Method for Making the Same”, Patent Application No. PCT/US10/42549, July 2010

31. Jaykumar, C., Zheng, Z., Joshi, U., Bryzik, W., Henein, N., Sattler, E., "Effect of Intake Pressure and Temperature on the Auto-Ignition of Fuels with Different Cetane Number and Volatility,"SAE 2012-01-1317.

32. Cavina, N., Poggio, L., Sartoni, G., "Misfire and Partial Burn Detection based on Ion Current Measurement," SAE 2011-24-0142.

33. Badawy, T., Henein, N., Bryzik, W.,"Closed Loop Control Using Ion Current Signal in a Diesel Engine," SAE 2011-01-2433.

34. Nargunde, J., Jayakumar, C., Sinha, A., Acharya, K. et al., "Comparison between Combustion, Performance and Emission Characteristics of JP8 and Ultra Low Sulfur 143 Diesel Fuel in a Single Cylinder Diesel Engine," SAE Technical Paper 2010-01-1123, 2010.

35. Schihl, P. and Hoogterp-Decker, L., "On the Ignition Behavior of JP8 in Military Relevant Diesel Engines," SAE Int. J. Engines 4(1):1-13, 2011.

36. "Kistler M5-Sensors, Type 6052A," Instruction Manual

37. Kistler Piezo-resistive High Pressure Sensor Specification Sheet (No. 03.4067).

38. Max Machinery, Inc. Model 710 Wall Mount Fuel Measurement System Manual.

39. Badawy, T., Rai, N., Singh, J., Bryzik, W., and Henein, N., "Effect of design and operating parameters on the ion current in a single-cylinder diesel engine," International Journal of Engine Research, 2011

ABSTRACT

EXPERIMENTAL INVESTIGATION ON COMBUSTION AND IONIZATION DURING COLD STARTING AND IDLING OF A DIESEL ENGINE

by

SAHIL DEODATTA SANE

December 2015

Advisor: Dr. Naeim A. Henein

Major: Mechanical Engineering

Degree: Master of Science

Diesel engine performance during cold starting is very crucial for smooth engine start at undesirable emission level. The development of cold start strategies that improve combustion stability relies mainly on the understanding of the combustion process during the cold starting. Even for modern diesel engines, the conditions during the cold start is far from normal operation characterized by large amount of unburned hydrocarbon emissions and long start to idling time. Thus, the use of an in-cylinder combustion sensor to measure the combustion quality during engine starting can significantly improve engine cold start control strategies. The ion current sensor has the potential to be used as onboard sensor to measure the combustion process during engine operation and can be used as feedback to the engine control unit.

The aim of this research is to study and determine the combustion instability and its impact on various combustion and ionization characteristics by performing cycle analysis for a comparison between engine performance using ultra low sulfur diesel (ULSD) and aviation jet propulsion (JP8) fuels during cold start at 25˚C. It also shows a comparison between two ion

current sensors during low load idling using the same fuels. For this purpose, the glow plug and fuel injector of VW 2.0L turbocharged diesel engine were modified and electrically insulated to be used as ion current sensors. The experimental test was conducted to study the combustion process and emission product produced during low load idling.

AUTOBIOGRAPHICAL STATEMENT

I was born in Mumbai, India on June 14th, 1989. My desire to gain the technical knowledge and to imbibe the practical skills took my career path towards core engineering field. I have completed my undergraduate education in mechanical engineering and earned a Bachelor's degree from Rajiv Gandhi Institute of Technology, Mumbai University, India in August 2011. My further interest to acquire an advanced and in-depth understanding in the field of internal combustion engines took me to Wayne State University, Detroit, Michigan in January 2013 to pursue of the Master's degree in mechanical engineering. During the course of my masters program, not only did I gain a thorough knowledge in combustion sciences but also got an opportunity to learn various simulation softwares. My passion of working on engine hardware was fulfilled by Prof. Dr. Naeim A. Henein, who gave me an opportunity to work in Center for Automotive Research as a Research Assistant (RA) under his guidance. My major goal was to study and analyze the heterogeneous combustion process during cold starting and idling of a diesel engine operated with an industrial ECU. It also comprised of designing a multi sensing fuel injector (MSFI) sensor in order to study ionization characteristics at the center of the combustion chamber. For this research, I conducted cold starting tests by using ULSD and JP8 fuel and performed an extensive analysis. My urge to take up more challenges in the industry and explore new techniques took me a step further when I started working as Diesel Engine Performance and Emission Calibration Engineer with John Deere since February 2015.